universität wien

Evolution of Crystallographic Texture and Mechanical Properties of Single- and Polycrystalline Mg (99.85 wt.%) Subjected to High-Pressure Torsion (HPT) Deformation

The Bilateral Doctoral Thesis

Bartłomiej J. Bonarski

2010-06-20

Scientific supervisors:

Prof. Borys Mikułowski (AGH – University of Science and Technology in Cracow, Poland)

Ao. Univ. Prof. Michael J. Zehetbauer (University of Vienna, Austria)

This doctoral thesis has been completed within the bilateral contract ("Cotutelle de Thèse") based upon a mutual agreement between the AGH – University of Science and Technology in Cracow (Poland) and the University of Vienna (Austria).

Physics of Nanostructured Materials

universität wien

DISSERTATION

Titel der Dissertation

Evolution of Crystallographic Texture and Mechanical Properties of Single- and Polycrystalline Mg (99.85 wt.%) Subjected to High-Pressure Torsion (HPT) Deformation.

angestrebter akademischer Grad

Doktor der Naturwissenschaften (Dr. rer.nat.)

Verfasserin / Verfasser:	Dipl. Ing. Bartłomiej J. Bonarski
Matrikel-Nummer:	0708379
Dissertationsgebiet (lt. Studienblatt):	Physik
Betreuerin / Betreuer:	Ao. Univ. Prof. Michael J. Zehetbauer Prof. Borys Mikułowski

Wien, am 20. Juni 2010

AKADEMIA GÓRNICZO-HUTNICZA
im. Stanisława Staszica w Krakowie

Wydział Metali Nieżelaznych
Katedra Materiałów Metalicznych i Nanoinżynierii

ROZPRAWA DOKTORSKA

Ewolucja tekstury krystalograficznej i własności mechanicznych mono- i polikrystalicznego magnezu (99.85 %wag.) odkształcanego metodą skręcania pod wysokim ciśnieniem (High-Pressure Torsion, HPT).

Mgr inż. Bartłomiej J. Bonarski

Promotorzy: Prof. dr hab. inż. Borys Mikułowski
Ao. Univ. Prof. Michael J. Zehetbauer

KRAKÓW, 20 czerwca 2010

I would like to express my sincere gratitude to my scientific supervisor, Prof. Borys Mikułowski, who accepted me as his PhD Student and granted me a perfect mixture of a free-hand and responsibility on this PhD route. I would like to thank him for giving me a chance of participating in a research stay at the University of Vienna which was a great experience and a wonderful time, and for a constant support and many valuable discussions during those years.

I am also grateful to my scientific supervisor Prof. Michael J. Zehetbauer for giving me the opportunity of working at his research group of Physics of Nanostructured Materials, inspiring me with the ideas, giving me a chance for representing the University at the numerous meetings and conferences and for a warm hospitality at his Group's Lab in Vienna.

My deepest and warm-heartedly gratitude goes to my beloved wife, Gabrysia for the wonderful and unforgettable years that we spent together in Vienna during realization of my PhD, filled with her cheerful support, warm understanding, patience and love.

I would like to thank my Parents and my Sister Karolina for their support and warm-heart during those years. My special thanks goes to my Father, for being always ready for supporting me with brilliant advices and expert's comments at the field of material science, and not only there.

Last but not least, I wish to express my cordial gratitude to the people I started to work with and who now I claim to call my Friends: Mag. Michi Kerber and Dr. Erhard Schafler and Dr. Daria Setman from Vienna. For their friendship and warm welcome which has turned the years away from the family into the great time I spent in Vienna, for the friendly understanding, hours of common work, and a great time when the work was done.

Abstract of bilateral Ph.D. Thesis

„Evolution of Crystallographic Texture and Mechanical Properties of Single- and Polycrystalline Mg (99.85 wt.%) Subjected to High-Pressure Torsion (HPT) Deformation"

High Pressure Torsion ("HPT") deformation is a processing mode which achieves nanostructured materials with outstanding physical properties in bulk shape. Therefore this method is in focus of international materials research in order to fully understand and control the processes governing the nanocrystallization of materials. A great lack in knowledge is about the HPT deformation of hexagonal metals and alloys at which the current PhD. Thesis aimed, by studying the evolution of the crystallographic texture occurring during and after HPT deformation of single- and polycrystalline magnesium of 99.85 wt.% purity, and by correlating this evolution with measurements of mechanical properties. The analyses showed that – with both the single as well as the polycrystalline materials – there was no influence of the initial material parameters – like the orientation or the size of crystallites – on the final texture and microstructure even with the very high plastic strains induced by HPT. The final texture and its intensities consisted of components which arose from shear of the HPT deformation but also from others which depend on the hydrostatic pressure as well as on the annealing time at ambient temperature after release of pressure. These dependences can be explained by the specific contributions of dynamic ("DRX", during HPT deformation) and static ("SRX", after HPT deformation) recovery/recrystallization processes. In order to distinguish between these processes, especially designed experiments were carried out where samples have been "frozen" at liquid nitrogen temperature before the investigations (samples type "F"), and compared with those which have been stored at ambient temperature after HPT deformation and investigated afterwards (samples type "RX"). In addition to the special effects to texture, the "RX" samples revealed the higher increase in strength, whereas the "F" samples exhibited a higher plasticity. As a result of thorough investigations of microstructure by different methods of electron microscopy, a bimodal structure consisting of both small, deformation-induced crystallites (grain size below 0.3 μm) and of much larger crystallites (grain size beyond 5 μm) arising from the recovery/recrystallization processes, was found. In analogy to the texture results, the fraction of recovered/recrystallized crystallites increased with increasing annealing time and with increasing HPT pressure.

Abstrakt der Dissertation

„Entwicklung der kristallografischen Textur und der mechanischen Eigenschaften von mittels Hochdrucktorsionsverformung hergestelltem ein- und vielkristallinem Magnesium (99.85 Gew. %)"

Die plastische Verformung mittels Hochdrucktorsion („High Pressure Torsion – HPT") ist eine Methode, mit der man nanostrukturierte Materialien mit außergewöhnlichen physikalischen Eigenschaften in massiver Form herstellen kann. Die Methode steht derzeit im Zentrum der internationalen wenden. Nur wenig ist von den Merkmalen der HPT Verformung hexagonaler Metalle und Legierungen bekannt, auf die die vorliegende Dissertation abzielt, indem sie die Entwicklung der kristallografischen Textur während und nach der HPT Verformung von ein- und vielkristallinem Mg mit Reinheit 99.85 Gew.% untersuchte und mit Messungen der mechanischen Eigenschaften korrelierte. Die Analysen zeigten zunächst, dass sowohl beim einkristallinen wie auch beim polykristallinem Material die Strukturparameter der Ausgangsmaterialien, wie z.B. die Orientierung und die Größe der Kristallite, auf die Charakteristik der Endtextur bzw. Mikrostruktur auch von höchsten HPT Verformungsgraden keinen Einfluss haben. Diese sind einerseits gekennzeichnet von Komponenten der Scherung, die von der HPT Verformung stammen, andererseits aber auch von Komponenten, die vom hydrostatischen Druck bzw. der der Entlastung folgenden Lagerung bei Raumtemperatur abhängen. Diese Abhängigkeiten können durch spezifische Beiträge der dynamischen ("DRX", während der HPT Verformung) und der statischen ("SRX", nach HPT Verformung) Erholung bzw. Rekristallisation erklärt werden. Um zwischen diesen Beiträgen zu unterscheiden, wurden spezielle Experimente durchgeführt, bei denen die Proben unmittelbar nach HPT Verformung bzw. vor den Untersuchungen in Flüssig-Stickstoff "eingefroren" wurden (Proben Typ „F"); diese wurden mit Proben verglichen (Proben Typ "RX"), die nach der HPT Verformung bei Raumtemperatur gelagert und erst dann untersucht wurden. Außer den speziellen Merkmalen der Textur zeigten die "RX" Proben eine höhere Festigkeit, während dagegen die "F" Proben eine höhere Plastizität aufwiesen. Intensive Untersuchungen mit verschiedenen Methoden der Elektronenmikroskopie zeigten eine bimodale Mikrostruktur, bestehend sowohl aus kleinen, verformungsinduzierten Kristalliten (Korngrösse unter 0.3µm), als auch aus rekristallisierten, wesentlich größeren Kristalliten (Korngröße über 5 µm). Analog zu den Texturuntersuchungen nahm der Anteil an erholten bzw. rekristallisierten Kristalliten mit zunehmendem hydrostatischem Druck bzw. zunehmender Auslagerungszeit bei Raumtemperatur zu.

Table of Contents

1 Introduction

1.1 Magnesium

Magnesium constitutes approximately 2% of total mass of the Earth's crust. It is number 6 on the list of the most abundant elements. With its density of 1.738 $kg \cdot m^{-3}$ (at a room temperature), which decreases to 1.584 $kg \cdot m^{-3}$ at the melting temperature of 650°C, being strongly influenced by the impurity level. Magnesium is a promising and reliable material for engineering applications which has been gaining more and more importance continuously in the last 80 years [1, 2]. An attractive combination of strength to weight ratio, ease of formability and alloying properties [3] place magnesium in the top of the list of the most promising engineering metallic materials, especially in the times when a tendency of saving energy drags more and more importance on the weight reduction of construction materials [4, 5].

What makes magnesium particularly interesting from the point of view of both the application and scientific reasons is its crystallographic structure. Mg crystallizes at 650°C into a hexagonal close packed (hcp) structure (with space group P63/mmc, space group number: 194) [6, 7].

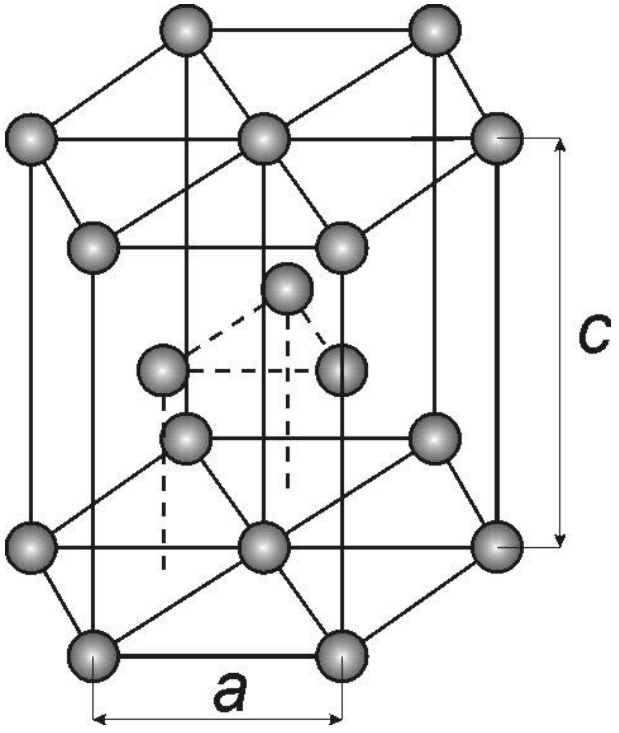

Fig. 1-1. Hexagonal close packed (hcp) structure of Mg. A single unit cell of hcp lattice consists of one third of the structure shown in the graph.

From the point of view of its application, Mg has proven to be an unique and promising material, mainly thanks to its light weight [6], whereas from the scientific point of view, deformation of Mg and its alloys makes this metal a very interesting research object, mainly because of its low-symmetry crystal structure (see section 1.2) [8, 9].

For the hexagonal close packed crystal (hcp) lattice there are three main slip systems available: basal, prismatic and pyramidal ones. Each of them consists of few sub-slip-systems with different dislocations with different Burgers vectors, as shown in Tab. 1-1 [10]. Depending mainly on the c/a ratio of the hexagonal structure, the critical resolved shear stresses (CRSS) are indicating which of them are activated during plastic deformation.

Edge dislocations

Major slip system	Burgers vector	Slip plane	Burgers vector types
Basal	$\langle 2\bar{1}\bar{1}0\rangle$	$\{0001\}$	*a*
Prismatic	$\langle \bar{2}110\rangle$	$\{01\bar{1}0\}$	*a*
	$\langle 0001\rangle$	$\{01\bar{1}0\}$	*c*
	$\langle \bar{2}113\rangle$	$\{01\bar{1}0\}$	*c+a*
Pyramidal	$\langle \bar{1}2\bar{1}0\rangle$	$\{10\bar{1}1\}$	*a*
	$\langle \bar{2}113\rangle$	$\{2\bar{1}\bar{1}2\}$	*c+a*
	$\langle \bar{2}113\rangle$	$\{11\bar{2}1\}$	*c+a*
	$\langle \bar{2}113\rangle$	$\{10\bar{1}1\}$	*c+a*

Screw dislocations

	Burgers vector	Burger vector types
	$\langle 2\bar{1}\bar{1}0\rangle$	*a*
	$\langle \bar{2}113\rangle$	*c+a*
	$\langle 0001\rangle$	*c*

Tab. 1-1. The most common slip systems with their Burgers vectors available for the hexagonal close packet (hcp) crystal lattice [11, 12].

1.2 Mg deformation

Magnesium is a hexagonal close packed metal with its $^{c}/_{a}$ ratio value closest to the theoretical value of 1.633 among all the other hcp metals. The exact theoretical value is: $\sqrt{\frac{8}{3}}$ which is to be achieved if the atoms were perfectly hard spheres. The real $^{c}/_{a}$ ratio for Magnesium amounts exactly 1.6236 [1, 6].

Magnesium's primary deformation system is constituted by a basal slip system on the planes of $\{0001\}$ family in directions $\langle 11\bar{2}0\rangle$ (along the *a* axis of the hcp lattice). The secondary slip system is the prismatic one, with slip planes of $\{10\bar{1}0\}$ family and the same $\langle 11\bar{2}0\rangle$ directions. Additional slip systems to be used are the $\{10\bar{1}1\}\langle 11\bar{2}0\rangle$ first order pyramidal slip system with an *a*-axis slip direction, a $\{10\bar{1}1\}\langle \bar{1}\bar{1}23\rangle$ first order pyramidal plane slip system with a *(c+a)* slip direction, and a $\{11\bar{2}3\}\langle \bar{1}\bar{1}23\rangle$ second order pyramidal slip system with a *(c+a)* slip direction. According to Critical Resolved Shear Stress (CRSS) values as given in Tab. 1-2: **(FPAS)**, **(FPCS)** and **(SPCS)** stand for ***First-order pyramidal*** *slip system with* ***a*** *Burgers vector*, ***First-order pyramidal*** *slip system with* ***c*** *Burgers vector* and for ***Second-order pyramidal*** *slip system with* ***(c+a)*** *Burgers vector*, respectively [13]. It is important to note that CRSS value for the secondary, prismatic slip system is approximately 80-times larger than for the primary system (basal slip). Such a significant difference, in the range of 2 orders of magnitude limits the plastic deformation of magnesium (especially at low temperatures) [13-17].

Slip system	Critical Resolved Shear Stress (CRSS) [MPa]
$\{0001\}\langle 11\bar{2}0\rangle$ basal	≈0.5
$\{10\bar{1}0\}\langle 11\bar{2}0\rangle$ prismatic	≈40
$\{10\bar{1}1\}\langle 11\bar{2}0\rangle$ (FPAS)	
$\{10\bar{1}1\}\langle \bar{1}\bar{1}23\rangle$ (FPCS)	≈50
$\{11\bar{2}3\}\langle \bar{1}\bar{1}23\rangle$ (SPCS)	≈40

Tab. 1-2. Slip systems and their Critical Resolved Shear Stress (CRSS) values for Mg [13, 18-21].

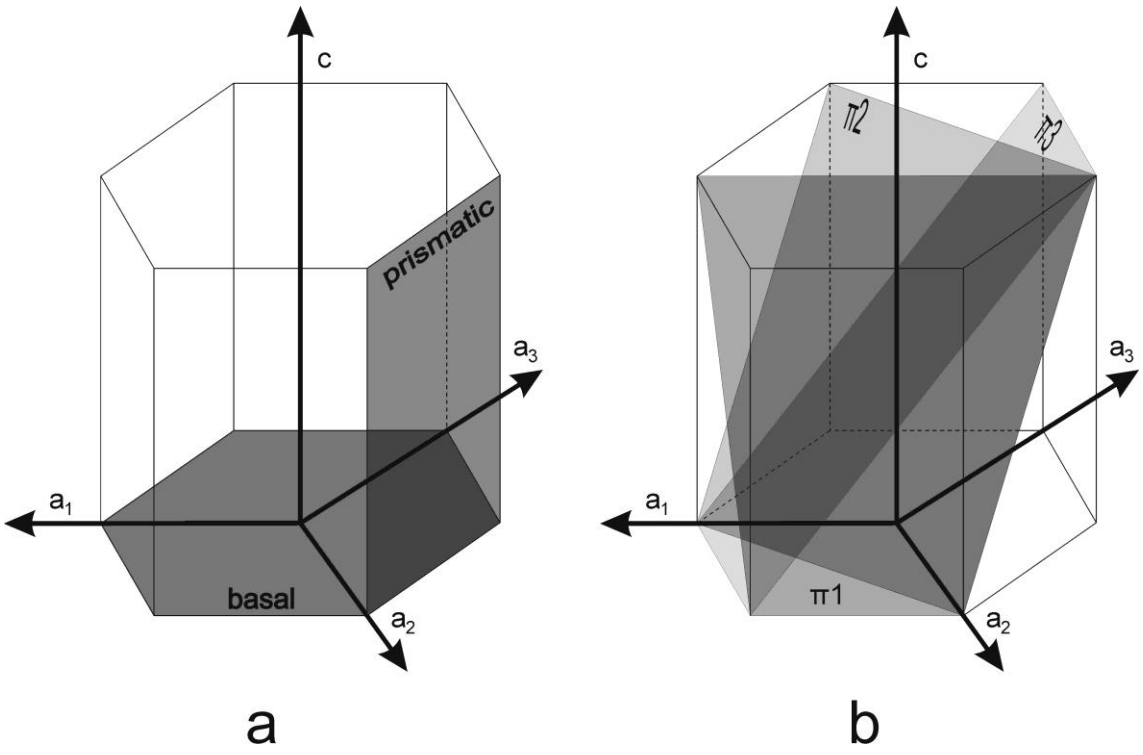

Fig. 1-2. Primary (a) and secondary (b) slip systems in Mg.

As shown in Tab. 1-2, there is a distinct difference in CRSS between the primary and secondary slip system, in the range of one order of magnitude. Together with low symmetry of the hexagonal close packed lattice, these are the main reasons of a non-uniform, inhomogeneous deformation of magnesium.

Type	Number of slip systems	Plane	Slip direction
basal $\langle a \rangle$	3	$\{0001\}$	$\langle 11\bar{2}0 \rangle$
prismatic $\langle a \rangle$	3	$\{\bar{1}100\}$	$\langle 11\bar{2}0 \rangle$
pyramidal $\langle a + c \rangle$ $(\pi 2)$	6	$\{11\bar{2}2\}$	$\langle 11\bar{2}3 \rangle$
tensile twin $(\pi 3)$	6	$\{10\bar{1}2\}$	$\langle 10\bar{1}1 \rangle$

Tab. 1-3. Deformation modes available in Mg [22, 23].

A number of slip and twinning systems is limited as shown in Tab. 1-3, mainly because of anisotropic structural symmetry of hcp lattice. A minimum of five independent slip systems are

required for an arbitrary shape change [24], but at the room temperature there are only four of them provided by the known slip systems. In each case, activation of the basal slip system does not allow a strain along the *c*-axis. With increasing temperature, more slip occurs in the $\{10\bar{1}1\}$ pyramidal planes but without a change in the direction [20, 25, 26]. Therefore twinning is an additional important deformation mode, which allows an arbitrary shape change by completing the required deformation modes. For the room temperature deformation of pure Mg, the CRSS values for $\{10\bar{1}1\}\langle 10\bar{1}\bar{2}\rangle$ depend on the compression and expansion directions and reach values in the range of ~76 to ~154 MPa [25, 27, 28].

As shown in Fig. 1-3, depending on the *c/a* ratio which characterizes the given hcp structure, a twinning shear has different values. The fact that *c/a* ratio strongly affects the possible slip modes by its CRSS values can be seen in Fig. 1-3 [29].

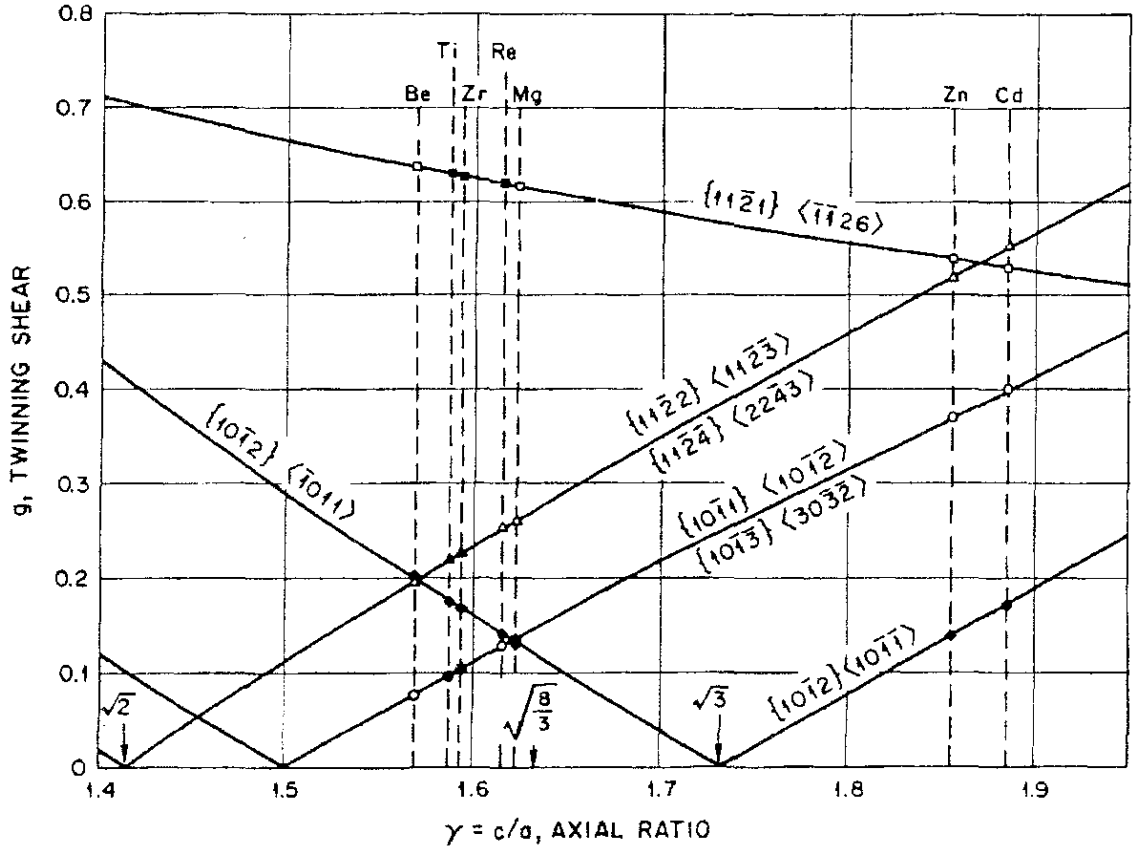

Fig. 1-3. Twinning shear of particular twinning systems with respect to the c/a ratio of the hcp crystal lattice [29].

According to Fig. 1-3, for Mg, three twinning modes: $\{10\bar{1}2\}\langle\bar{1}011\rangle$, $\{10\bar{1}1\}\langle10\bar{1}\bar{2}\rangle$ and $\{10\bar{1}\bar{3}\}\langle30\bar{3}\bar{2}\rangle$ are the most preferred ones [29].

An interesting study of twinning in Mg can be found in the work of Wonsiewicz [25], where the mechanism of twinning with following retwinning is described. The twinning on $\{10\bar{1}2\}$ occurs in tension perpendicular, or compression in parallel to the $\{0001\}$ basal plane and reorients the basal plane through 86.3°. Under an opposite system of loading, $\{10\bar{1}1\}$ twins can form, and then retwin on $\{10\bar{1}2\}$. A similar double twinning process on a plane $\{10\bar{1}3\}$ can be observed (see details in Fig. 1-4) [25].

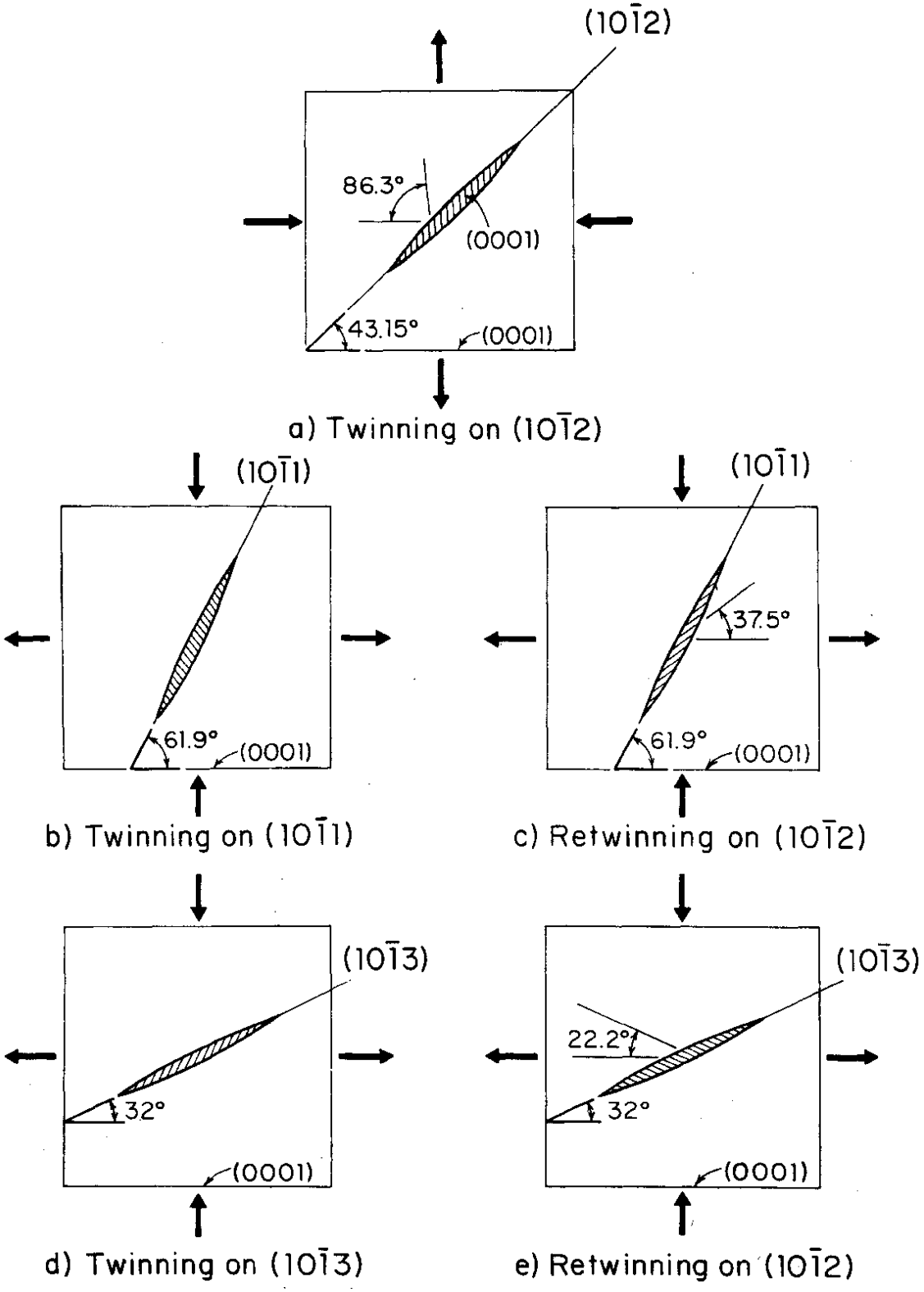

Fig. 1-4. Details of twinning in magnesium [25].

1.3 Severe Plastic Deformation (SPD) methods

During the last years Severe Plastic Deformation (SPD) has gained increasing importance in achieving bulk nanostructured metals and alloys [30, 31], which exhibit not only enhanced strength values [32, 33] but also considerable extents of ductility compared to common nanocrystalline materials [34]. High-Pressure Torsion (HPT) offers a number of advantages on Equal-Channel Angular Pressing (ECAP) and other SPD methods, namely the precise control of important deformation parameters (such as the hydrostatic pressure and the deformation induced strain), the possibility to measure in-situ SPD stress-strain characteristics, and the realization of highest hydrostatic pressures, strains and smallest grain sizes [35-37].

1.3.1 High-Pressure Torsion

The first idea of plastic deformation of metals by torsion and compression were proposed by Bridgman as early as in 1943 [38]. The main and interesting advantage of such a combination of plastic deformations is the fact that during "twisting under compression" a metal rod endures even up to very large strains [38]. The general idea of plastic deformation by torsion under compression proposed by Bridgman (as shown in Fig. 1-5a) was improved by the application of a hydrostatic pressure (induced by specially designed anvils) and is being used at present (see Fig. 1-5c and Fig. 3-4) [39].

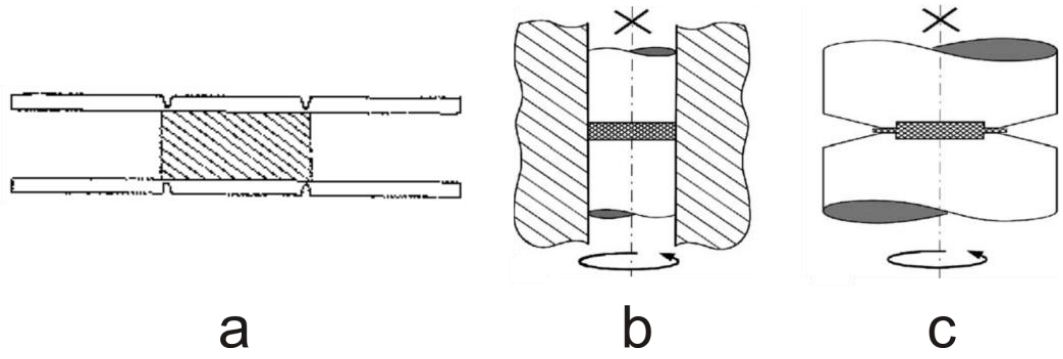

Fig. 1-5. Conception of a deformation by torsion under pressure: (a) first experiment idea proposed by Bridgman [38], (b) idealized and (c) practical setups of today's HPT devices. [40]

The torsional shear strain induced during high-pressure torsion can be calculated according to the formula [39-42]:

$$\gamma = \frac{2\pi r n}{h}$$

Equ. 1-1. Torsional shear strain in HPT deformation.

where: *r* is the radius of the sample (corresponding to the radius for which *γ* is calculated), *n* is the number of rotations applied during the deformation, and the *h* is the sample thickness. Note that in the relevant literature the results are often presented and calculated with *h* relating to the initial sample thickness, but in the presented dissertation *h* is always taken as it is after the deformation process. The main reason for this consideration is the fact that during this specific type of deformation, the sample thickness is reduced. Normally, this thickness reduction happens to be not larger than 17% (as observed during the experiments, see section 3.2). In the presented dissertation wherever the shear strain is considered, it applies to the torsional shear strain, calculated according to the above mentioned formula (Equ. 1-1).

In order to compare the shear strain induced by HPT with strains induced by conventional deformation modes, one should convert torsional shear strain (γ_t) into equivalent strain (ε_{vM}) according to the von Mises criterion [30], as follows:

$$\varepsilon_{vM} = \frac{\gamma_t}{\sqrt{3}}$$

Equ. 1-2. Equivalent von Mises strain in HPT deformation.

The idea of studying the texture changes of materials subjected to torsion, deformed under hydrostatic pressure conditions, was successfully applied to the regular lattice metals, such as Cu, Ni, Al [33, 43-45]. However, for hexagonal lattice metals, HPT literature data is at least poor and limited mainly to Ti [33, 46]. There are only a few works concerning pure Mg microstructure changes after HPT [37, 47], whereas the research devoted to an advanced texture analysis is not available at present in the relevant literature.

1.3.2 Other SPD methods

Severe Plastic Deformation (SPD) methods gained increasing attention in the recent decade mainly due to its ability to produce ultra-fine grained structures, those which have a grain size, of – by definition – less than 100 nm, which exhibit elevated strengths (and other advanced properties) as well [48].

There are a few criteria allowing particular SPD methods to distinguish from each other, as follows [48]:

- continuous SPD without change of strain path (like *High-Pressure Torsion - HPT*),
- accumulating of strain path (*Equal Channel Angular Pressing - ECAP* route A),
- accumulating variation of strain with reversal of strain path (*Cyclic Extrusion Compression - CEC*, *KoBo* extrusion),
- accumulating variation of strain with variable strain path (*Accumulative Roll-Bonding - ARB, ECAP* route *Bc*).

1.3.2.1 Equal Channel Angular Pressing (ECAP)

The general idea of *Equal-Channel Angular Pressing* (ECAP) is to induce plastic deformation by shear by pressing the material through a channel (of squared or round section) which contains two intersecting channels of the same cross section. The main deformation area spreads around the channels' intersection. What makes this method very efficient is the fact that after passing through the channel, the overall shape and dimensions of the specimen remain unchanged, which gives the possibility of repeating the entire procedure, achieving even larger strains.

During ECAP deformation, the entire sample volume undergoes shear deformation in uniform way (of course, except the very edge part of the extruded billet). The equivalent strain can be calculated according to the formula [49]:

$$\varepsilon_N = cosh^{-1}(N \cdot cot\phi)$$

Equ. 1-3. Equivalent strain in ECAP deformation.

where *N* is the number of ECAP passes and ϕ is the channels' intersection angle (refer to Fig. 1-6). For the most common used channels geometry (which is ϕ=90° and ψ=20°) the strain for 1 pass equals $\varepsilon_1 \approx 1$ [30]. To compare with conventional shear strains one should follow the following

formula, including the exact channel intersection and outer curvature angles (as indicated in Fig. 1-6) [50] :

$$\gamma = 2cot\left(\frac{\phi}{2}+\frac{\psi}{2}\right)+\psi cosec\left(\frac{\phi}{2}+\frac{\psi}{2}\right)$$

Equ. 1-4. Shear strain in ECAP deformation.

Further developments of ECAP method led to various strain paths, called routes, as shown in Fig. 1-7.

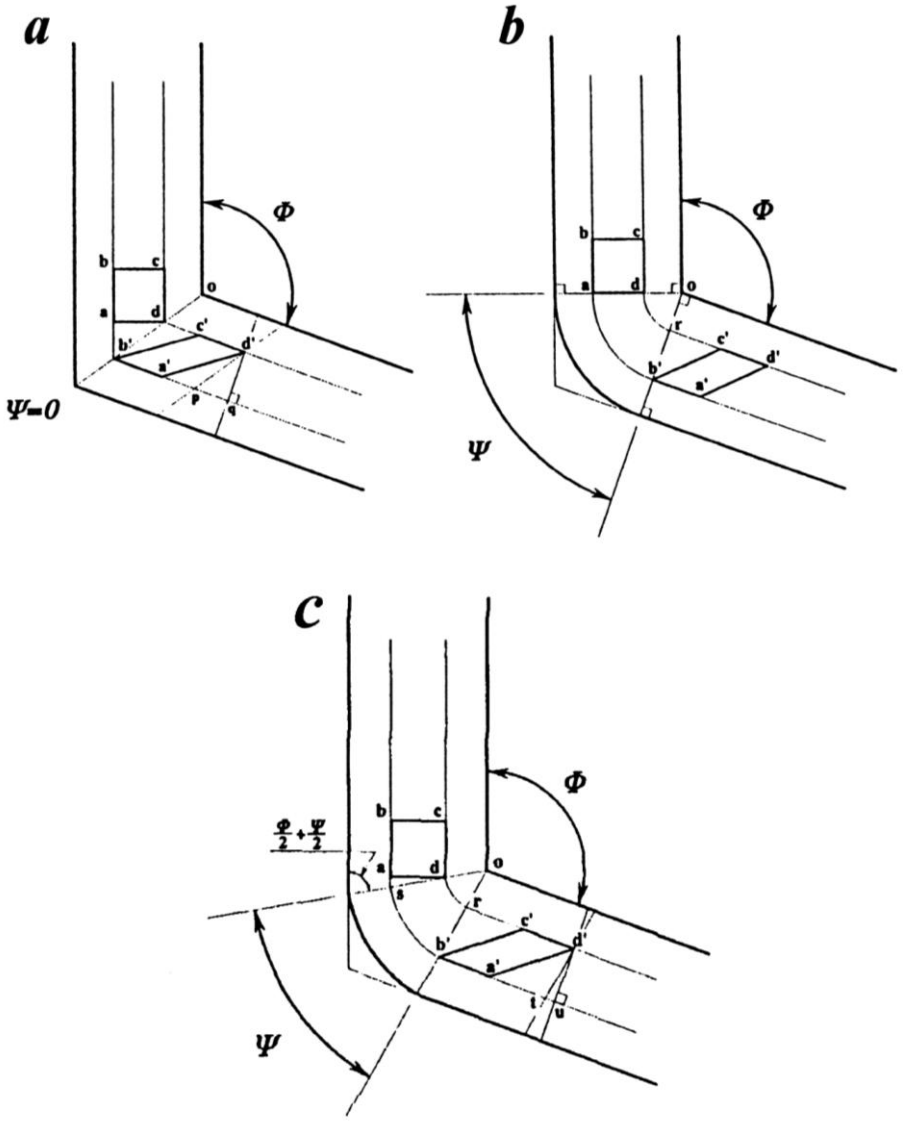

Fig. 1-6. Schematic idea of Equal-Channel Angular Pressing. The intersection of two channels is defined by *φ*, and the outer curvature of the intersection is defined as *ψ*. Three variants of ECAP geometry are shown: (a) *ψ=0°*, (b) *ψ=π-φ* and (c) *ψ* between 0 and *(π-φ)*. [50]

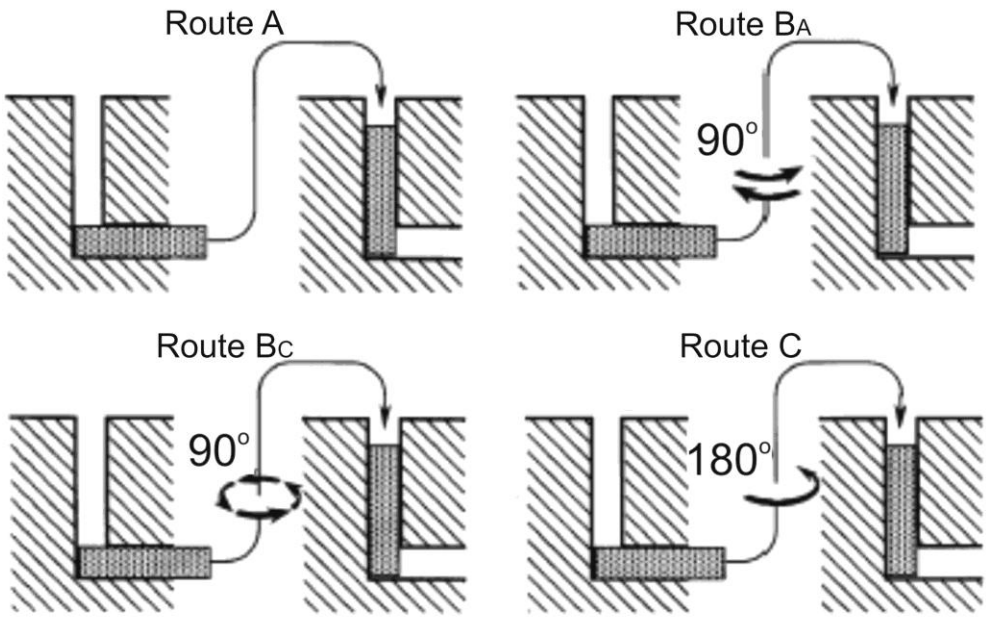

Fig. 1-7. Variants of ECAP deformations, routes A, B_A, B_C and C by different inter-pass billet positioning. [51]

ECAP is so far one of the best studied methods applied to all the conventional metals used in advanced materials engineering, revealing its great capabilities of enhancing strength and ductility for Cu [52, 53], Al [54], Ni [55], Ti [33] and Mg, and its alloys as well [56, 57].

1.3.2.2 Accumulative Roll-Bonding (ARB)

Accumulative Roll-Bonding is another example of an interesting SPD method, developed recently, in which the rolling is to be the main deformation mechanism. Its ability of inducing large plastic strains is reached by a repeatable process of rolling, and folding of the material into two even parts between each rolling pass [58, 59]. The schematic idea of ARB is shown in Fig. 1-8.

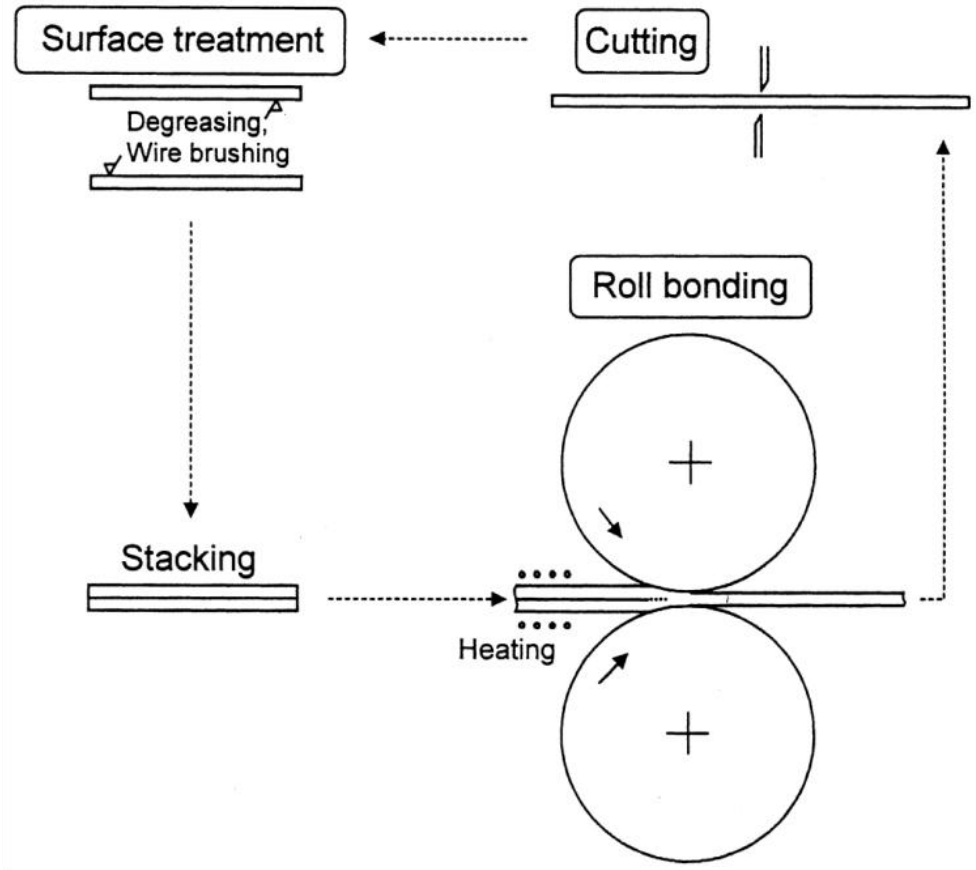

Fig. 1-8. Idea of Accumulative Roll-Bonding (ARB) deformation process [58].

After each rolling-bonding cycle, the processed material's thickness is reduced. As the material is always folded into two parts, the number of layers grows geometrically, with their thickness following the equation:

$$h = \frac{h_0}{2^n}$$

Equ. 1-5. Thickness reduction in ARB deformation method.

where h_0 is the initial material thickness and n is the number of cycles [58].

Taking into consideration the von Mises yield criterion and assuming no lateral spreading of the rolled material, the equivalent plastic strain can be expressed as follows:

$$\varepsilon_{vM} = \left[\frac{2}{\sqrt{3}}\ln\left(\frac{1}{2}\right)\right] \cdot n$$

Equ. 1-6. Equivalent von Mises strain for ARB deformation.

where *n* is the number of passes (see Fig. 1-8), which can be estimated as [58, 59]:

$$\varepsilon_{vM} \approx 0.8 \cdot n$$

Equ. 1-7. The equivalent plastic strain in ARB with respect to the applied number of passes.

.

An important advantage of the ARB method is the fact that it can be combined with other SPD methods, resulting in enormous plastic strains. An example of such a combination can be achieved by ARB processing of Cu and Zr plates to obtain fine Cu-Zr multilayer composition and then deforming it by HPT. As a result of such a plastic processing combination an amorphization of the obtained nanostructure is observed [60].

1.3.2.3 Cyclic Extrusion Compression (CEC)

The Cyclic Extrusion Compression (CEC) method is a combination of extrusion and compression in one, repeatable deformation cycle. An initial sample shape remains unchanged after each pass, which allows arbitrarily large plastic strains to be achieved without changing the processed material outer diameters [61, 62].

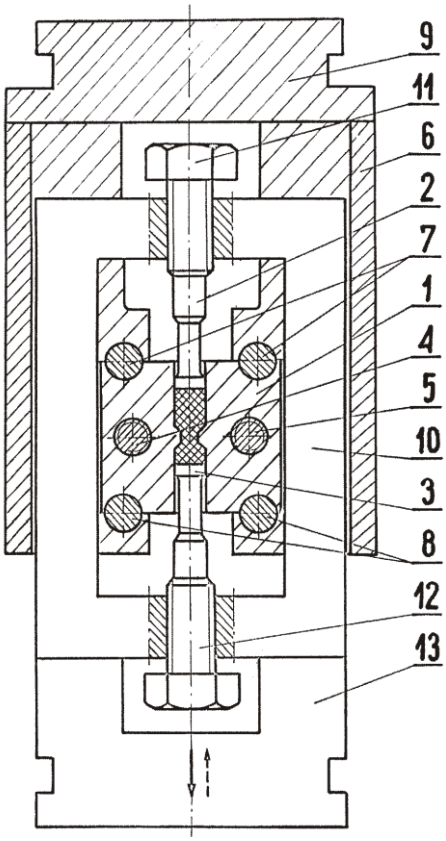

Fig. 1-9. Diagrammed sketch of CEC device. The die (1) is held with the bolts (4,5,7 and 8) to the frame (6). One of the anvils (9) is the stationary one, whereas the second one (13) with yoke (10) is moving up and down. Then two rams (2,3) are compressed by the bolts (11,12) [63].

Repetition of the extrusion compression cycle leads to accumulating true plastic strain which can be expressed as follows:

$$\varepsilon = 4n \ln\left(\frac{d}{d_0}\right)$$

Equ. 1-8. True plastic strain in CEC deformation method.

where *n* is the number of cycles and $\frac{d}{d_0}$ is a die to chamber diameters ratio (as shown in Fig. 1-9) [64].

2 Aim of the doctoral thesis and experimental methods chosen

This dissertation is aimed at characterization of the texture and microstructure changes in 99.85 wt.% purity Mg (see Tab. 3-1) subjected to severe plastic deformation by *High-Pressure Torsion (HPT).*

The primary aim of the dissertation is to determine the texture evolution during and after HPT in single- and polycrystalline magnesium. The secondary task of this PhD project is to evaluate the correlation between the evolved texture with the mechanical properties, as well as the possibility of enhancing pure Mg mechanical properties by application of HPT method. Another interesting task is to determine the texture heritance with respect to the initial texture and/or grain size.

Crystallographic texture evolution is to be studied in both, poly- and single-crystalline materials. The polycrystalline material analysis, by means of the coarse- and fine-grained structure, is aimed at determining the initial grain size and texture influence on the final material (after HPT processing). The task of the single crystalline analysis is to determine, by an experimental method, the precise orientation migration path during HPT deformation. For this purpose a set of four initial orientations has been selected (see section 3.1.1).

A selection of the particular initial single crystal orientation was done according to the expected activation of the deformation modes during HPT deformation process (for further details see section 1.2). The single crystal facility available at the AGH (Cracow, Poland) had to be modified in order to obtain the orientation of the single crystals desired by the investigation plan within this thesis.

The designed deformation process is to be carried out with an HPT facility in a variety of hydrostatic pressures for the polycrystalline material (from 1 to 4 GPa) and for one pressure for single crystalline samples (1.5 GPa). The main investigation method for determining the texture evolution is the advanced crystallographic texture analysis. For mechanical properties of the deformed magnesium, microhardness as well as the tension tests were carried out. In order to complete the analysis, a microstructural observation by means of *Transmission Electron Microscopy (TEM)* and *Scanning Electron Microscopy (SEM)*, especially a latter one in combination with *Electron Back-Scattered Diffraction (EBSD)* techniques, have been planned.

3 Experimental

3.1 Investigated material

The research were aimed at samples from single and polycrystalline magnesium of 99.85 wt.% purity (see Tab. 3-1), subjected to the High-Pressure Torsion deformation. Single crystalline research was carried out with four selected orientations, while polycrystalline material was investigated in the coarse- and fine-grained state (as-cast and hot-extruded material, respectively).

The exact chemical composition of the investigated material is according to Tab. 3-1. Chemical analysis of the investigated material was carried out by atomic absorption spectrometry (AAS Pye-Unicam SP9).

Element	Mn	Si	Fe	Cu	Ni	Mg
Weight [%]	0.095	0.025	0.025	0.0015	<0.001	balance

Tab. 3-1. Investigated material composition in wt [%].

3.1.1 Single crystalline Mg

Single crystals of given purity Mg (Tab. 3-1) were grown in order to obtain samples with selected four initial orientations: $[10\bar{1}1]$, $[11\bar{2}2]$, $[11\bar{2}0]$ and $[0001]$ (see Fig. 4-1),

3.1.1.1 Mg Single crystal growth

In order to obtain single crystal Mg samples suited for HPT of desired crystalline orientations, large single crystals were produced using a modified Bridgman's method. A special zone-furnace was constructed at Department of Metallic Materials and Nanotechnology (at the AGH – University of Science and Technology in Cracow, Poland). With slight overpressure argon atmosphere, ingots shaped out of commercial purity Mg were melted. A special construction of the furnace provided a relatively sharp temperature gradient. A slow and continuous one-way movement (in the range of 0.5 $^{mm}/_{min}$) melted the ingot, until slow directional crystallization was achieved (as shown in Fig. 3-1). For further details see [65].

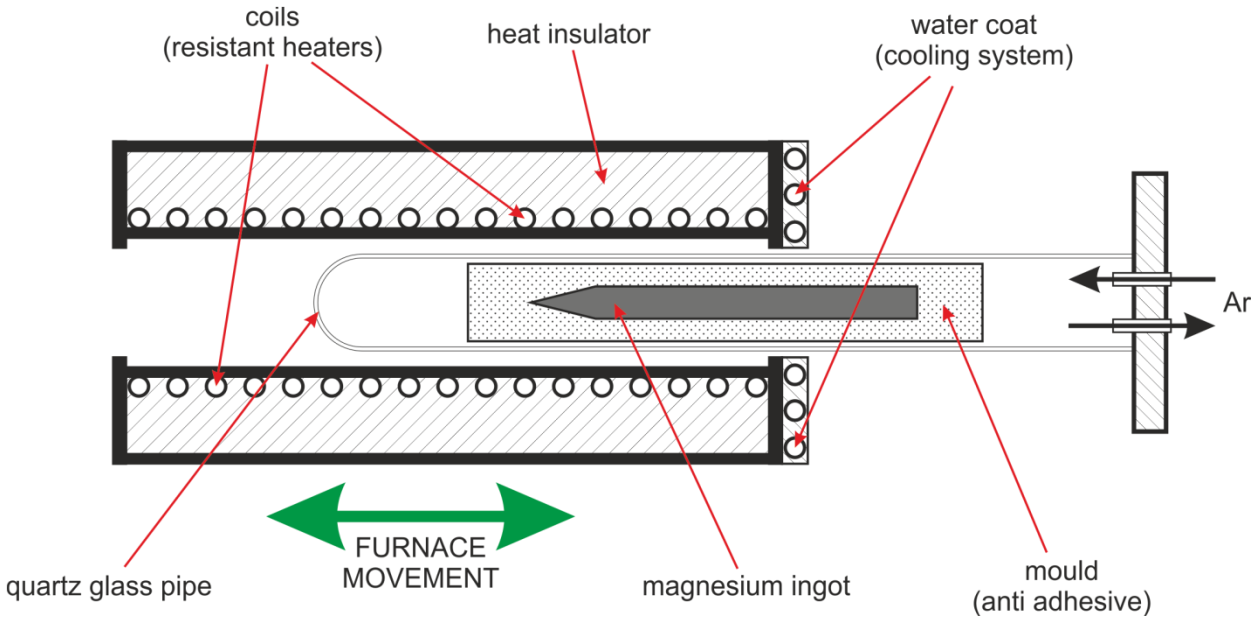

Fig. 3-1. Resistant furnace used to grow magnesium single crystals.

The above mentioned method allowed the production of magnesium single crystals in geometry suitable to cut off samples for HPT experiments of desired four orientations.

Initial orientations of Mg single crystals subjected to HPT deformation were carefully chosen to provide information about general deformation modes expected (see section 1.2). The selected initial single crystal orientations were: two types of pyramidal $[10\bar{1}1]$ and $[11\bar{2}2]$, prismatic $[11\bar{2}0]$ and basal orientations $[0001]$, denoted as 'I', 'II', 'III' and 'IV', respectively (exactly as shown in Fig. 4-1).

3.1.2 Polycrystalline Mg

For the polycrystalline material investigation two kinds of samples were prepared. The first group of samples was prepared from as-cast magnesium with grain size of order of millimeters, as shown in Fig. 3-2. The as-cast Mg samples are considered to be a texture-free material, as the grain size was too large to consider the texture – under acceptable statistic conditions – as well as for the designed HPT experiments (sample size was small with respect to grain size).

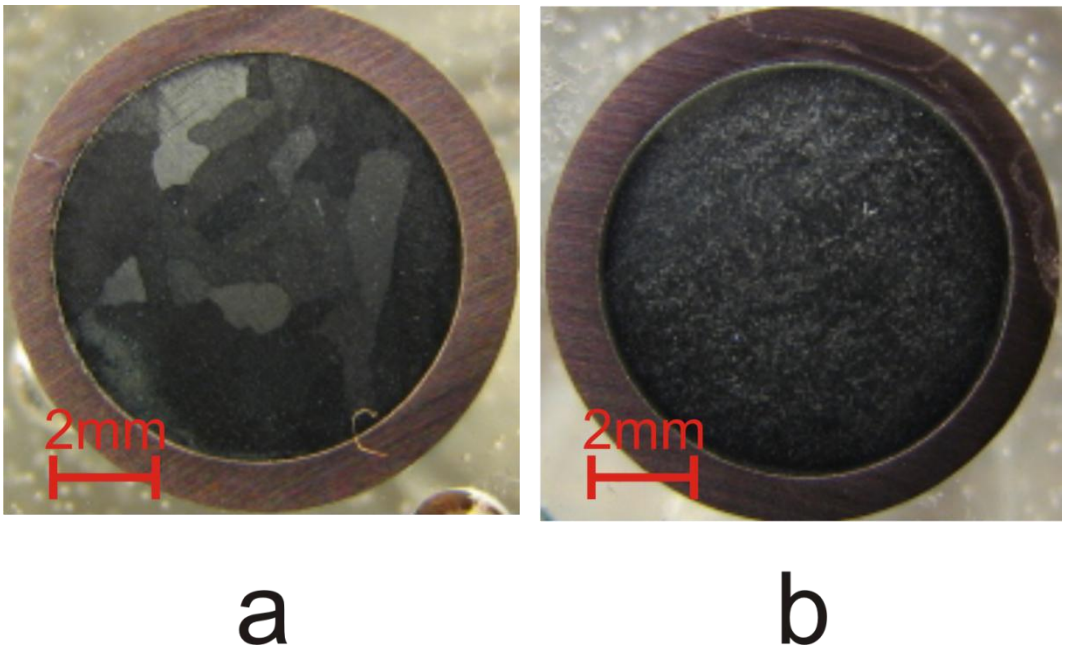

Fig. 3-2. Light microscopy images of the initial material samples prepared for HPT experiments: (a) as-cast Mg and (b) hot-extruded Mg (according to section 3.1). Cu ring attached to each of the samples as shown in Fig. 3-7 (for details refer to section 3.2).

The second sort of samples was prepared by hot-extrusion at 350°C from 30mm diameter ingots into rods of 10 and 14 mm in diameter. Hot-extruded Mg revealed grain size in the range of 10 to 40 µm (see Fig. 3-2) and a sharp, typical extrusion texture (see Fig. 3-3). As mentioned in section 3.2, the strain range available for HPT was limited. Therefore to achieve higher strains of Mg, samples were placed inside Cu ring, which effectively ensured stable deformation up to the desired strains. In order to prepare samples suitable for HPT equipment, disc samples were cut using an electro spark erosion cutter into discs of 10 mm in diameter and 1 mm in thickness, and 14 mm in diameter and 2 mm in thickness, respectively, to the designed HPT experiments.

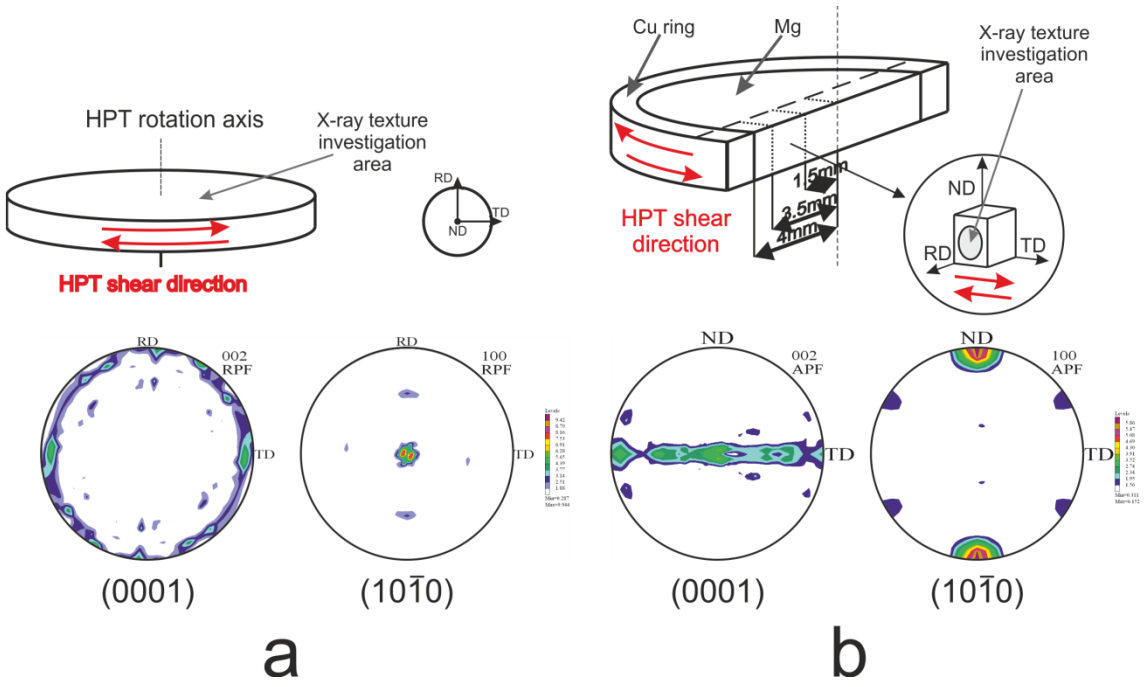

Fig. 3-3. The initial textures of investigated polycrystalline Mg as seen in two reference systems: (a) surface and (b) radial, as shown on basal (0001) and prismatic $(10\bar{1}0)$ pole figures.

3.1.2.1 'Frozen' and 'Recrystallized' material

As the preliminary texture analysis revealed that strong recovery/recrystallization affects the sample after the HPT processing (during storing of deformed material at room temperature) [65], a special experiment was designed to estimate the specific fractions of dynamic and static recovery on HPT deformed polycrystalline Mg. The ***dynamic*** recovery/recrystallization (called ***DRX***) includes all the relaxation, grain growth, recovery and recrystallization processes which take place *during* the deformation (in this case – the HPT experiment), whereas the ***static*** recovery/recrystallization ***(SRX)*** denotes all the changes of microstructure and mechanical properties changes which occur in the deformed material *after* the deformation, in this case during storage of the HPT samples at room temperature (natural ageing). The main idea was to compare the HPT-deformed samples, strongly affected by static recovery (by storing them at RT), with other, being less affected by static recovery. The differences between the two sample sorts were that the recrystallized material (stored at RT, called 'RX') is affected by both, the dynamic (DRX) and static recovery/recrystallization (SRX), while other set of samples was - immediately after deformation - placed in liquid nitrogen – this sample set

is called the ‘frozen’ one (F). The sample was then carefully handled in order to perform the same test as for the RX material to have a good comparison opportunity and determine DRX and SRX activity. By comparing the initial textures (Fig. 3-3) and textures of HPT-deformed material (Fig. 4-17 - Fig. 4-24) one can notice that pole figures show a drastic and complete reconstruction of the texture.

3.2 High-Pressure Torsion (HPT)

The High-Pressure Torsion (HPT) experiments were carried out at the Erich Schmid Institute (ESI) in Leoben, Austria. This particular HPT facility provides the rare opportunity of in-situ deformation torque recording [39]. This enables the shear stress – shear strain in-situ characteristics calculations in order to estimate the stress and material behavior during the HPT deformation, which can be especially interesting at a selected single crystal orientation subjected to the deformation. It is to be noted, that in-situ measurements of the deformation torque used during HPT processing is used to recalculate the *nominal* shear stresses of HPT deformation.

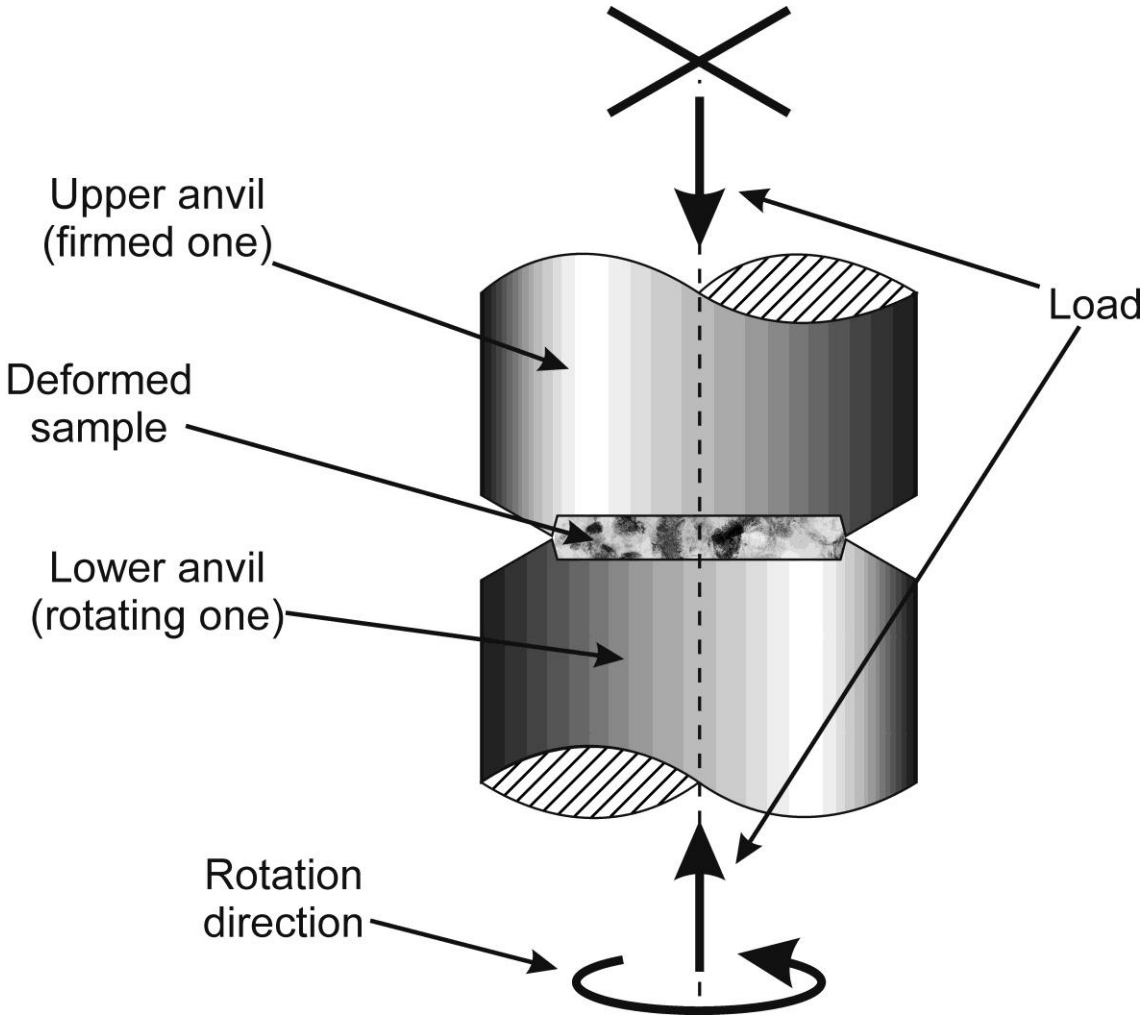

Fig. 3-4. The experimental setup of High-Pressure Torsion (HPT) deformation device used. The deformation is being realized by shear induced by two rotating in opposite directions plungers, inducing high hydrostatic pressure on the sample at the same time.

The maximum load exerted on the sample by the hydraulic press at this facility amounts to 400 kN. As the hydrostatic pressure depends directly on the diameter of the sample according to the dependence $P = \frac{L}{A}$ (*P* – pressure, *L* – load, *A* – sample surface area), the maximum HPT hydrostatic pressure can be achieved by decrease of the sample diameter applied. For the samples with 10 mm diameters hydrostatic pressures of 2 and 4 GPa were applied, whereas samples with 14 mm diameters were processed at 1 GPa of hydrostatic pressure. All single crystalline samples were deformed at the same hydrostatic pressure value of 1.5 GPa, which provided optimum conditions for a stable deformation process of the single crystals up to relatively low strains of *γ≤20* (as compared to the polycrystalline samples).

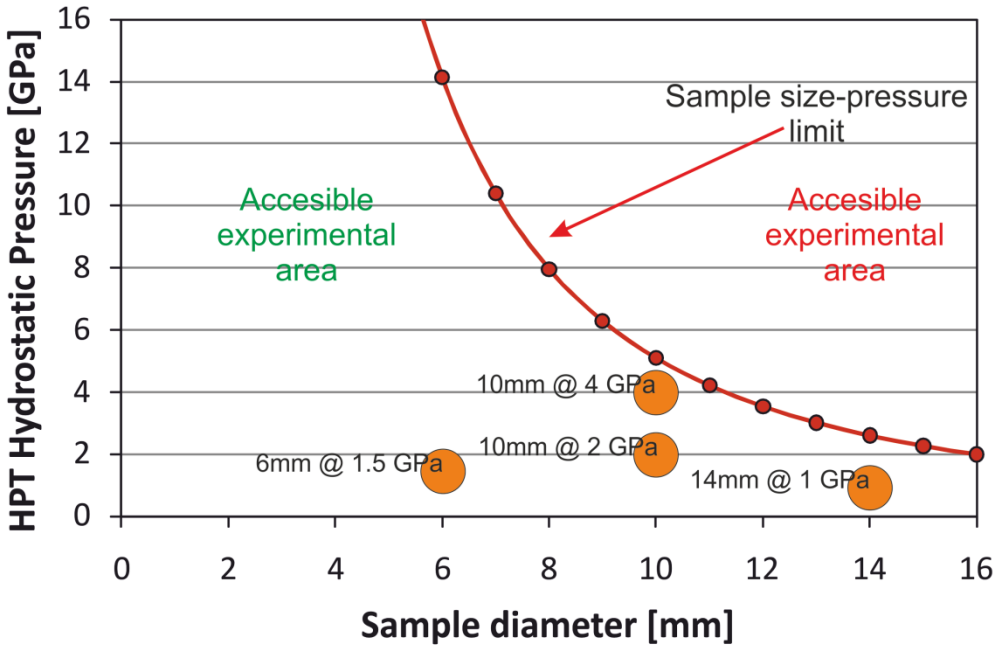

Fig. 3-5. Experimental limits of HPT facility at ESI Leoben (Austria). Maximum available load is 400 kN (red line).

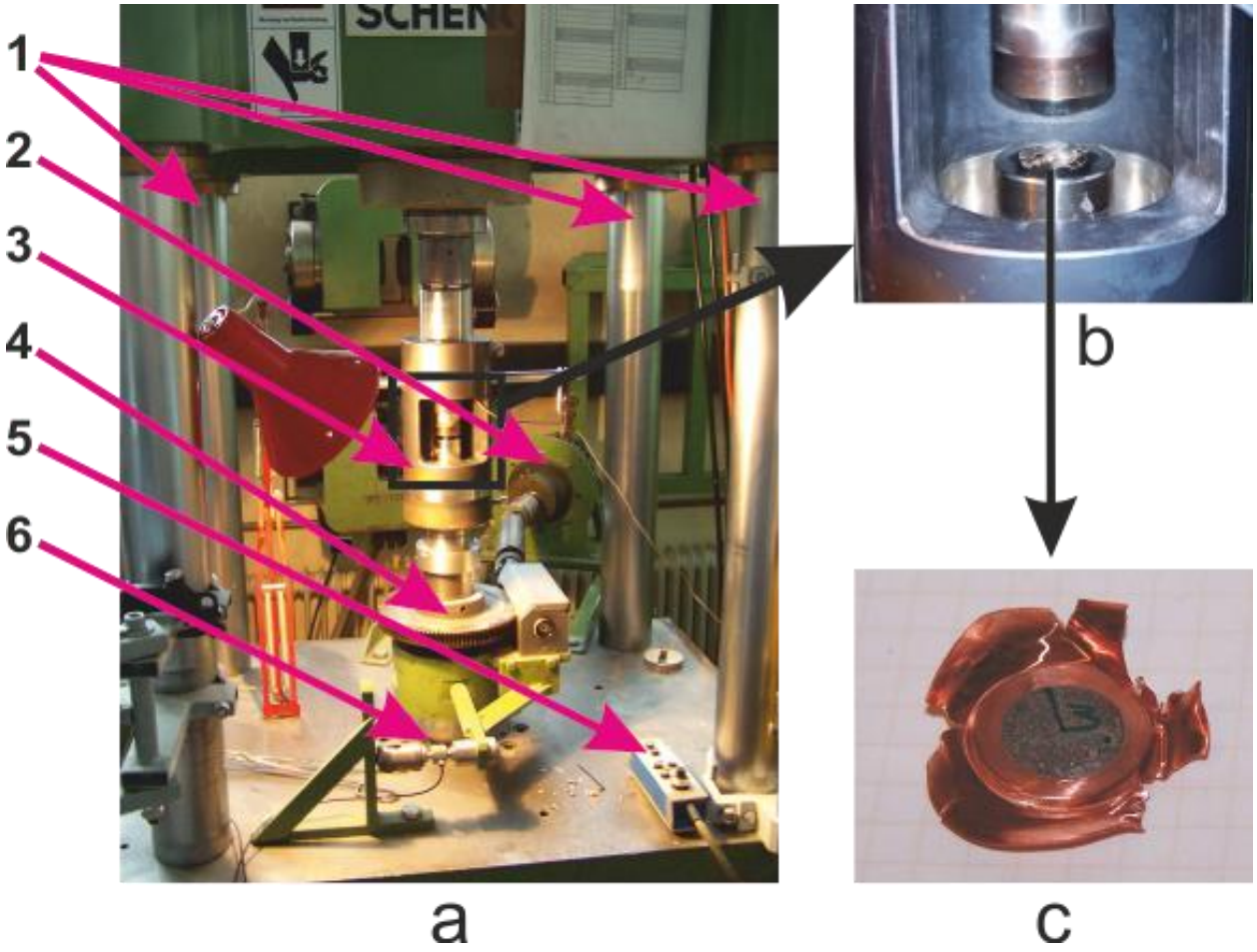

Fig. 3-6. The High-Pressure Torsion experimental facility at ESI Leoben (Austria). General HPT equipment with press and drive (a), sample chamber (b) and sample after the deformation (c). Meaning of numbers in Fig. 3-6 (a): 1 - hydraulic press pistons/rails, 2 – electric engine for torsion generation, 3 – sample chamber, 4 – drive gear wheel, 5 – coarse press control panel, 6 – torque sensor.

The first experiments with HPT of magnesium revealed problems with the process stability at high strain deformation. A non-uniform flowing out of the material, caused unstable deformation, affecting not only the deformation process but also in-situ force monitored during HPT (as shown in Fig. 3-7, further details in [65]). Being a relatively soft material, Mg exhibits a tendency for unstable (not uniform) material flow across the plungers during the deformation process. As shown in Fig. 3-7, the deformation of bare Mg sample was difficult, unstable due to relatively high softness of pure Mg, which revealed a tendency to flow off the plungers in a non-homogenous way. After such an unstable deformation, bare Mg samples tended to reveal some internal cracks being healed at the same time due to the presence of high hydrostatic pressure, as it can be seen on the sample side

(see Fig. 3-7, lower right). As in usual case, the HPT deformation works in a homogenous way all around the sample in a non-excessive way – as it can be seen at the sample in Fig. 3-8, on the right hand side. Moreover, an excessive flow of the material caused the plungers to touch each other, which can be destructive for the HPT facility and strongly disturbs the deformation process (see the end of the red curve in Fig. 3-7), which prohibits deformation of pure Mg up to higher, desired strains. Application of a copper ring, attached to the Mg sample, brought a solution which allowed performing deformation up to the expected high strains [65]. As the main purpose of the designed experiment was to prepare Mg samples by HPT deformation and not only the deformation process itself, the use of Cu-ring was acceptable. It is to be noted that the application of Cu-ring 'reinforces' the sample and significantly increases the shear stress during HPT deformation (as one can observe the increase of in-situ nominal shear stress level of Mg with Cu ring sample in Fig. 3-7). This decreases the significance and value of the in-situ recorded deformation curves, yet a comparison among the deformed samples can be still made as the Cu ring increases the stress level by the same value every time.

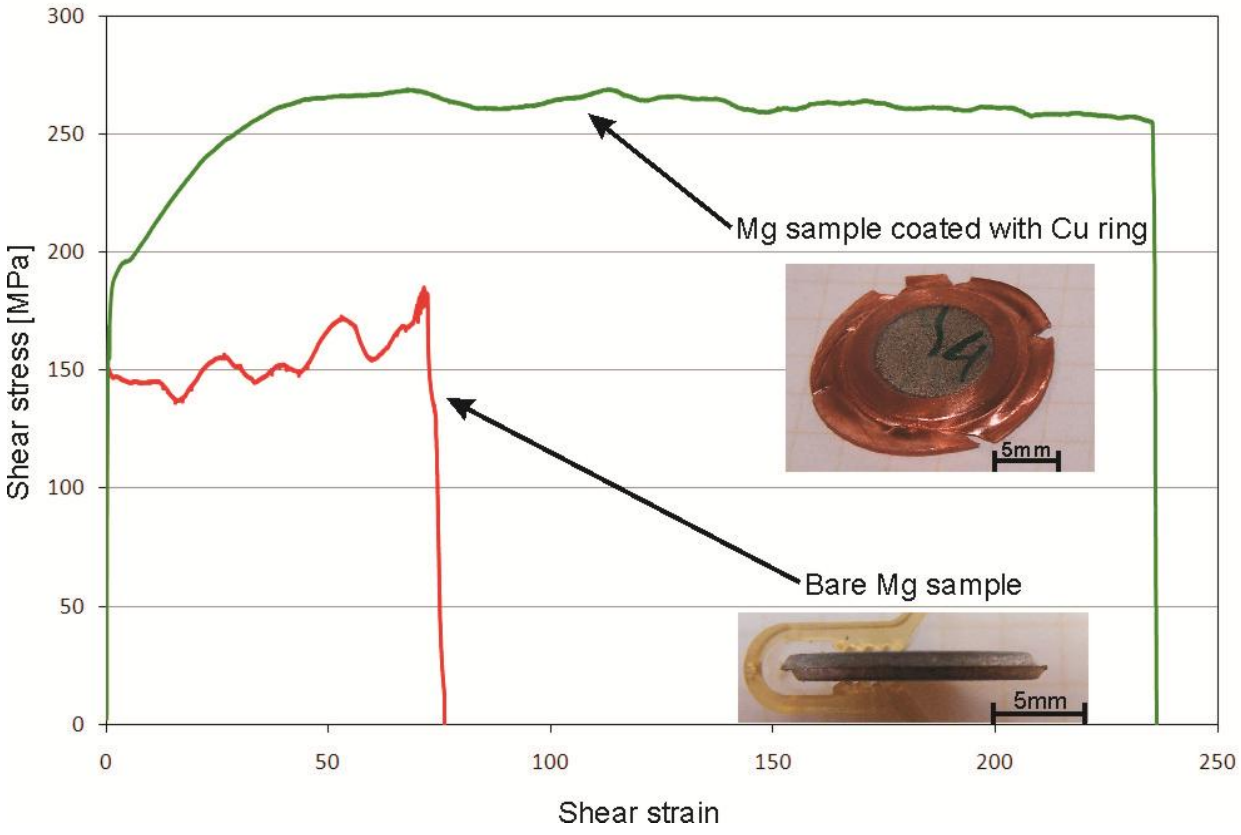

Fig. 3-7. HPT In-situ recorded stress-strain characteristics of sample deformation without (bare Mg sample, red) and with the Cu ring attached (green). Both samples have an overall diameter of 14 mm.

HPT experiments were planned for commercial purity Mg (99.85 wt %) of two different states of material. The first one was as-cast Mg, which revealed a grain size of order of millimeters, whereas the second part was Mg hot-extruded at 350°C with the grain size in the range of 20 to 40 μm.

Fig. 3-8. Magnesium samples with Cu ring attached prepared for HPT experiments (on the left hand), and the same sample after HPT deformation at the right hand (mark on the sample attached for verification of the number of rotations applied).

3.3 X-ray crystallographic texture

For the texture experiments two surfaces of sample cross-sections were considered. Single crystal samples were investigated in order to estimate an overall migration of sample orientation, and for this purpose no special cross section was selected. Polycrystalline material samples were investigated at the 'radial' cross section whereas single crystal sample experiments were carried out at normal to HPT axis sample surfaces, according to Fig. 3-9. For the normal surface reference setup (Fig. 3-9 a) ND, RD and TD refer to the normal (along HPT axis), radial and conventionally-considered transverse directions, respectively. In this setup TD is equal to the radial direction, though in another direction than RD. However, for the 'radial' cross sections (Fig. 3-9 b) ND, RD and TD refer to the normal (again, along the HPT rotation axis), radial and tangential directions, respectively. For the extended reference system, the definition used refers to Fig. 3-9.

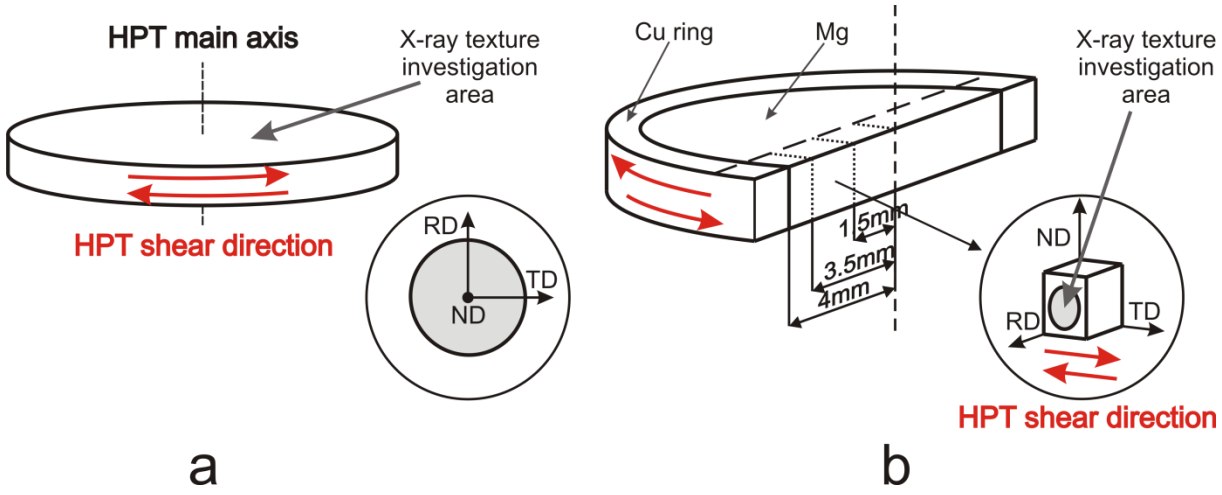

Fig. 3-9. Preparation of the single (a) and polycrystalline (b) samples for the texture investigation with pole figure reference axis given for both sample setups.

In order to obtain good-quality texture results, selected sample surfaces were mechanically ground and finally polished on water papers up to grade of 2000. Then the sample surfaces were rinsed in ethanol and dried with pressured air.

The texture investigations were carried out with a D-8 Discovery X-Ray system from Bruker/AXS supplied with a GADDS *(General Area Diffraction Detection System)* area detector. The X-ray radiation was generated at 40 kV and 40 mA with a copper anode operating with a wave length of λ = 1.540598 Å for Cu$K\alpha_1$. The beam was collimated to a spot size of 300 µm in order to provide measuring textures from sample areas where the shear keeps the same direction. X-ray texture measurements were performed by the reflection method basing on four reflections (see Tab. 3-2) used for the Orientation Distribution Function (*ODF*) calculation. The ODF was calculated by the Arbitrary Defined Cells (ADC) method [66] with LaboTex 3.0 [67] texture analysis software.

Reflection	2Theta (2θ) [°]
$\{10\bar{1}0\}$	32.189
$\{0002\}$	34.395
$\{10\bar{1}1\}$	36.622
$\{10\bar{1}2\}$	47.820

Tab. 3-2. Bragg's reflections and related pole figures of Mg lattice planes used for calculation of texture functions. 2-Theta positions are corresponding to the CuKα_1 radiation used.

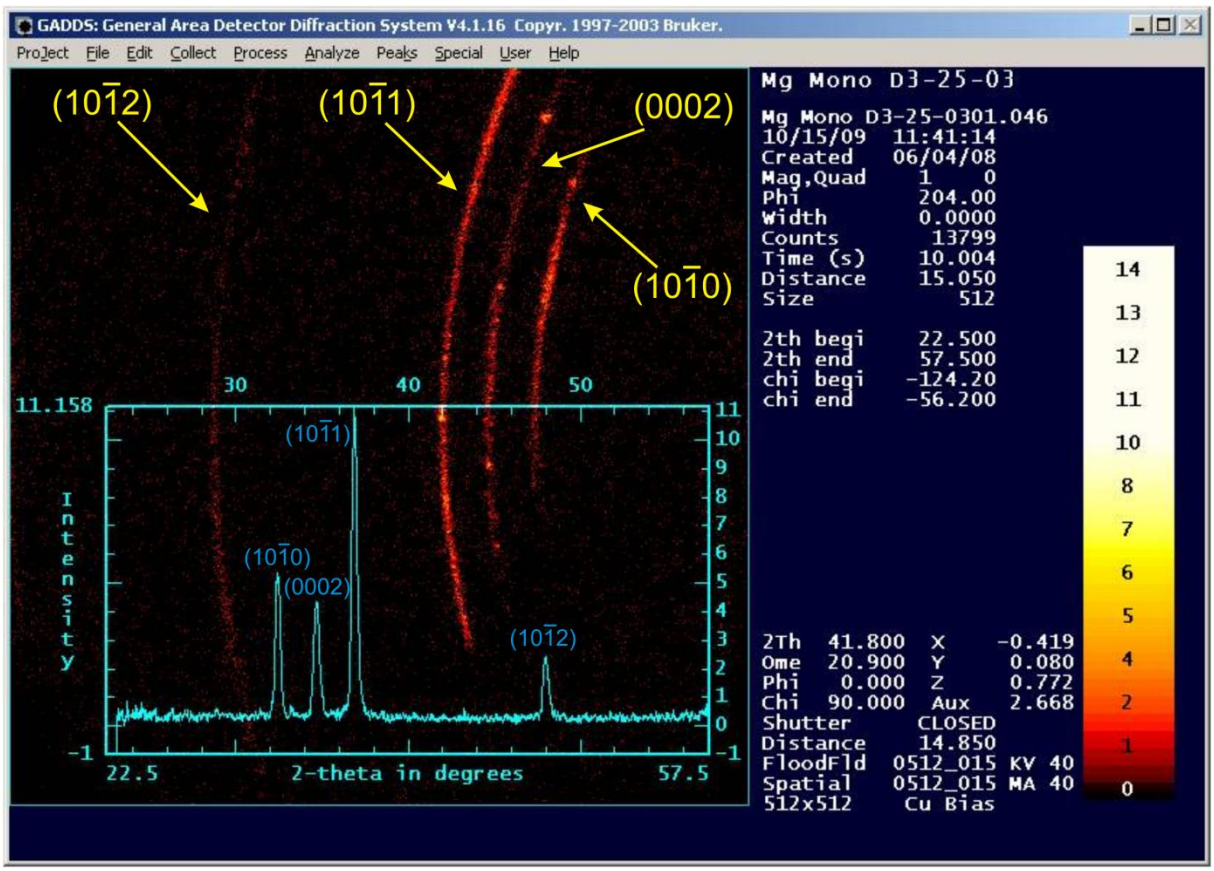

Fig. 3-10. The main user interface of GADDS (General Area Detector Diffraction System) control program. On the main area (left) reflection can be seen (as appeared in the form of red rings) and Chi-angle integrated image of registered frame (note that on the main detection area, 2-Theta angles are in order from right to left, whereas the integrated chart represents the regular, left-to-right order).

The GADDS area detector which was used in the experiments can cover up to approximately 35° of 2-Thetra range at one fixed position (refer to Fig. 3-10). As for the four main reflections in magnesium (listed in Tab. 3-2) all of them can be registered within the same detector position, which significantly shortens the measurement time as compared to an equipment supplied with a point detector (from approximately 5 hours with a point detector, down to 35 minutes with GADDS system). As it can be seen in Fig. 3-10, a single reflection appears as a ring on the main program work area, and at one time several reflections can be recorded within one frame. Therefore, special software has to be used in order to 'merge' the recorded pattern into one coherent image of counts. This task is to be accomplished with the MultexArea software (by Bruker/AXS).

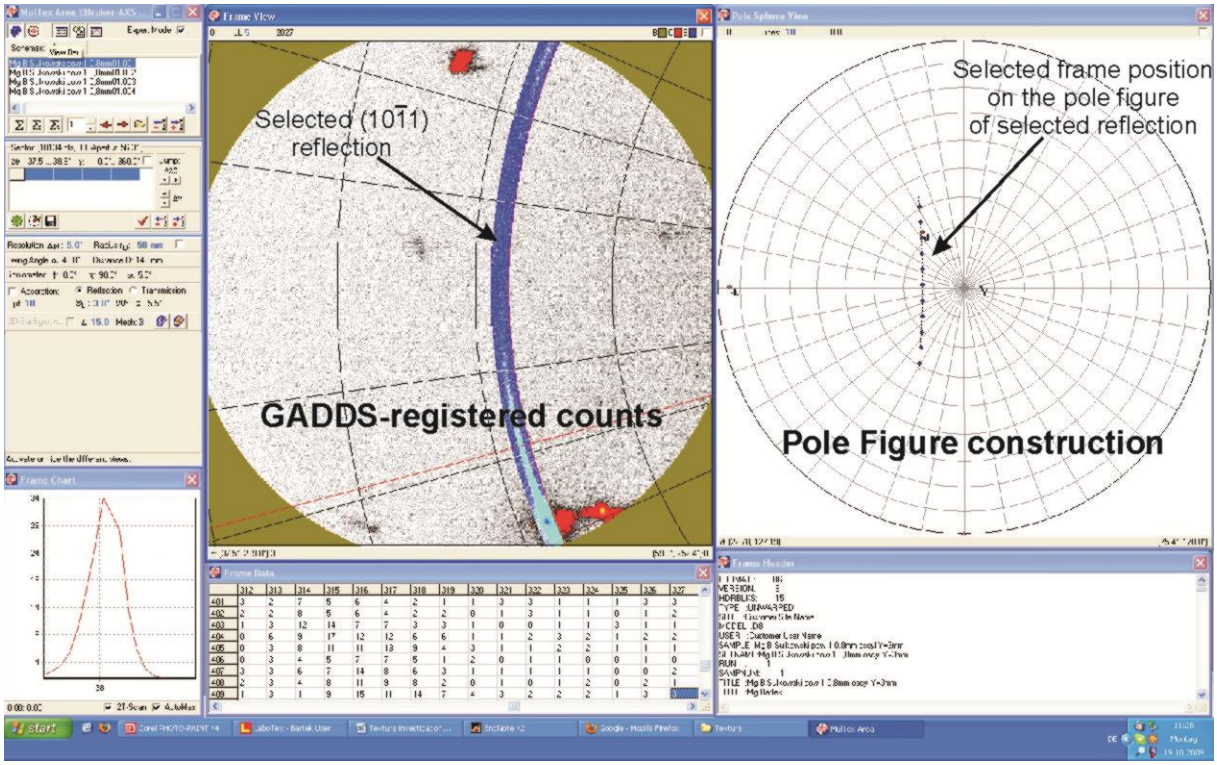

Fig. 3-11. The main user interface of MultexArea software. Reflection $(10\bar{1}1)$ selected (center, upper) in order to evaluate $(10\bar{1}1)$-type pole figure (right, upper).

As shown in Fig. 3-11, MultexArea software allows selecting a single, desired reflection peak and extracting it from the detector frames, one by one, in order to construct a coherent, measured pole figure (of this one, specific reflection). This data is next to be processed by LaboTex 3.0 software [67] for a more advanced texture analysis.

As shown in Fig. 3-12, full recalculated pole figures (RPF) are presented which are recalculated from the *Orientation Distribution Function (ODF).* ODF is calculated by the iteration-based method [68] basing on the measured parts of pole figures. In order to enhance the component analysis, ODF symmetrization from triclinic to monoclinic was applied. By knowing ODF, full recalculated pole figures, additional pole figures (APF) (especially those, which were not measured) and inverted pole figures (IPF) of desired direction can be displayed and analyzed. The ODF itself can provide valuable information concerning dominant components, their position, volume fractions and overall texture "sharpness".

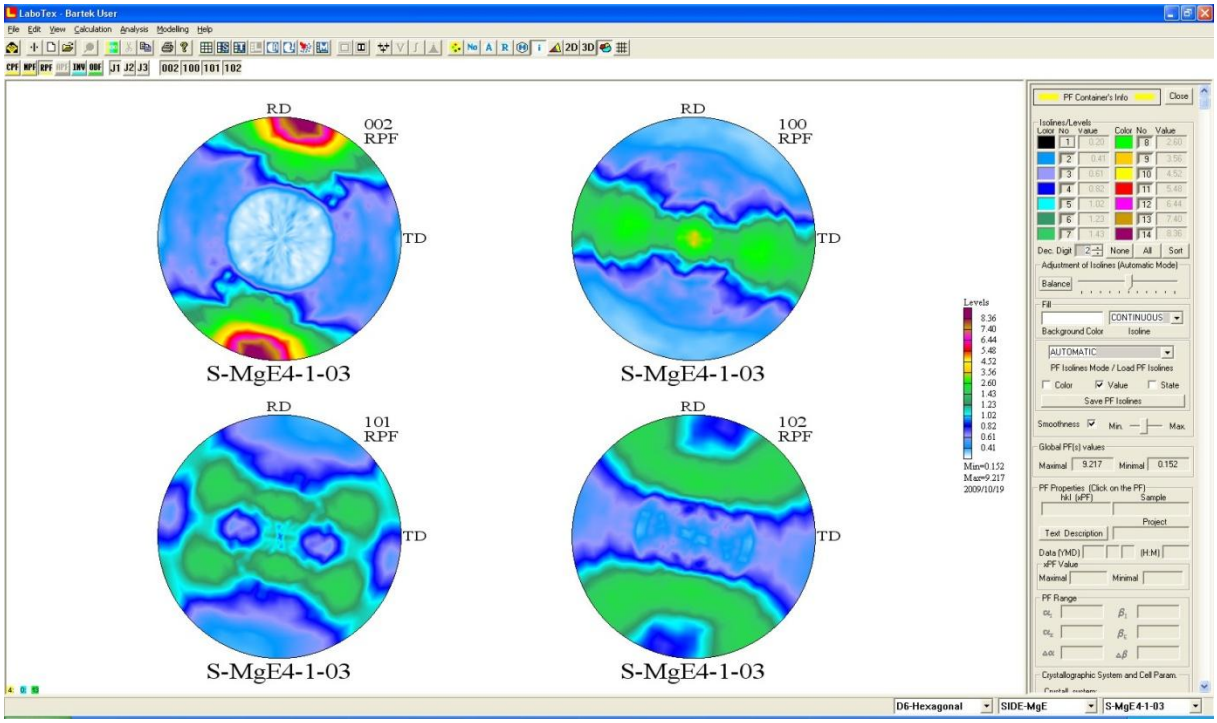

Fig. 3-12. The main user interface of the LaboTex 3.0 package [67]. Four main pole figures of the HPT-deformed Mg sample are displayed.

This kind of information can be derived from the ODF, by an analysis of an overall 'sharpness' of the texture, as well as particular components volume fractions. For this purpose, textures were evaluated in the terms of the texture index (or maximum texture intensity) *J* which is an integral parameter comprising all orientations *g* with their probability densities *f(g)*:

$$J = \oint [f(g)]^2 dg$$

Equ. 3-1. Texture index formula [69].

For a more quantitative characterization of the texture sharpness, values of normalized texture index J_n were derived, following the expression [69]:

$$J_n = \frac{J-1}{J+1}$$

Equ. 3-2. Normalized texture index formula [69].

While the maximum texture intensity *J* can take values within a range of $\{1, \infty)$ representing totally random distributions and single crystals, respectively, the normalized texture index J_n varies in the range of {0,1) [69]$\{0, 1)$.

For the calculations of the volume fraction of the selected, dominating components, Integration Method supported by LaboTex was used. The tolerance of the component position was limited to the usual value of 15° in all three dimensions of the ODF space (ϕ1, Φ and ϕ2).

For polycrystalline magnesium samples an advanced texture analysis, based upon pole figures and ODF section, was used, whereas for the single-crystalline samples, the tracing of the change of orientation on the Inverted Pole Figures (IPF) was more suitable for acquiring information about the orientation changes during HPT deformation.

3.4 Tension tests

The tension test provides most of the mechanical properties of metals as there are the strength, ductility and the strain. A few variants of HPT-deformed polycrystalline Mg samples (deformed at different hydrostatic pressures up to the different shear strain) were subjected to the tension tests at room temperature and at the same strain rate in order to estimate influence of HPT strain on the mechanical properties as well as to correlate with the evolved crystallographic texture.

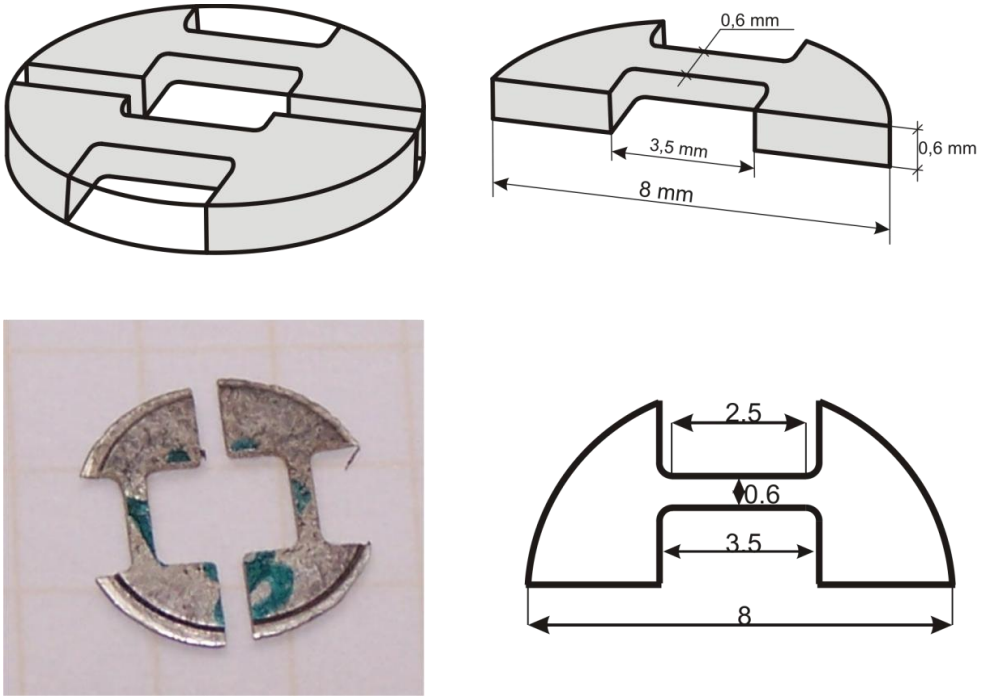

Fig. 3-13. Sample preparation procedure – from the HPT specimen into the samples suitable for tension tests. As shown in the figure: sample design (upper row), HPT-sample cut off (lower right) and tension sample geometry (lower left).

As shown in Fig. 3-13, the samples for the tension test are cut off directly from HPT deformed specimens. A special electro-spark cutting head was prepared in order to produce the tension samples at the highest possible accuracy. An initial diameter of HPT samples can be either 8 or 10 mm, which is just enough to cut the sample with a 2.5 mm long tension base, located in the middle of the HPT-sample radius (see Fig. 3-13).

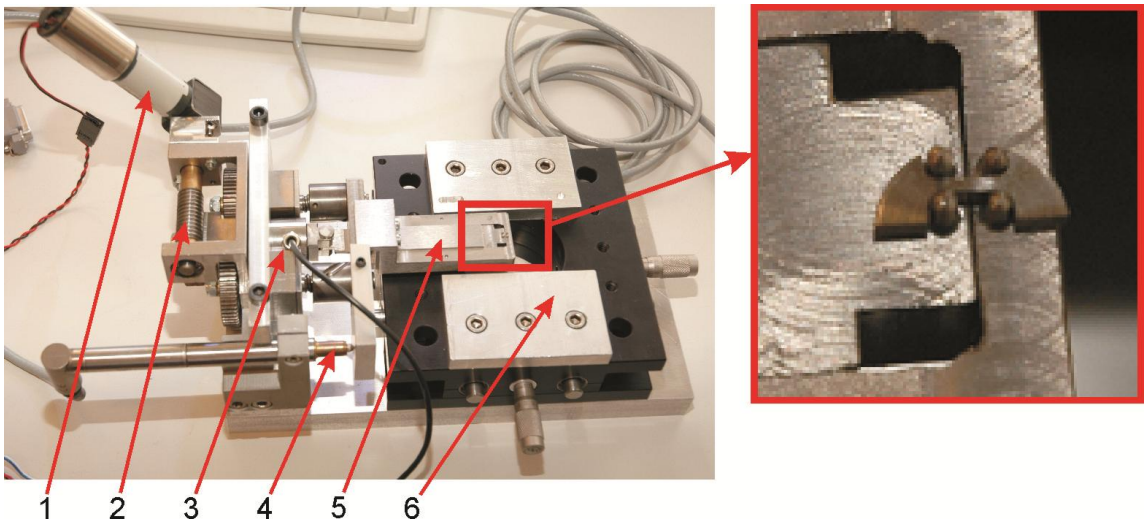

Fig. 3-14. Portable tension tests facility used in experiments. 1 – electric motor, 2 – transmission, 3 – force measuring unit, 4 – displacement measuring unit, 5 – sample traverse, 6 – XY table (to be applied with optional AFM microscope). Sample mounting as shown in close-up.

The tension tests were performed at the Research Group of Physics of Nanostructured Materials Lab (University of Vienna), with a tension machine, specially designed for experiments with HPT samples (as shown in Fig. 3-14). Tension tests were carried out at room temperature, with the strain rate of $\dot{\varepsilon} = 1.4 \cdot 10^{-3}[s^{-1}]$ being the same for all samples. In-situ registered force and elongation were recalculated into stress-strain characteristics of the investigated samples.

3.5 Microhardness measurements

In order to correlate the texture development with the mechanical properties also microhardness measurements were carried out. For comparison reasons indentations at exactly the same cross-sections as the texture measurements (as shown in Fig. 3-15) were done.

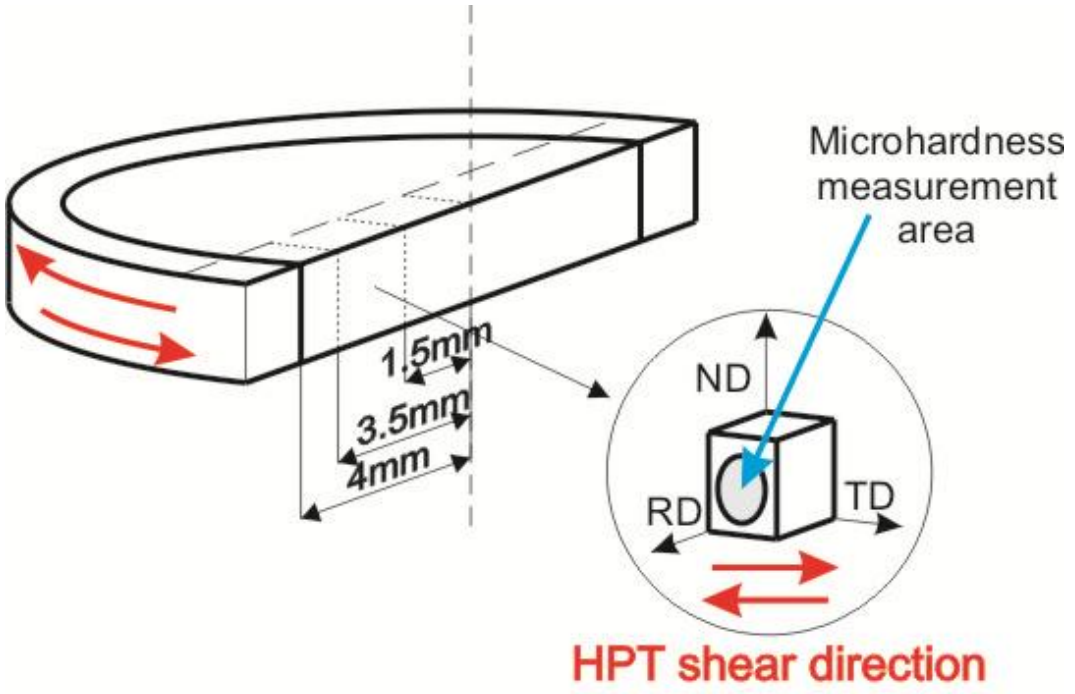

Fig. 3-15. Microhardness measurements experimental setup with respect to the HPT deformation setup. Radial cross section as shown in the graph was chosen to correlate with the texture measurements results.

Microhardness measurements were done with a Wolpert 2100 Indenter with a Vickers indenter. As magnesium is a rather soft material, a load of 0.01 kg was chosen (0.1 N indentation force) and applied for 10 s. Using the automated sample table, surface mapping was performed, by taking the indentations as a grid on the sample surface.

An average microhardness indentation diagonal (in Vickers method indenter comprises a pyramid) amounted to 22 µm. As microhardness measurements did not reveal significant, monotonic hardness distribution on the sample surface, typical of the HPT-deformed metals (with low recovery

rate), as reported in [70] microhardness was presented as an averaged value for the sample cross-section investigated.

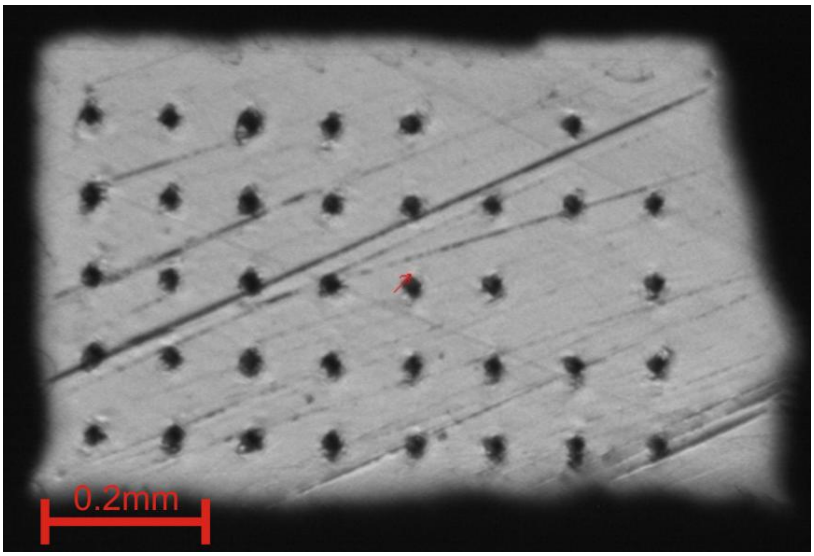

Fig. 3-16. Light-microscope image of indentations of sample surface tested microhardness.

3.6 Microstructure observations

An inspection of the material's (micro-) structure is one of the most informative investigations. This can be achieved by means of both transmission and scanning electron microscopy. The latter offers the possibility of *Electron Back-Scatter Diffraction (EBSD)* imaging.

3.6.1 Transmission Electron Microscopy (TEM)

The highest possible magnifications can be reached with TEM and its further developed variants. For materials science this level of magnification allows tracing the evolution of microstructure. For such a sophisticated investigation method, a special procedure of sample preparation needs to be strictly obeyed in order to provide the data of desired reliability.

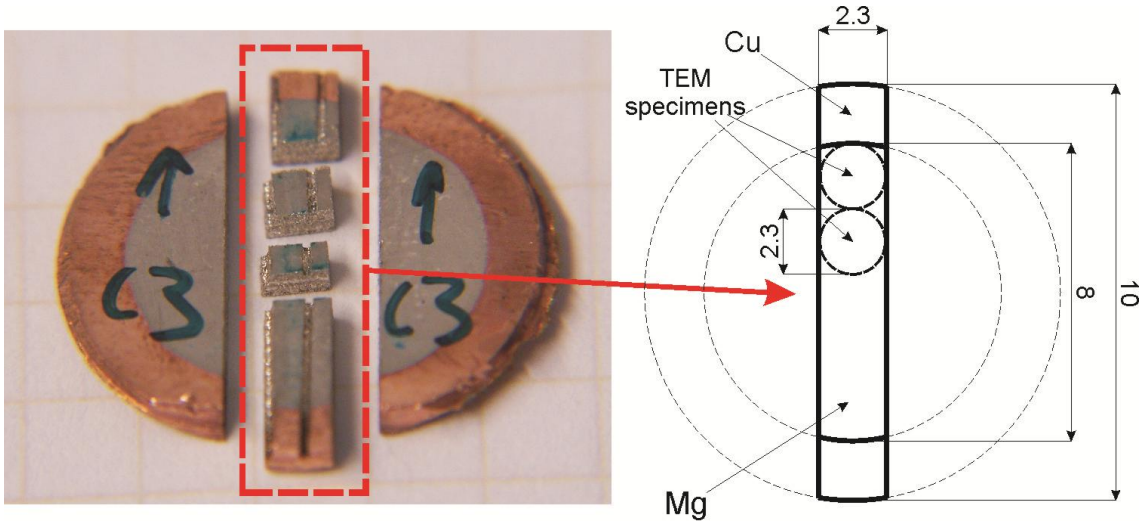

Fig. 3-17. Preparation of TEM specimens from deformed HPT sample. Example shown on the picture is 14 mm diameter Mg sample with Cu ring attached.

With the preparation a 2.3 mm wide strip along with the sample diameter, as shown in Fig. 3-17, is cut from the HPT sample. This has to be done at best by an electro-spark cutter, which can be accurate and does not affect the entire sample but the parts directly in the place of cut. Secondly, such a prepared strip is mechanically ground and then polished with water papers of grade of up to

4000 until it reaches the final thickness of 0.2 mm. At first, one side is polished, then the second one, to ensure that final thin strip will be exactly extracted from the middle of sample thickness. Next, a disc of 2.3 mm in diameter is punched out of the thin strip. Such prepared Mg discs are electropolished by the double-jet system Tenupol-3 by Struers. Typical electro polishing has to be carried out at 5°C and a voltage of 20 V in a 1% volume solution of perchloric acid *($HClO_4$)* in ethanol *(C_2H_5OH)*. This procedure allows the preparation of Mg thin foils specimens suitable for TEM observations which were carried out with a Philips CM200 TEM microscope at a voltage of 200 kV in both dark and bright field modes.

3.6.2 Electron Back-Scatter Diffraction (EBSD) in Scanning Electron Microscopy (SEM)

When extremely high magnifications are not necessary to characterize the microstructure evolution, SEM imaging can be a powerful and sufficient research tool, especially when one needs to define the orientation of the grains in the observed area, which can be performed using EBSD techniques. However, in the case of Mg, the preparation procedure of the samples for EBSD investigations is complicated and requires precision in order to achieve reliable results.

Mg samples were prepared to investigate the same surface as for the texture measurement as shown in Fig. 3-18, which is not exactly the same cross-section as for TEM imaging (because of sample preparation requirements, Fig. 3-17). For the single crystal samples, the surface normal to the HPT rotation axis was investigated.

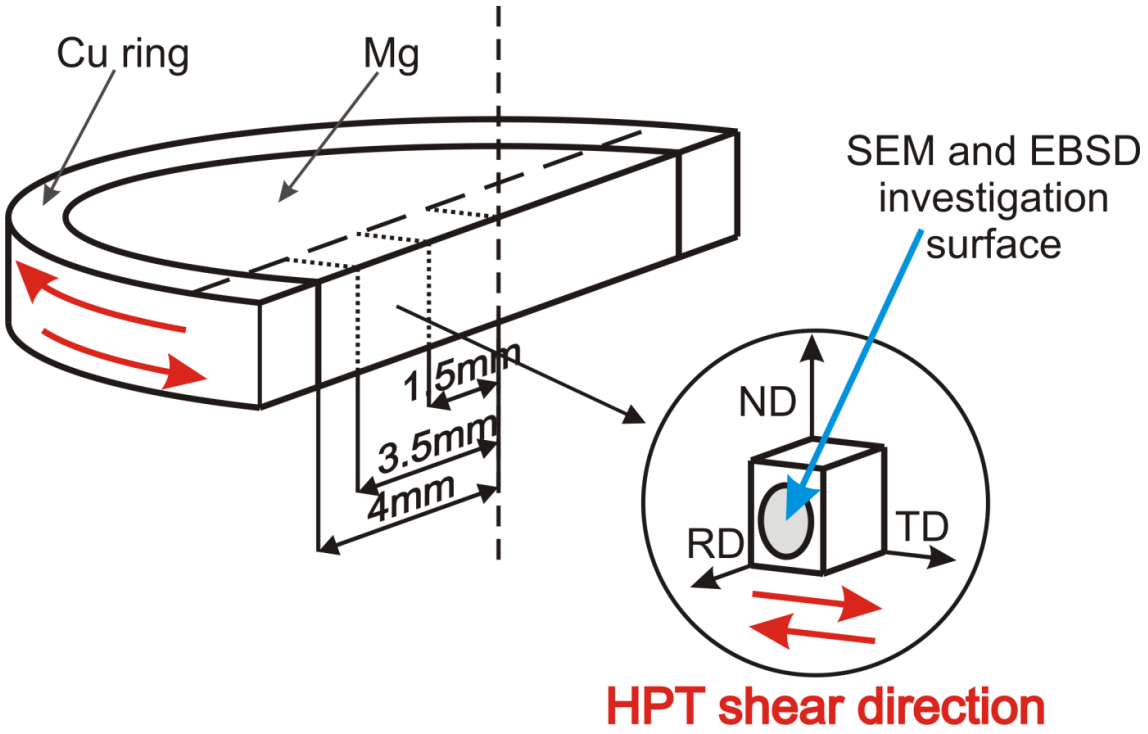

Fig. 3-18. Preparation of polycrystalline Mg specimens for SEM and EBSD experiments. Investigated surface is exactly the same one as used for texture and microhardness testing.

As the specimens are cut from HPT sample by electro spark erosion, according to Fig. 3-18, the investigated surface needs to be carefully prepared. The first step is a mechanical polishing on water papers with granularity up to 2500. The next step is mechanical polishing with LaboPol-2 polisher from Struers with the use of 200 mm MD Doc polishing wheel rotating at the speed of 250 rpm. Polishing was carried out with the use of DP-Lubricant Red (Struers) lubricant with suspension DP-Suspension P 3 µm (which is a diamond suspension on the basis of ethanol and propanol). Then samples were rinsed with ethanol *(C_2H_5OH)*, and dried with pressured air. Final polishing was carried out with the same Struers polisher using 200 mm MD Chem polishing wheel rotated at 250 rpms. The polishing solution was a mixture of the same lubricant but this time with OP-U suspension (which is the suspension on the basis of silica and water). Rinsed with ethanol and dried with pressured air, samples were ready for SEM and EBSD imaging. SEM imaging was carried out with a Hitachi S-3400N microscope operating at 20 kV supplied with HKL-OXFORD Instruments system for EBSD experiments. EBSD imaging was carried out at a standard procedure of tilting the specimen by 70° off the beam line.

4 Results

As for the single crystals investigation four initial orientations were considered as shown in Fig. 4-1. The selected initial orientations are called: **'I'** - for the *pyramidal* one $[10\bar{1}1]$, **'II'** - for another *pyramidal* one, the $[11\bar{2}2]$, **'III'** – for the *prismatic* one $[11\bar{2}0]$ and **'IV'** for the *basal* one, the $[0001]$. This definition is used for the initial orientations nomenclature in all the following sections regarding single crystal investigations.

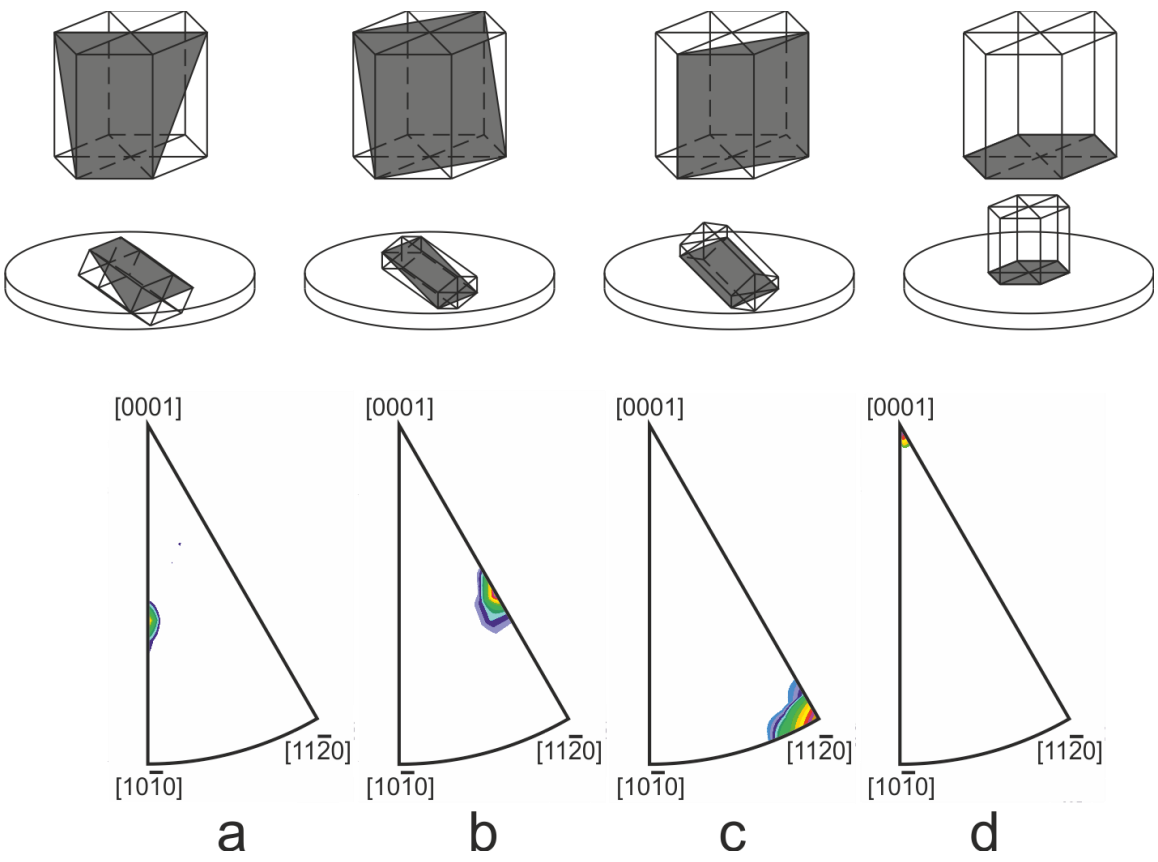

Fig. 4-1. Measured initial orientations of selected Mg single crystals samples prepared for HPT deformation: $[10\bar{1}1]$ (a), $[11\bar{2}2]$ (both called 'pyramidal ones') (b), $[11\bar{2}0]$ called 'prismatic' one (c) and $[0001]$ called 'basal' one (d). Above each initial orientation, hexagonal unit cell orientation with respect to the HPT sample geometry is shown.

4.1 In-situ stress-strain curves

4.1.1 Single crystals

The single crystalline samples of pure Mg were selected and prepared in order to represent four different orientations from the standard hexagonal triangle (see Fig. 4-1).

The single crystal orientations were selected in order to perform easy activation of preferred slip systems as well as of twinning during deformation by High-Pressure Torsion. As it can be seen in Fig. 4-1, orientations are called *'I', 'II', 'III'* and *'IV'* (for the sake of simplicity) and represent orientations: $[10\bar{1}1]$, $[11\bar{2}2]$ (both pyramidal ones), $[11\bar{2}0]$ (prismatic one) and [0001] (basal one), respectively.

Single crystalline samples were deformed at the same hydrostatic pressure of 1.5 GPa, up to a 0.75 full rotation (which corresponds to the torsional strain of about γ=18), as for the single crystal material, the early stage of HPT deformation is mostly interesting (in contrast to the polycrystalline samples, which were deformed up to much higher torsion strains).

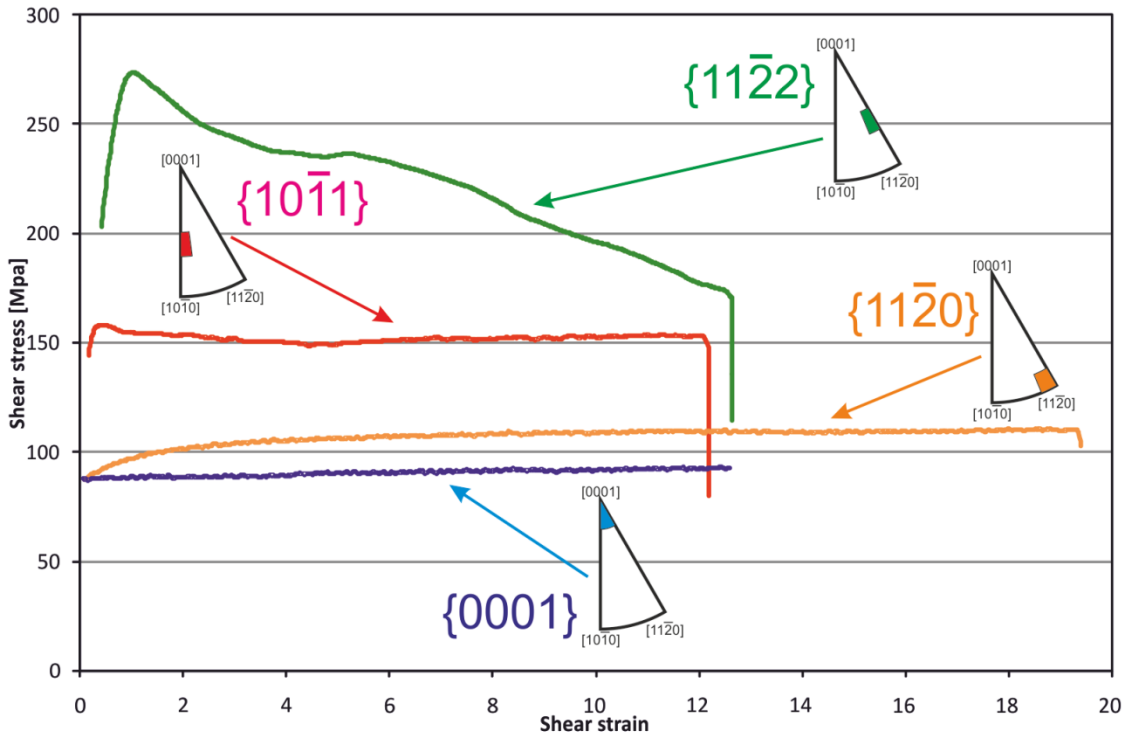

Fig. 4-2. In-situ recorded HPT deformation characteristics of the four different single crystalline Mg samples deformed at 1.5 GPa up to the same amount of 0.5 rotations. The shear strain varies according to differences in thickness reduction (see section 3.2 and 5.1). Initial orientations as given on the graph.

As the HPT strain depends mainly on the radius (and some on the final thickness of the deformed sample) samples deformed up to the same amount of rotations can be characterized by different shear strain (according to Equ. 1-1) if the sample thickness reduction is slightly different. One should remember that the same radius should be considered when comparing the samples, therefore all the presented data always apply to the same radius on the sample. This can be seen in Fig. 4-2, where all the single-crystalline samples were deformed up to the same amount of 0.5 rot, but some of them reveal deviations from the expected shear strain.

4.1.2 Polycrystals

The polycrystalline magnesium samples were deformed by High-Pressure Torsion from two different initial material stages. The first one was as-cast, coarse grained Mg whereas the second one was fine-grained, hot extruded Mg. As mentioned in section 3.2, a copper ring was applied to improve the stability of the deformation process (see Fig. 3-7). The difference in the structure (and texture) between coarse grained and fine grained samples did not affect the deformation characteristics during HPT deformation process. As it can be seen on the following graphs, samples tend to reach the same level of shear stress, and the hardening characteristics are similar, regardless of the initial material state.

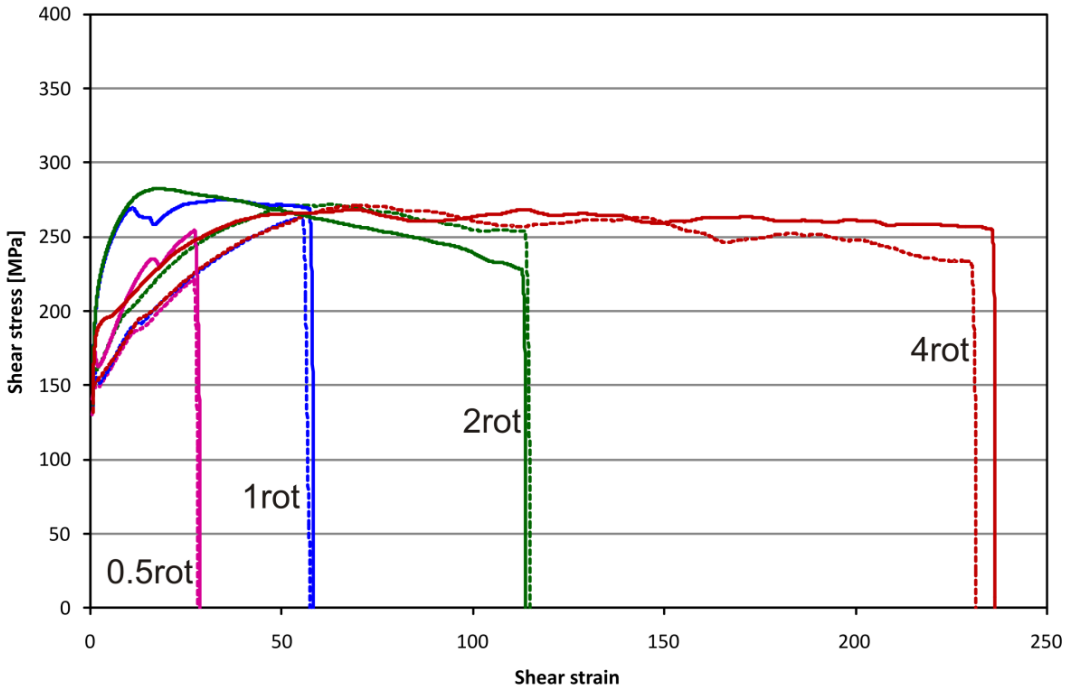

Fig. 4-3. In-situ recorded HPT deformation characteristics of polycrystalline Mg samples with Cu ring attached, deformed at 1 GPa. Number of full rotations applied is given in the graph. Solid and dotted lines correspond to fine-grained (hot extruded) and coarse-grained (as-cast) initial material, respectively.

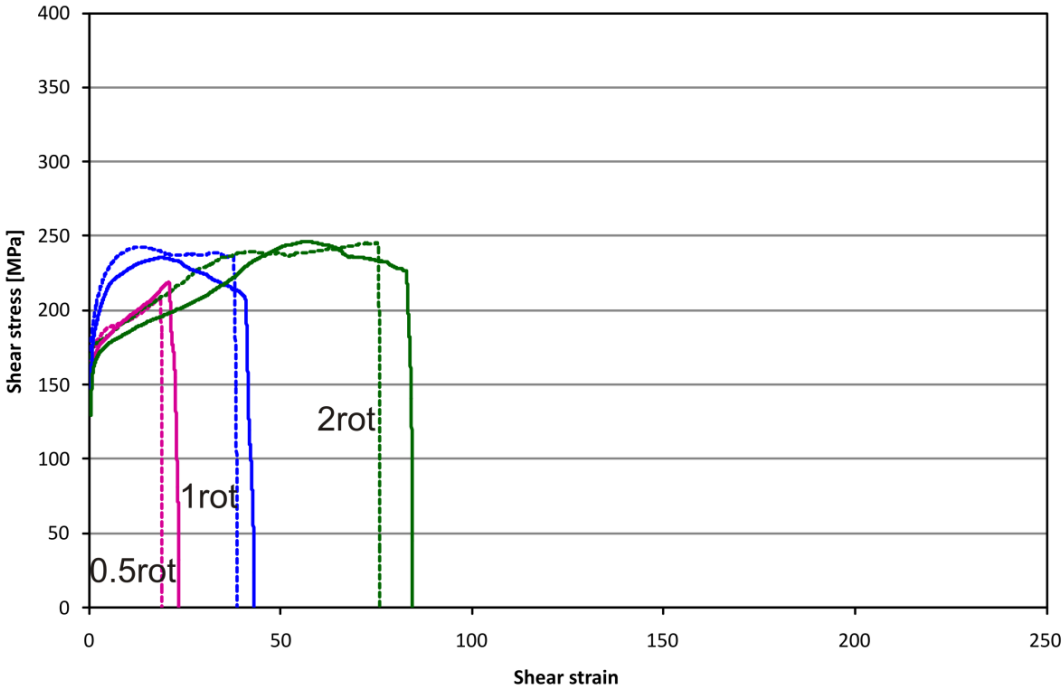

Fig. 4-4. In-situ recorded HPT deformation characteristics of polycrystalline Mg samples with Cu ring attached deformed at 2 GPa. Number of full rotations applied is given in the graph. Solid and dotted lines correspond to fine-grained (hot extruded) and coarse-grained (as-cast) initial material, respectively.

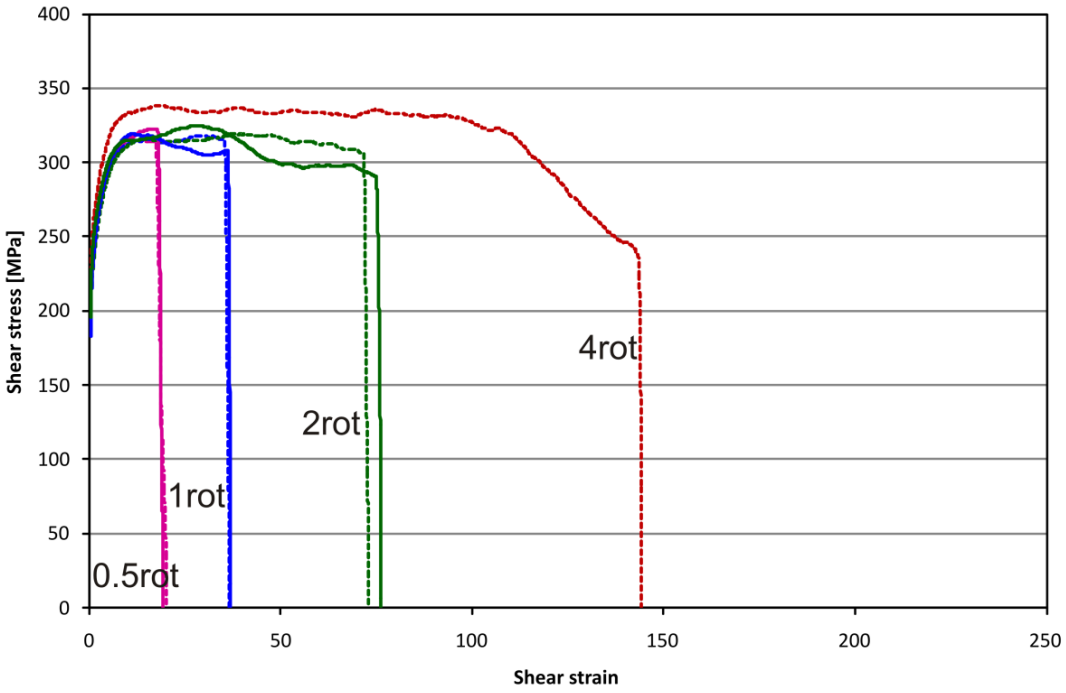

Fig. 4-5. In-situ recorded HPT deformation characteristics of polycrystalline Mg samples with Cu ring attached deformed at 4 GPa. Number of full rotations applied is given in the graph. Solid and dotted lines correspond to fine-grained (hot extruded) and coarse-grained (as-cast) initial material, respectively.

As it can be seen in Fig. 4-6, the shear stress induced during HPT deformation increases markedly when the Cu-ring sample 'reinforcement' is applied. Pure Mg samples were of 8 mm diameter, whereas the samples denoted as Mg with Cu ring were of 10 mm overall diameter (radials: 4 mm of Mg + 1 mm of Cu). Typical shear stress values for 8 mm pure Mg samples amounted to 120 and 240 MPa for 2 and 4 GPa, respectively, whereas for 10 mm sample (Mg 'reinforced' with Cu ring) the shear stress reached the values of 160 and 320 MPa for the same set of 2 and 4 GPa hydrostatic pressures applied. Both sets of samples were deformed up to 2 full rotations. As the thickness reduction is slightly bigger in the case of pure Mg samples, they reach higher shear strain values (see section 3.2).

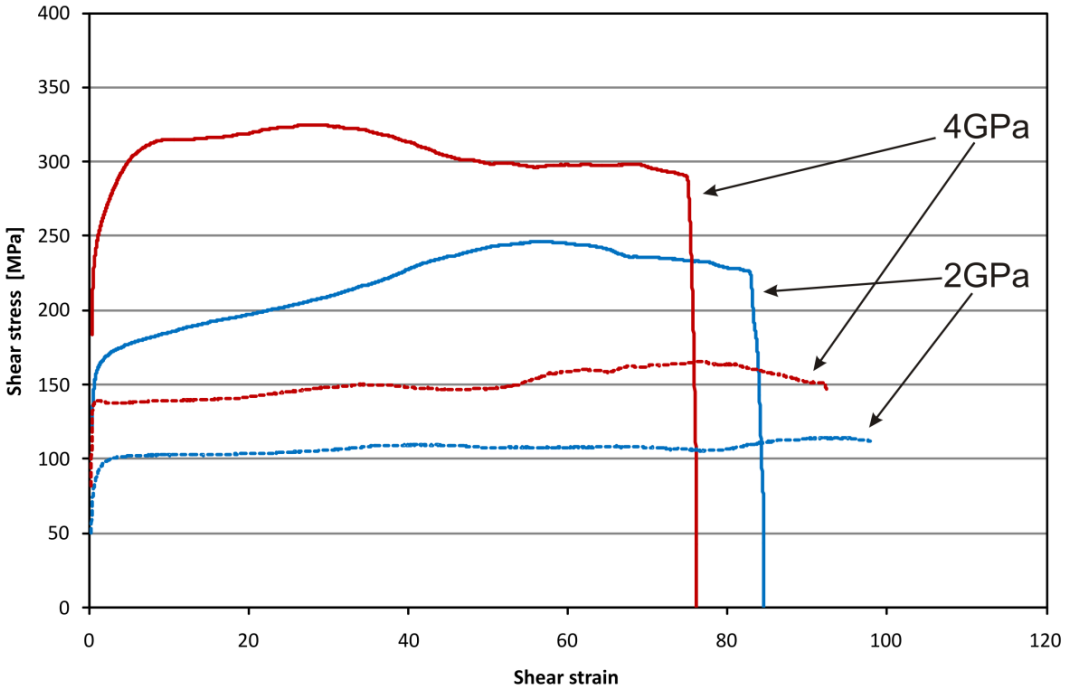

Fig. 4-6. In-situ recorded HPT deformation characteristics of Mg samples (with diameter of 8 mm) and Mg samples with Cu ring attached (with an overall diameter of 10 mm) deformed at 2 and 4 GPa. Bare Mg samples marked with dashed lines, whereas samples with Cu ring are marked with solid lines.

4.2 X-ray textures

4.2.1 Single crystals

The pure Mg single crystalline samples of selected orientations (Fig. 4-8) were deformed by High-Pressure Torsion at the hydrostatic pressure of 1.5 GPa by relatively low strains (as compared to the polycrystalline experiments). In contrast to polycrystalline material, low strains were essential for the orientation changes during HPT deformation. Therefore the samples were deformed applying HPT rotations from 0.1 to 0.75, which corresponds the torsional shear strain up to the value of about $\gamma \leq 20$, according to Equ. 1-1.

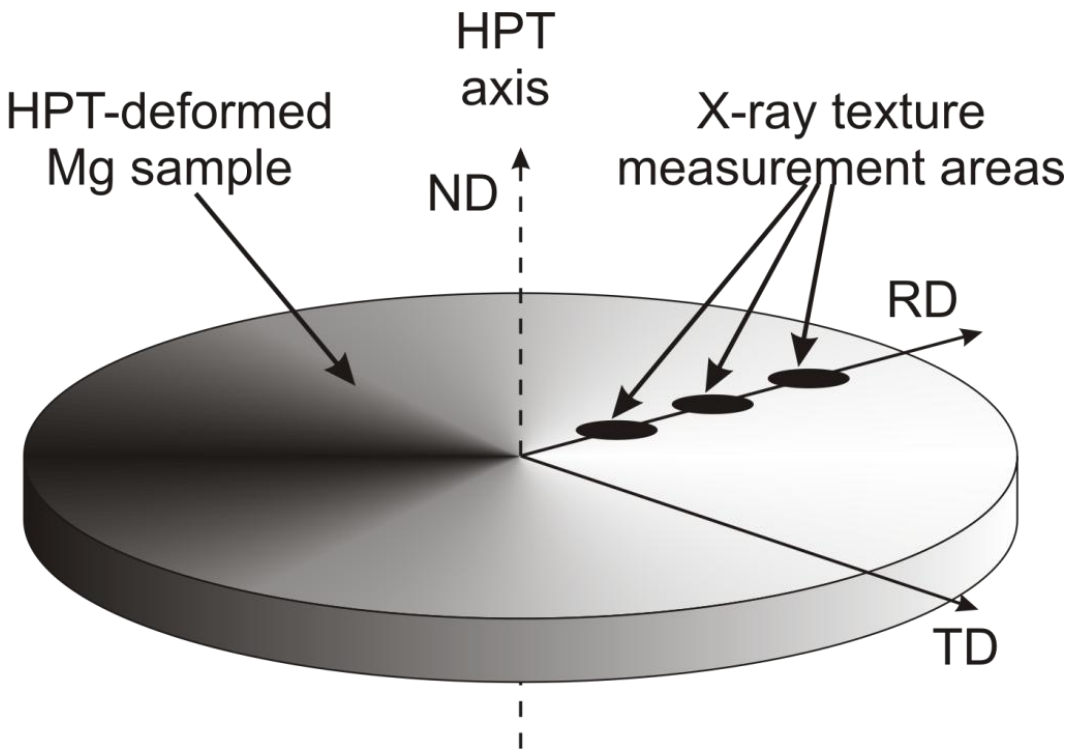

Fig. 4-7. Experimental setup for texture measurement of Mg single crystal samples deformed by HPT.

The single crystal orientations described by Inverted Pole Figures (IPF) (Fig. 4-8) are representative for all the samples of given series used in the HPT experiments. 4 principal orientations were investigated: $[10\bar{1}1]$, $[11\bar{2}2]$ (both 'Pyramidal'), $[11\bar{2}0]$ ('Prismatic') and $[0001]$

('Basal'), as shown in Fig. 4-1 and in Fig. 4-8, and for simplification they will be further denoted as I, II, III and IV, respectively (refer to Fig. 4-8).

For the HPT deformation of single crystal samples the most important information is the change of the initial orientation. The analysis of the Inverted Pole Figures (IPF) is an efficient method to trace these changes, therefore all the texture results (related to single crystal samples) are presented with IPFs.

Due to a strong strain gradient in HPT-deformed discs [70], three measurement points were selected along the sample radius (as shown in Fig. 4-7), enabling a more accurate texture strain study.

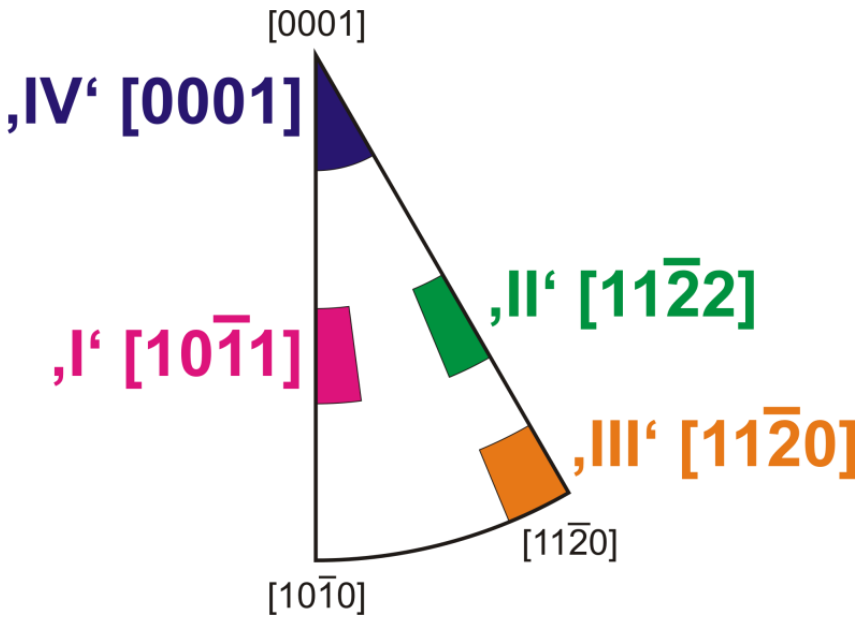

Fig. 4-8. Key map for texture components notation, used in the present dissertation (according to colors of the corresponding orientations used in following graphs).

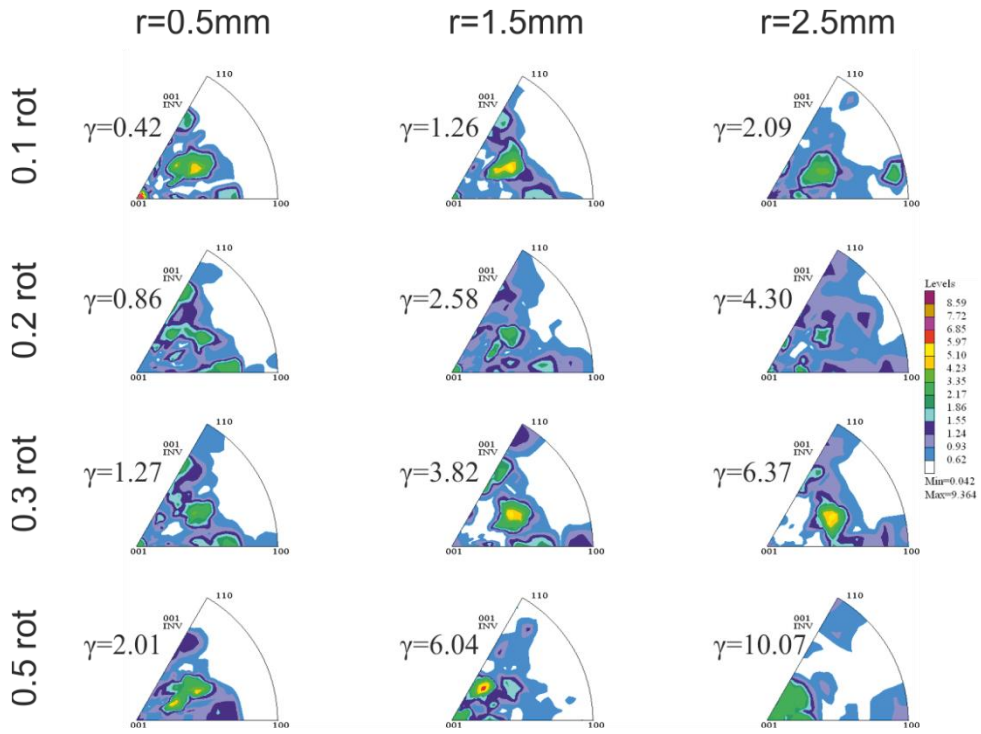

Fig. 4-9. Evolution of texture in HPT deformation of Mg single crystal of $[10\bar{1}1]$ initial orientation (denoted as „I") as seen on Inverted Pole Figures (IPF) of [0001] direction as a function of applied HPT rotations amount and radius of the measured area on the sample. Torsional shear strains as given on the graph next to corresponding IPFs.

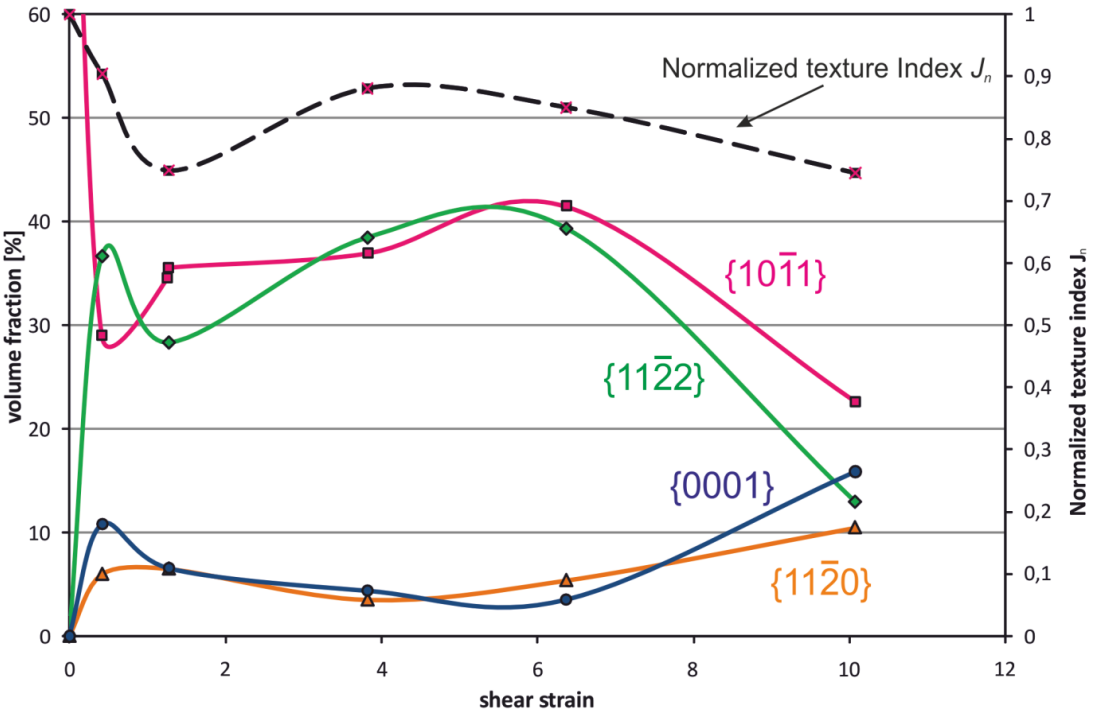

Fig. 4-10. Evolution of normalized texture index and the volume fraction evolution for the main four texture components as a function of HPT shear strain for orientation 'I' $[10\bar{1}1]$ (pyramidal system).

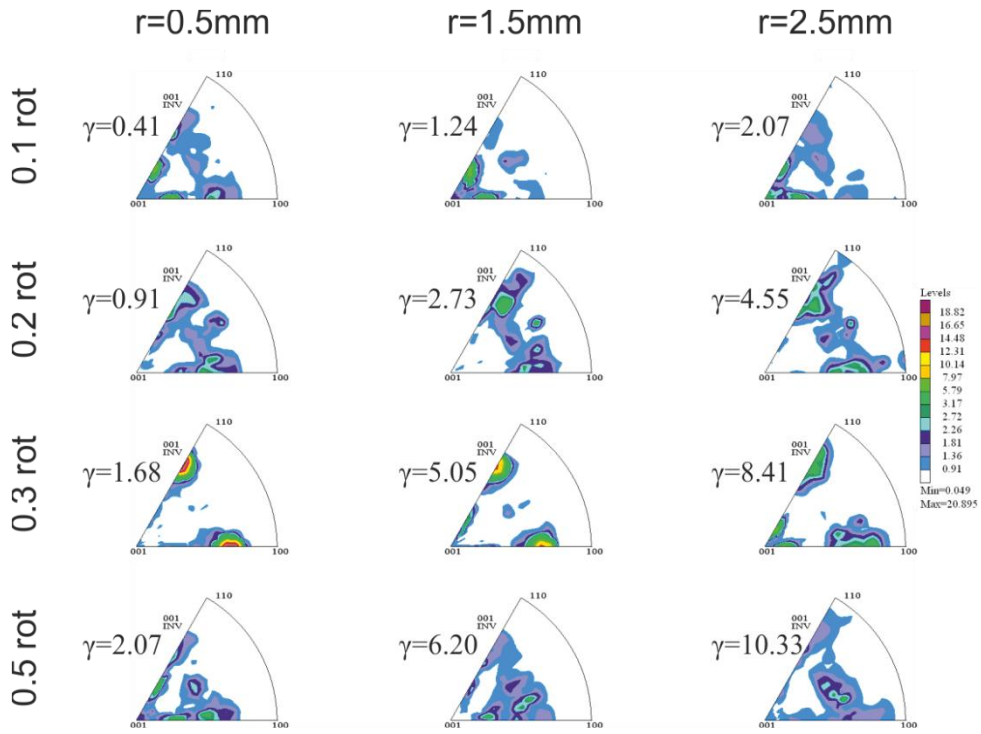

Fig. 4-11. Evolution of texture in HPT deformation of Mg single crystal of $[11\bar{2}2]$ initial orientation (denoted as „II“) as seen on Inverted Pole Figures (IPF) of [0001] direction as a function of applied HPT rotations amount and radius of the measured area on the sample. Torsional shear strains as given on the graph next to corresponding IPFs.

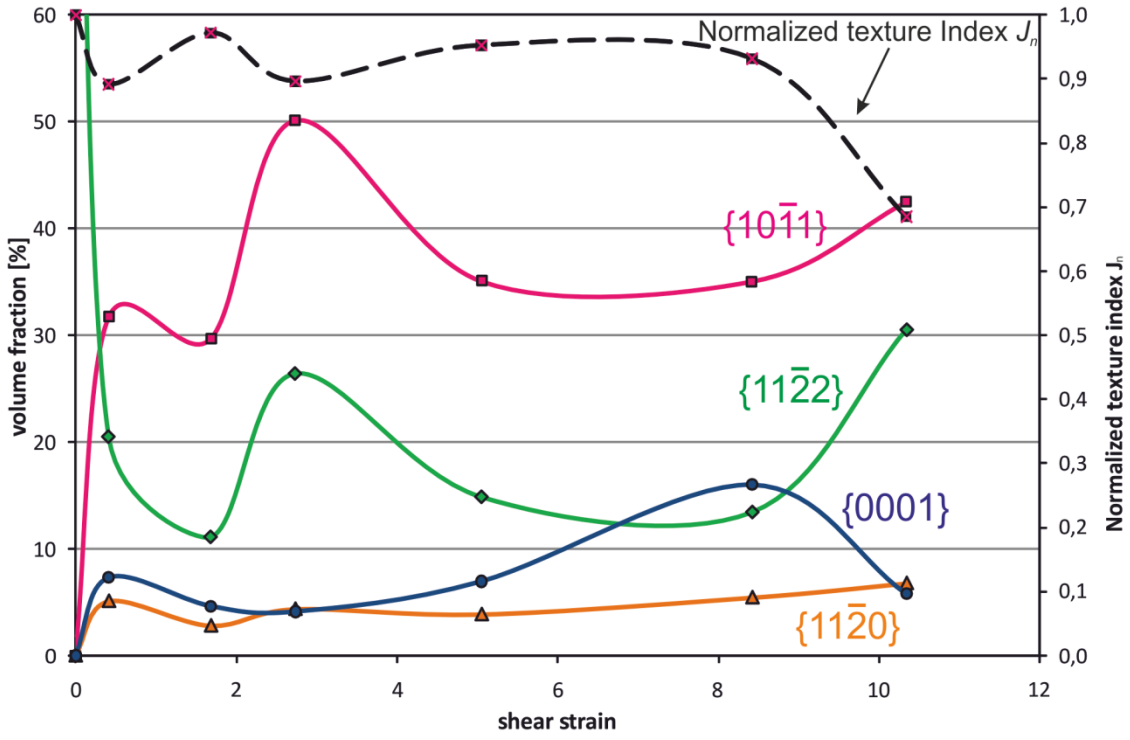

Fig. 4-12. Evolution of normalized texture index and the volume fraction evolution for the main four texture components as a function of HPT shear strain for orientation 'II' $[11\bar{2}2]$ (pyramidal).

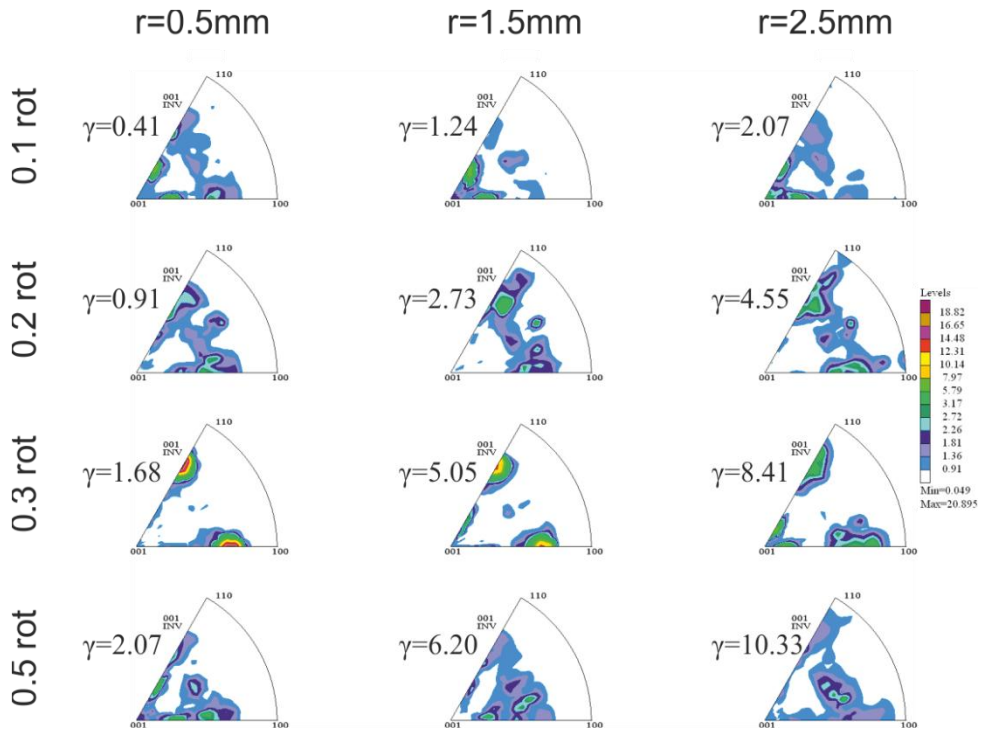

Fig. 4-13. Evolution of texture in HPT deformation of Mg single crystal of $[11\bar{2}0]$ initial orientation (denoted as „III") as seen on Inverted Pole Figures (IPF) of [0001] direction as a function of applied HPT rotations amount and radius of the measured area on the sample. Torsional shear strains as given on the graph next to corresponding IPFs.

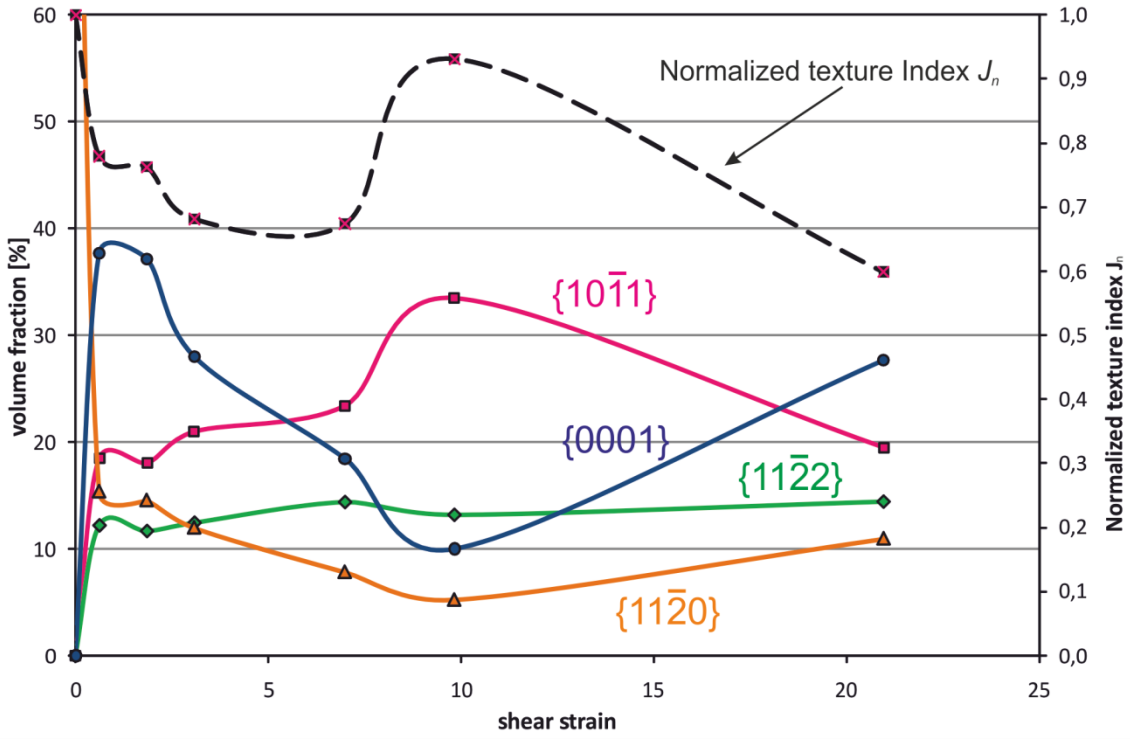

Fig. 4-14. Evolution of normalized texture index and the volume fraction evolution for the main four texture components as a function of HPT shear strain for orientation 'III' $[11\bar{2}0]$ (prismatic).

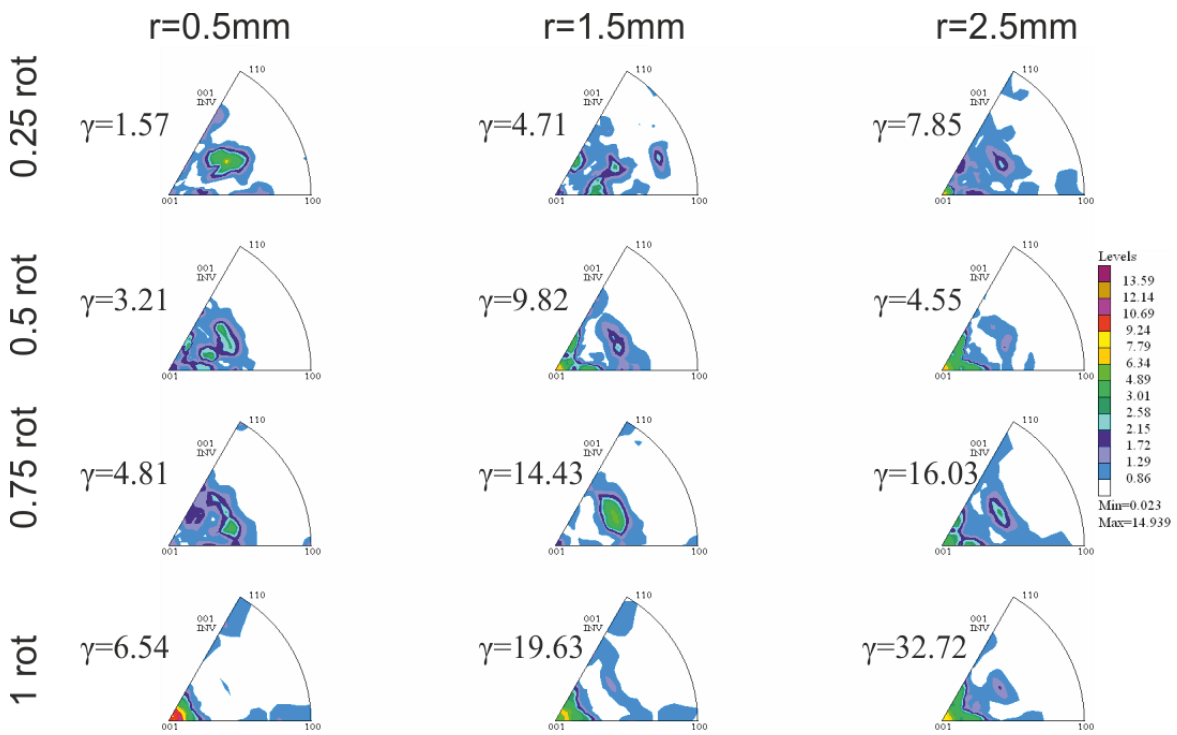

Fig. 4-15. Evolution of texture in HPT deformation of Mg single crystal of [0001] initial orientation (denoted as „IV") as seen on Inverted Pole Figures (IPF) of [0001] direction as a function of applied HPT rotations amount and radius of the measured area on the sample. Torsional shear strains as given on the graph next to corresponding IPFs.

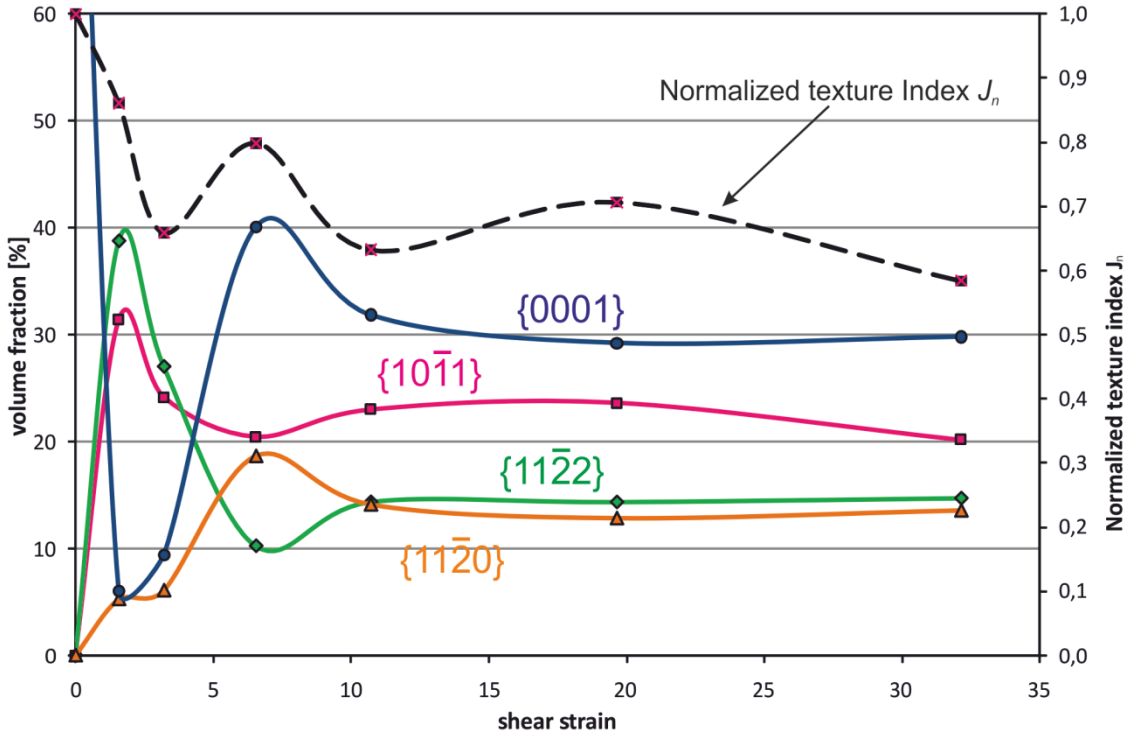

Fig. 4-16. Evolution of normalized texture index and the volume fraction evolution for the main four texture components as a function of HPT shear strain for orientation 'IV' [0001] (basal).

4.2.2 Mg Polycrystals

For the first X-ray texture investigations, a normal sample surface was used, as it is common for other materials deformed by HPT, such as Cu, Ni investigation [71, 72]. As such experiments did not provide sufficient texture information, another – radial – sample section was considered (see Fig. 3-9).

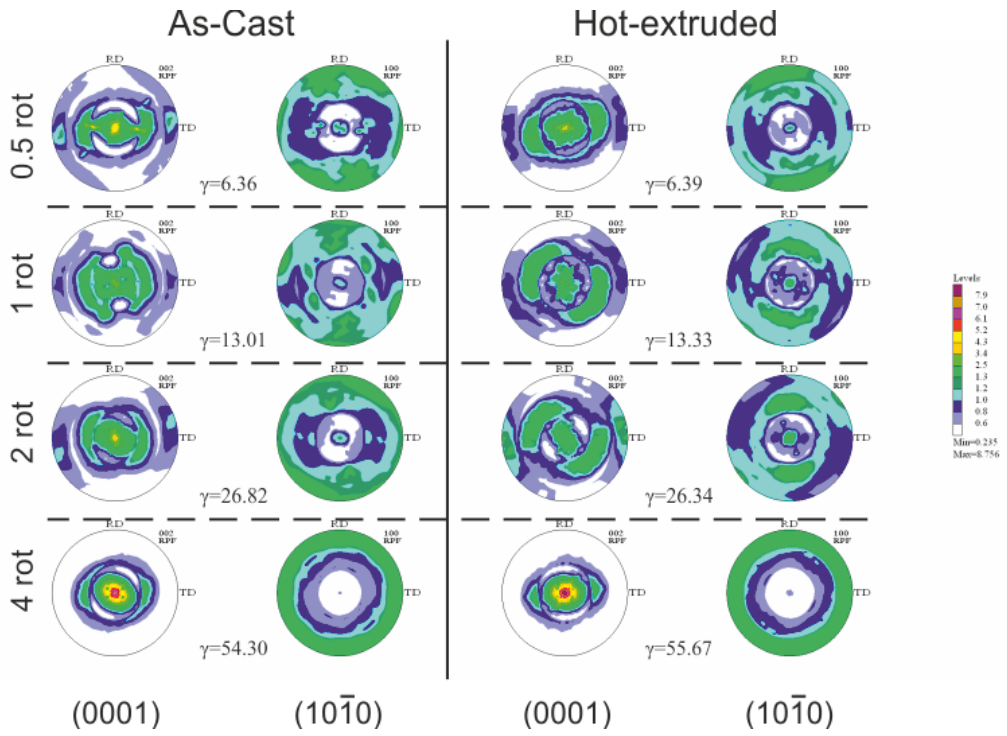

Fig. 4-17. The recalculated pole figures (RPF) of As-cast and Hot-extruded (left and right, respectively) Mg after HPT deformation at hydrostatic pressure of 1 GPa up to different amount of rotations. X-ray textures were measured at normal sample surface (as shown in Fig. 3-9).

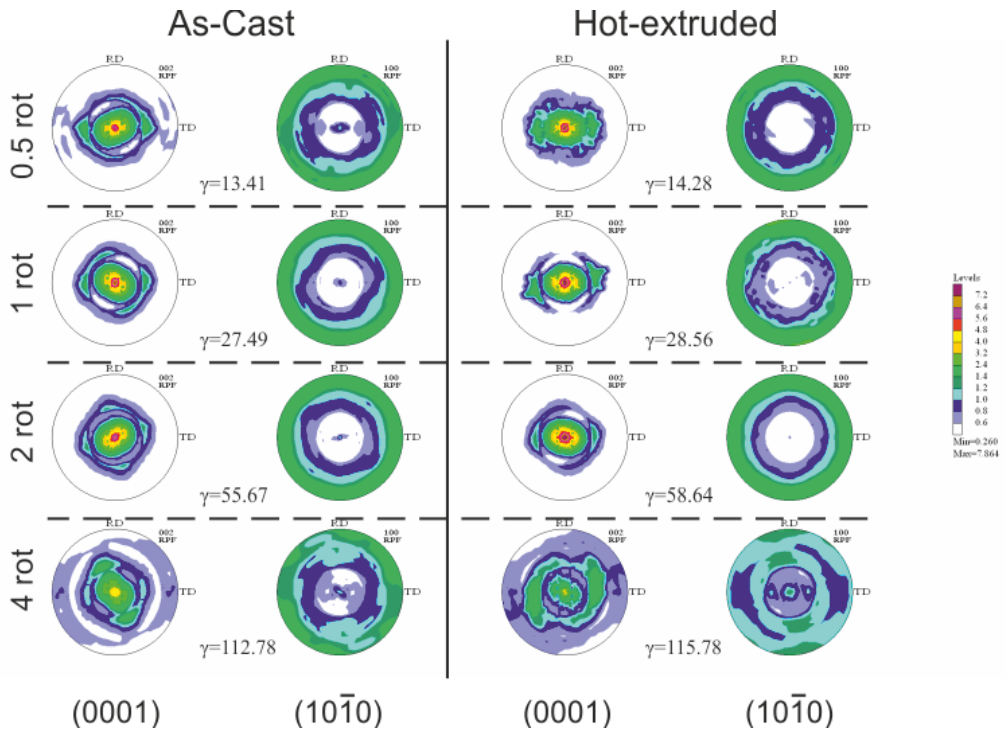

Fig. 4-18. The recalculated pole figures (RPF) of As-cast and Hot-extruded (left and right, respectively) Mg after HPT deformation at hydrostatic pressure of 2 GPa up to different amount of rotations. X-ray textures were measured at normal sample surface (as shown in Fig. 3-9).

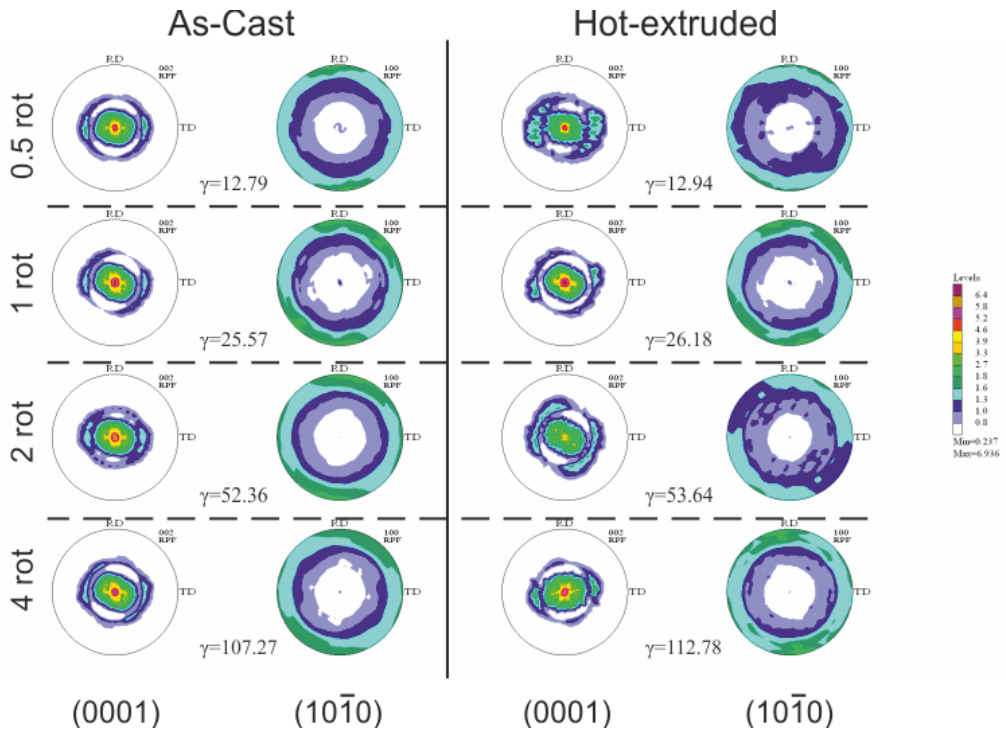

Fig. 4-19. The recalculated pole figures (RPF) of As-cast and Hot-extruded (left and right, respectively) Mg after HPT deformation at hydrostatic pressure of 4 GPa up to different amount of rotations. X-ray textures were measured at normal sample surface (as shown in Fig. 3-9).

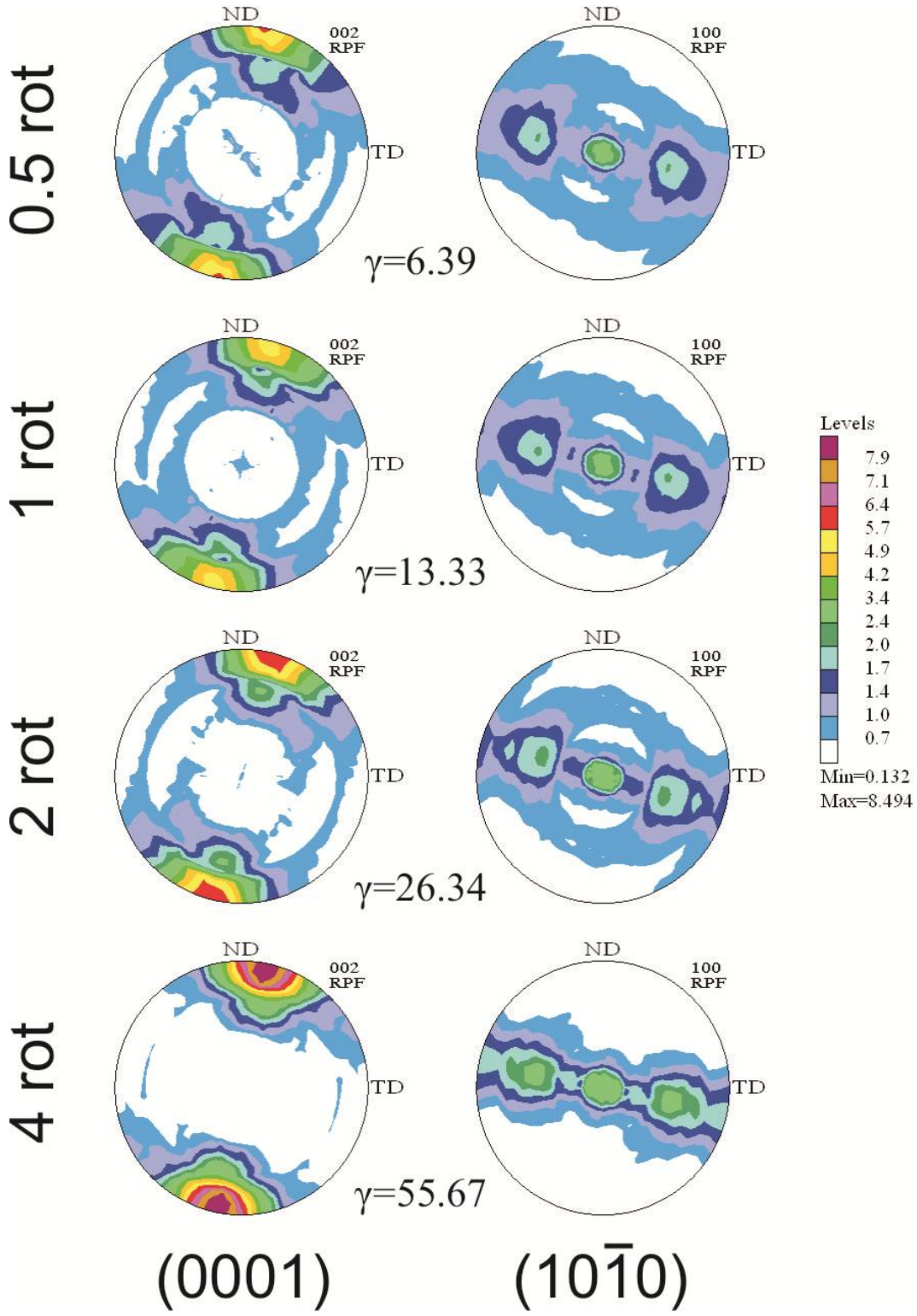

Fig. 4-20. The recalculated pole figures (RPF) of Hot-extruded Mg after HPT deformation at hydrostatic pressure of 1 GPa up to different amount of rotations. X-ray textures were measured at radial cross-section of HPT sample (as shown in Fig. 3-9).

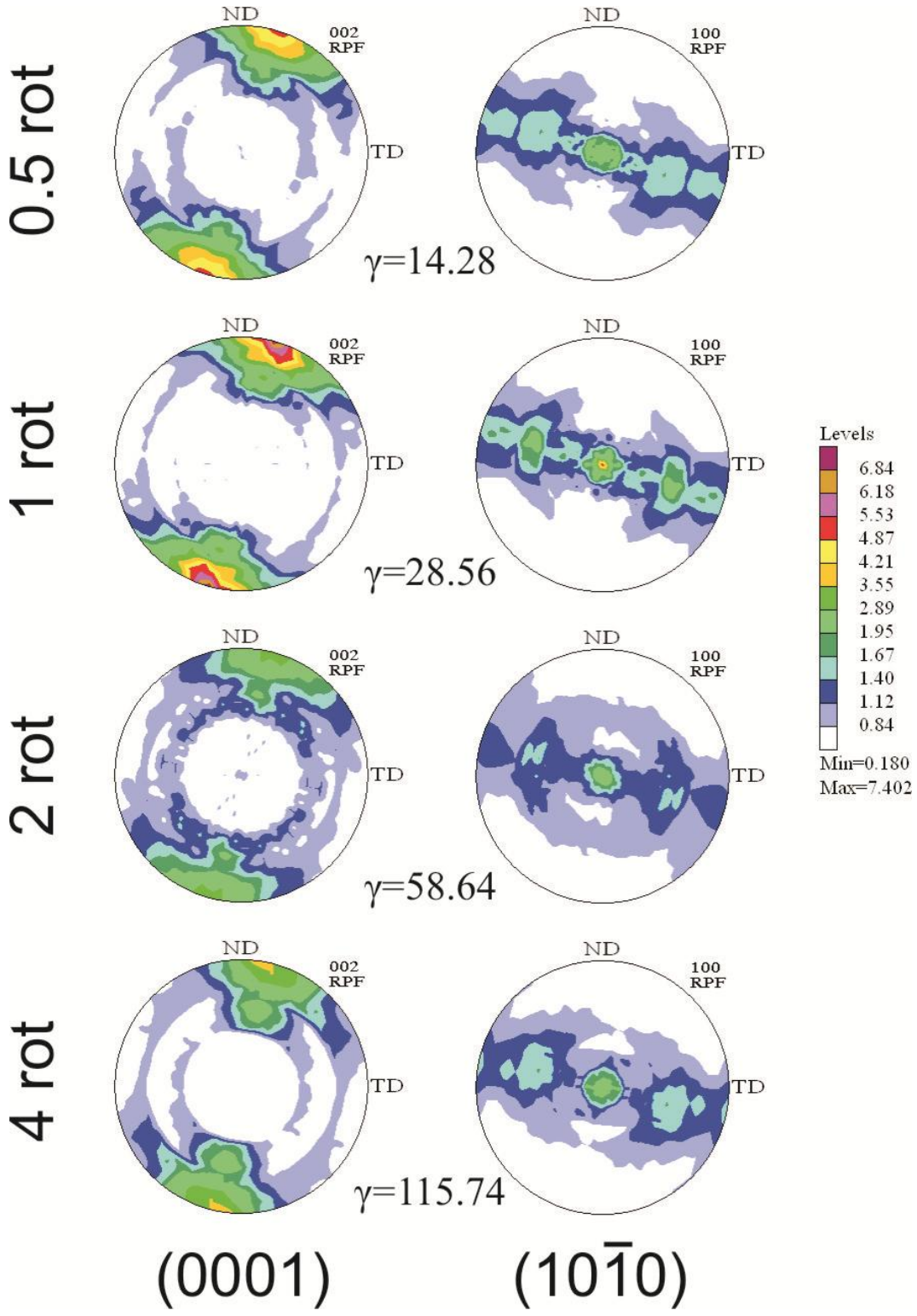

Fig. 4-21. The recalculated pole figures (RPF) of Hot-extruded Mg after HPT deformation at hydrostatic pressure of 2 GPa up to different amount of rotations. X-ray textures were measured at radial cross-section of HPT sample (as shown in Fig. 3-9).

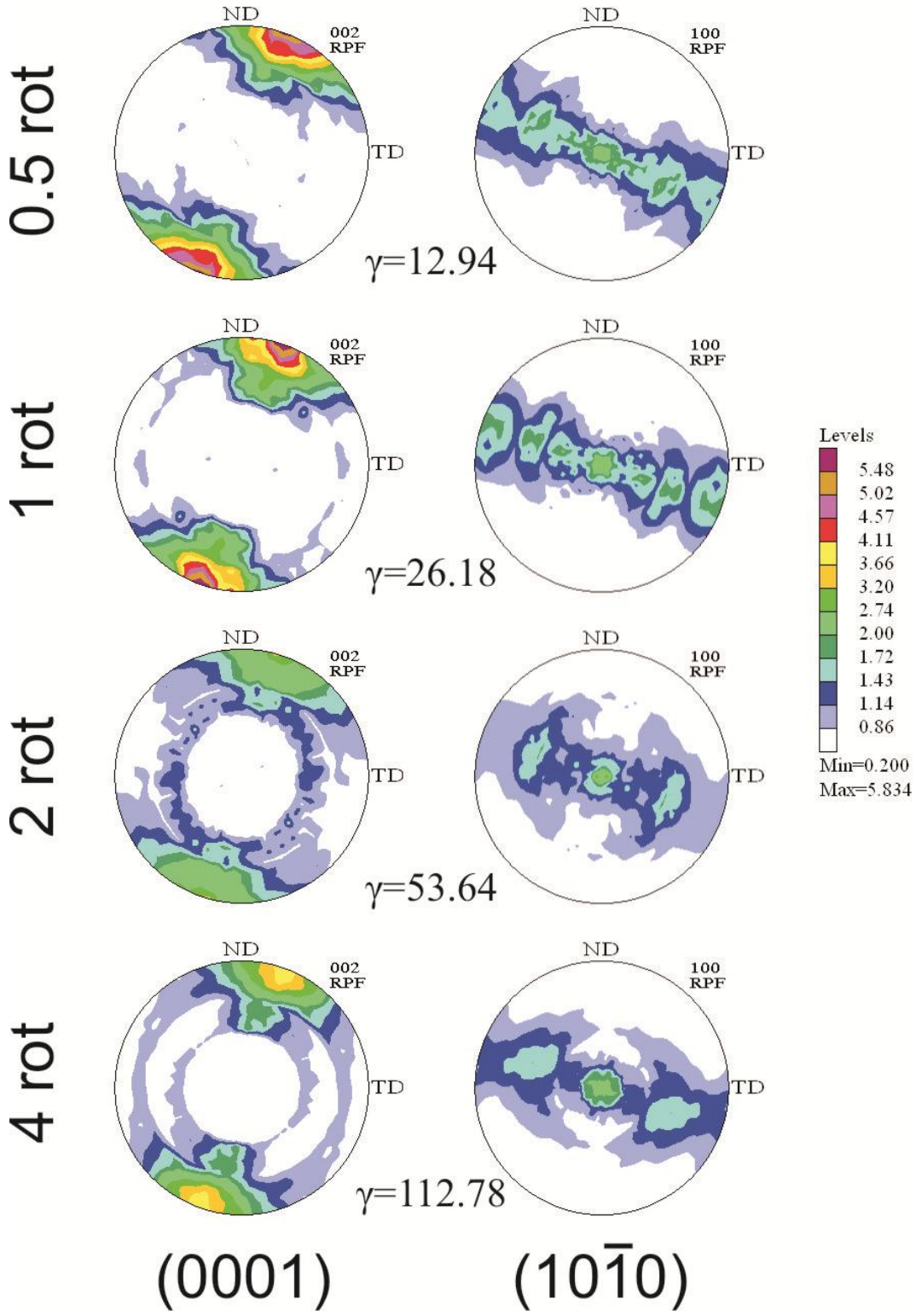

Fig. 4-22. The recalculated pole figures (RPF) of Hot-extruded Mg after HPT deformation at hydrostatic pressure of 4 GPa up to different amount of rotations. X-ray textures were measured at radial cross-section of HPT sample (as shown in Fig. 3-9).

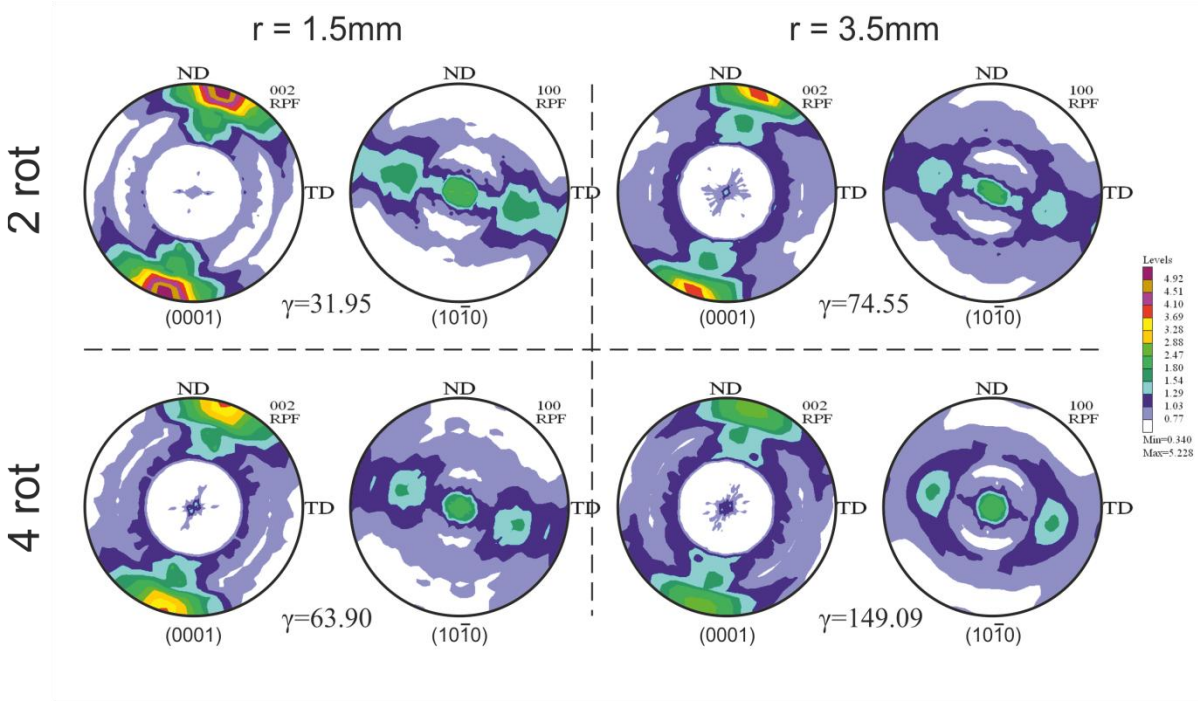

Fig. 4-23. The Recalculated Pole Figures (RPF) of HPT-deformed Mg samples frozen directly after deformation. HPT hydrostatic pressure amounted to 2 GPa. X-ray textures were measured at radial cross-section of HPT sample (as shown in Fig. 3-9).

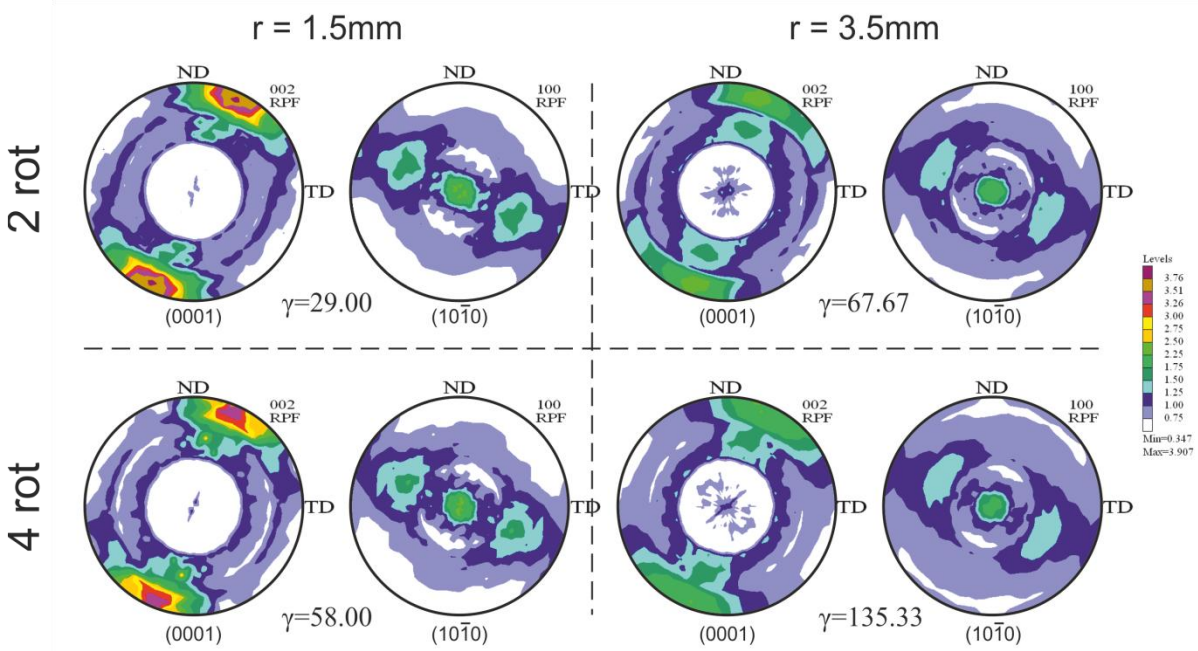

Fig. 4-24. The Recalculated Pole Figures (RPF) of HPT-deformed Mg samples frozen directly after deformation. HPT hydrostatic pressure amounted to 4 GPa. X-ray textures were measured at radial cross-section of HPT sample (as shown in Fig. 3-9).

4.3 Tension tests

These tests were carried out at a room temperature and a strain rate of $\dot{\varepsilon} = 1.4 \cdot 10^{-3}[s^{-1}]$. The hot-extruded material (refer to section 3.1.1) after the HPT deformation was investigated by the tension tests. Experimental results of 'Frozen' (F) and 'Recrystallized' (RX) samples (see section 3.1.2.1) were compared with each other and with the initial material (see Tab. 4-1). The strain was calculated for true strain formula, as follows:

$$\varepsilon = \ln \frac{l}{l_0}$$

Equ. 4-1. True strain for the tension tests.

where *l* corresponds to the actual base length and l_0 is a constant initial base length (equals to 2.5 mm, as shown in Fig. 3-13).

HPT Hydrostatic Pressure [GPa]	RX	F
2	41.5	55.5
4	38.3	50.6
Initial	66.4	

Tab. 4-1. Elongation in [%] at the tension tests measured for the polycrystalline Mg samples deformed in HPT compared to the initial material (before the HPT). RX and F stand for the 'Recrystallized' and the 'Frozen' material state (see section 3.1.2.1)

The HPT samples were deformed up to the same strain of approximately $\gamma \simeq 65$, which was achieved by HPT deformation up to the 2 full rotations (according to Equ. 1-1). The initial material (according to section 3.1.1), was hot extruded magnesium (at 350°C) and had an average grain size of about 40 µm.

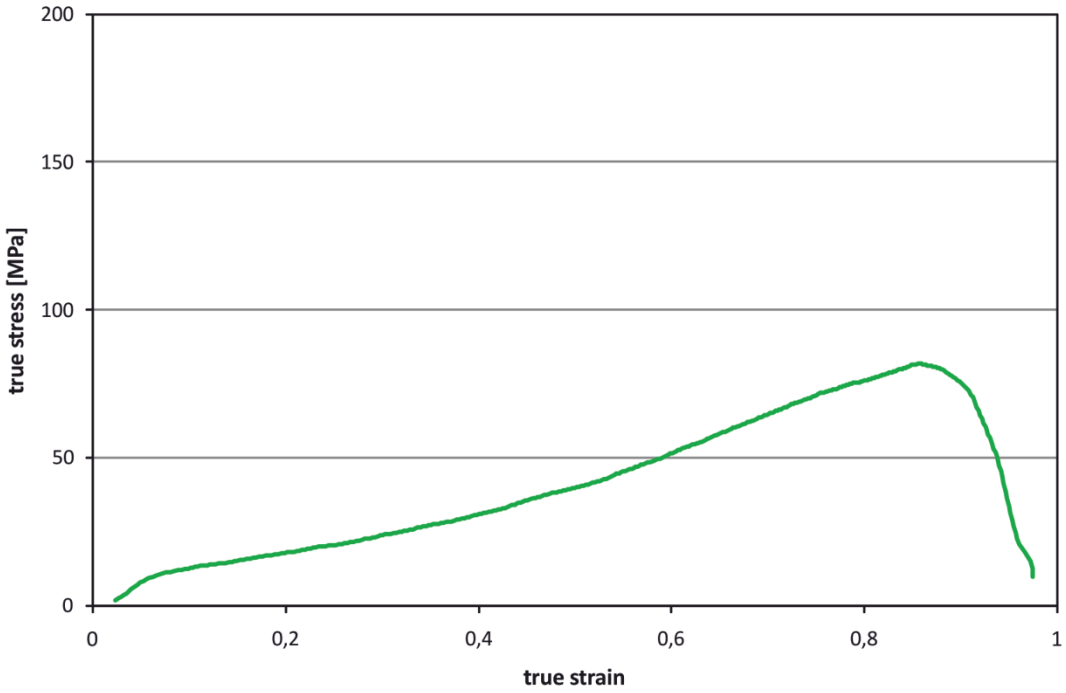

Fig. 4-25. True stress – true strain characteristics of an initial Mg sample (cut from disc prepared for HPT deformation) subjected to tension tests at room temperature.

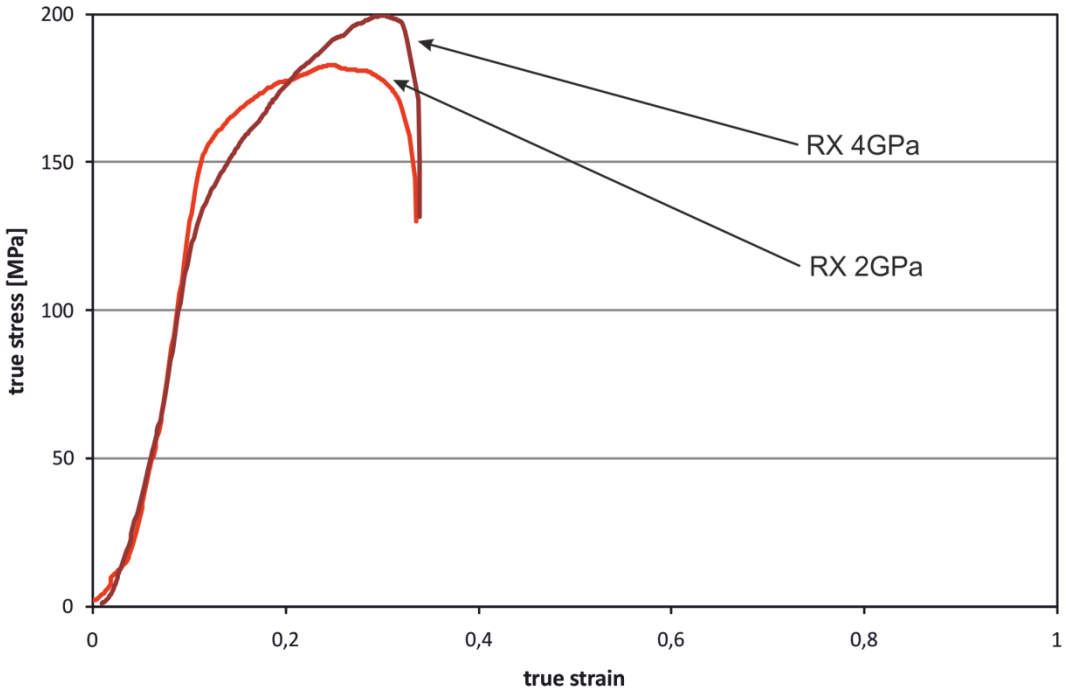

Fig. 4-26. True stress – true strain tension characteristics of recrystallized (RX) magnesium samples subjected to HPT deformation at 2 and 4GPa.

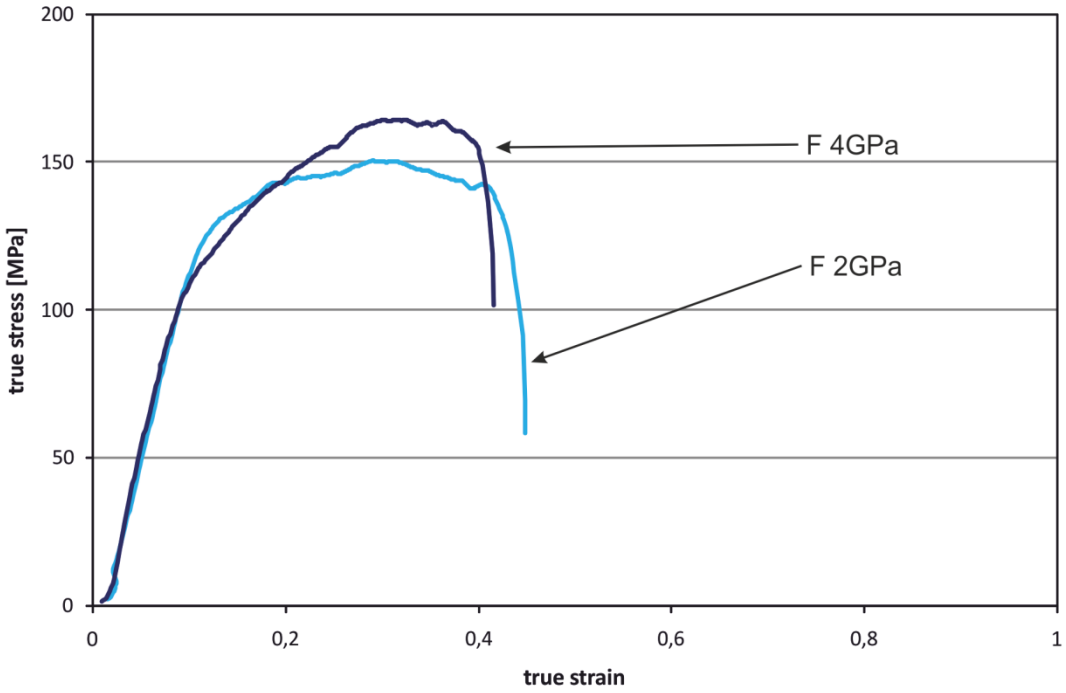

Fig. 4-27. True stress – true strain tension characteristics of frozen (F) magnesium samples subjected to HPT deformation at 2 and 4GPa.

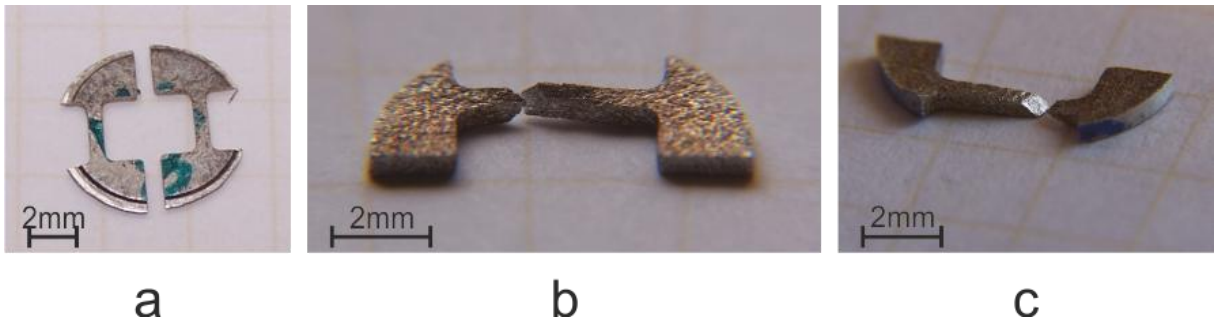

Fig. 4-28. HPT magnesium samples prepared and after tension tests. Tension samples as cut from HPT-deformed specimen (a), hot-extruded magnesium sample (not subjected to HPT deformation) after tension tests (b) and HPT-deformed Mg sample after tension tests (c).

4.4 Measurements of microhardness

Due to the strong strain gradient across the torsion axis of the HPT-deformed samples it is expected that with the increasing radius, microhardness increases in parallel with accumulated shear strain. This phenomenon has been reported for the most common HPT deformed metals, such as Al, Ti or Cu [36, 46, 70]. By applying severe plastic deformation at room temperature, the microhardness distribution is to be strongly affected by the (static) recovery rate, strongly depending on the particular material. It has been reported [70] that for the materials with a relatively fast recovery rate, the microhardness distribution after the HPT does not reveal the characteristic increase as a function of sample radius. The first results of microhardness measurement across the sample normal surface show no clear trends of microhardness either neither to increase nor to decrease.

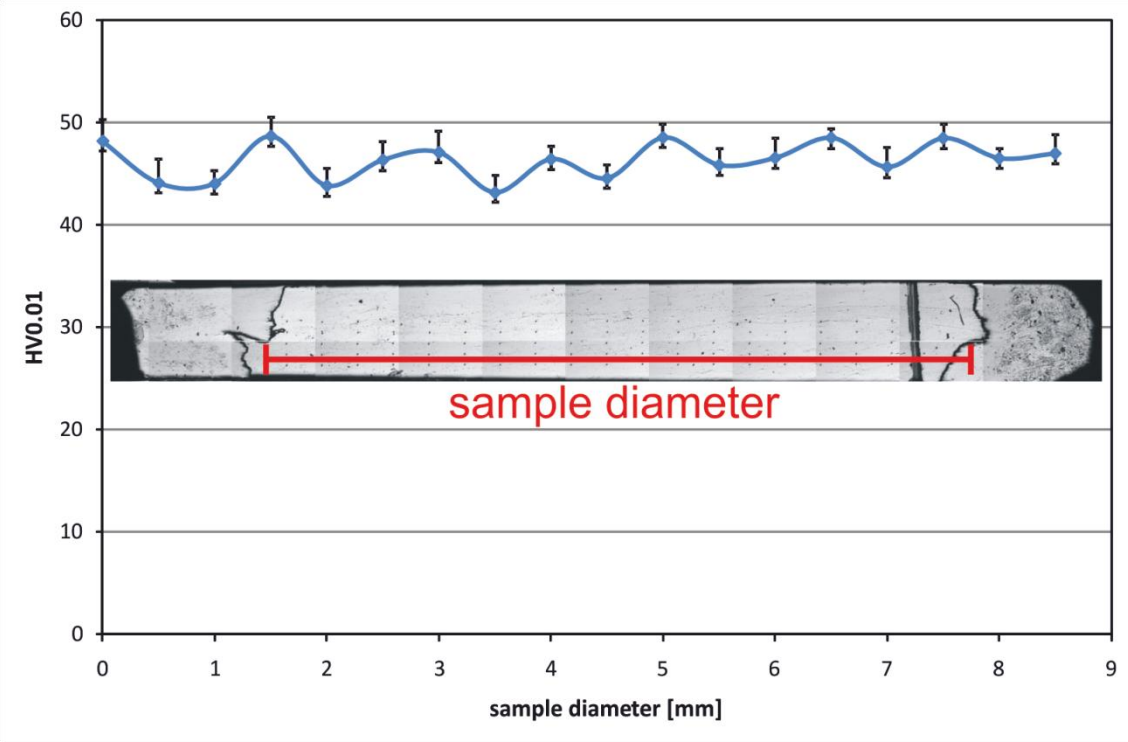

Fig. 4-29. Microhardness measured along the HPT sample diameter.

In the case of the material with a fast recovery rate, such as magnesium, diameter microhardness investigation setup showed no strain dependence, therefore microhardness was measured on the same radial cross section - as used for texture measurements - at the same radius of 3.5 mm for each sample. Although, no strain dependence has been found in the microhardness, as

shown in Fig. 4-29, microhardness has been measured on the same radial cross section as used for the texture measurements. Microhardness was then averaged for entire investigated area and presented in 2-D and 3-D as an average microhardness representative for the given sample surface.

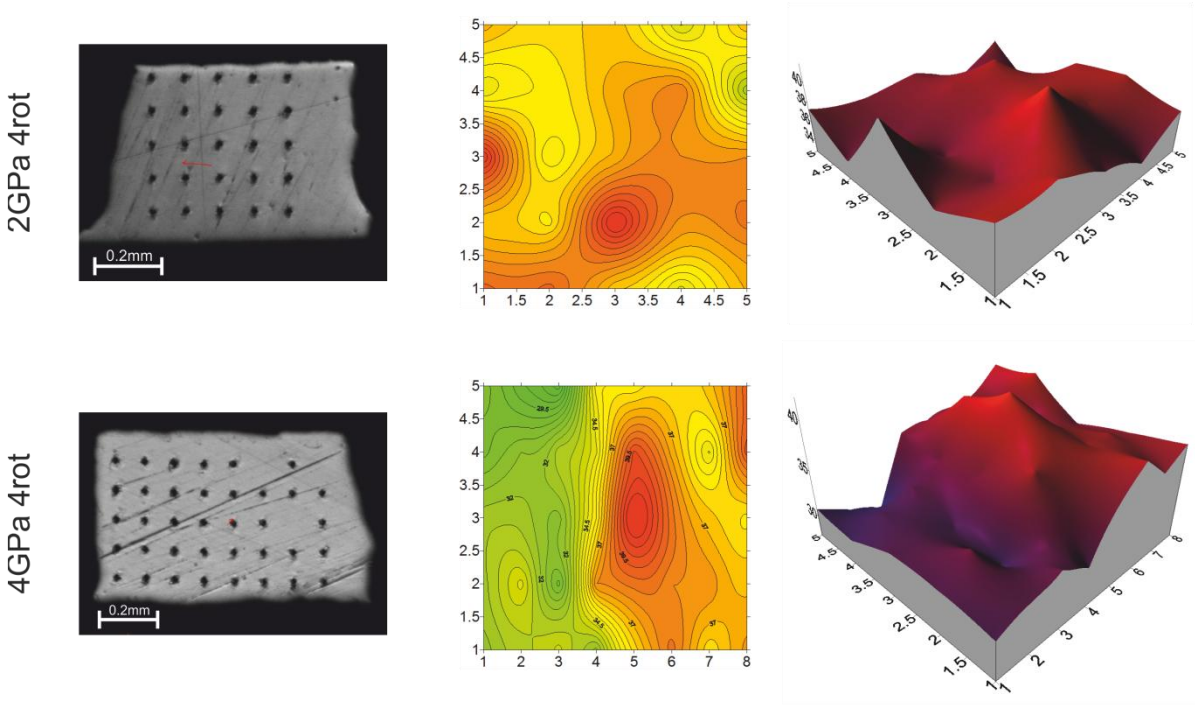

Fig. 4-30. Microhardness: area investigated (left), 2-D and 3-D representation for area investigated (middle and right, respectively) for polycrystalline Mg samples deformed by HPT at 2 and 4 GPa (upper and lower row, respectively).

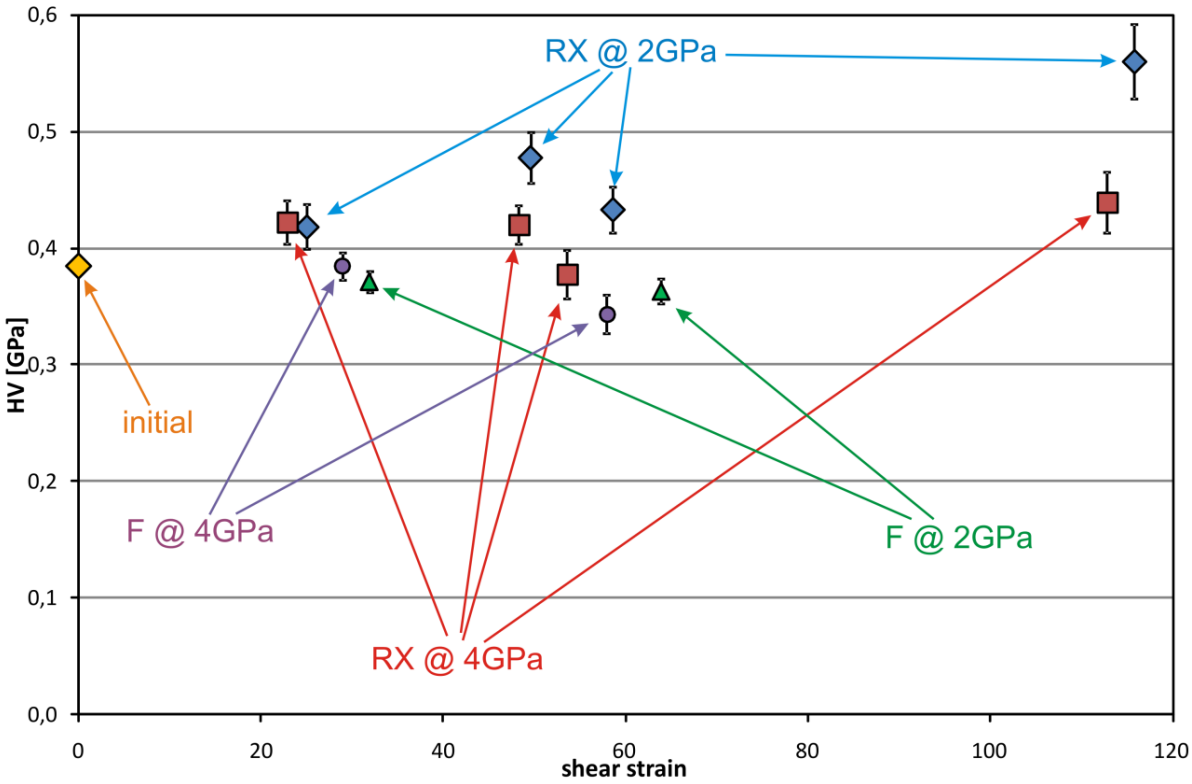

Fig. 4-31. Microhardness of HPT-deformed samples. RX stands for recrystallized and F for frozen material.

4.5 Observations of microstructure

Contrary to the local and global texture investigation, which can derive information on the number of grains involved, very localized microstructural investigation provide a good supplement of overall structure changes for the materials in the ultra-fine grained regime. To enter the desired magnification level, an electron microscopy has to be applied. The Electron Back-Scattered Diffraction (EBSD) investigations were carried out by a system HKL-OXFORD Instruments being a part of SEM Hitachi S-3400N operated at 20kV. A standard procedure of recording EBSD data with 70° sample tilt was applied.

4.5.1 Mg single crystals

As orientation changes and structure fragmentation are particularly interesting in the case of single crystal deformation, a SEM investigation was carried out (as shown in Fig. 3-9).

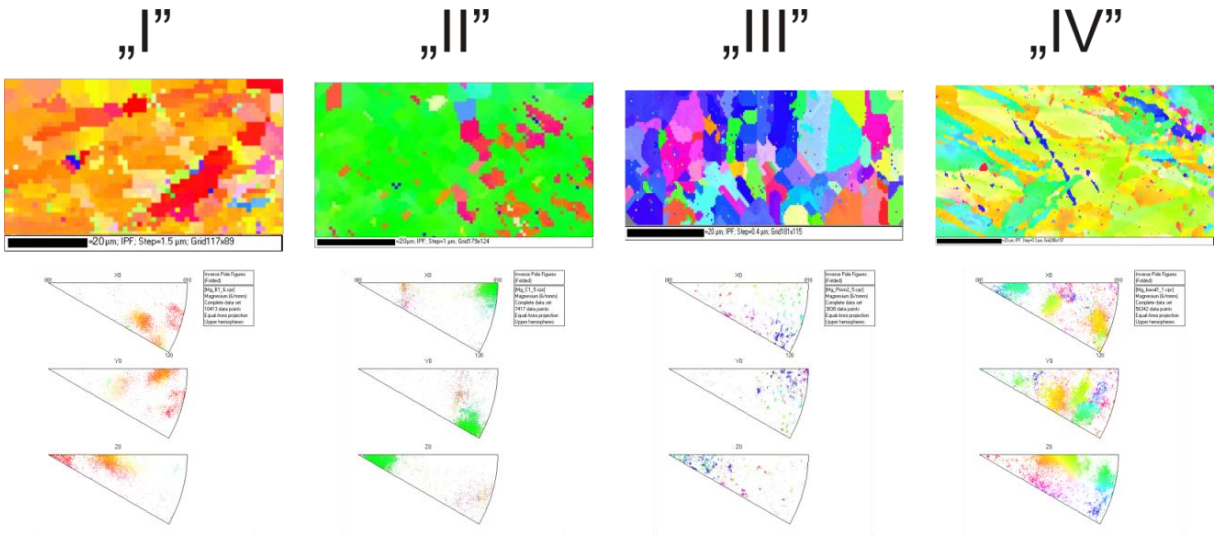

Fig. 4-32. EBSD images recorded for the four single crystal orientations after HPT deformation up to 0.1 rot (shear strain γ≈3). Below, orientation maps in the basic triangle are shown.

The EBSD investigations revealed a microstructure at its early stage of fragmentation, which leads to strong grain size reduction (as shown for polycrystalline material). Twins can be identified within the structure. Reorientation between particular twins shows two typical values of 86.3°, which is a typical reorientation value around c-axis with twinning on $\{10\bar{1}2\}$ plane [25]. The second type of the observed disorientation borders between grains was the value of around 56°, which may be the evidence for reorientation of basal planes around c-axis due to the twinning on $\{10\bar{1}1\}$ plane [25, 73]. However, in the case of polycrystalline Mg, no evidence for twinning was observed, neither by EBSD nor by X-ray texture investigations. The absence of twins in the polycrystalline samples could be explained by the excessive recovery/recrystallization processes, affecting the microstructure during and after the HPT processing.

4.5.2 Mg polycrystals

The EBSD investigations were carried out at the same (radial) cross section as the X-ray texture measurements. The samples were deformed at 2 and 4 GPa at the same strain value of shear strain i.e. approximately at γ=65. EBSD data were collected in steps of 0.15 µm.

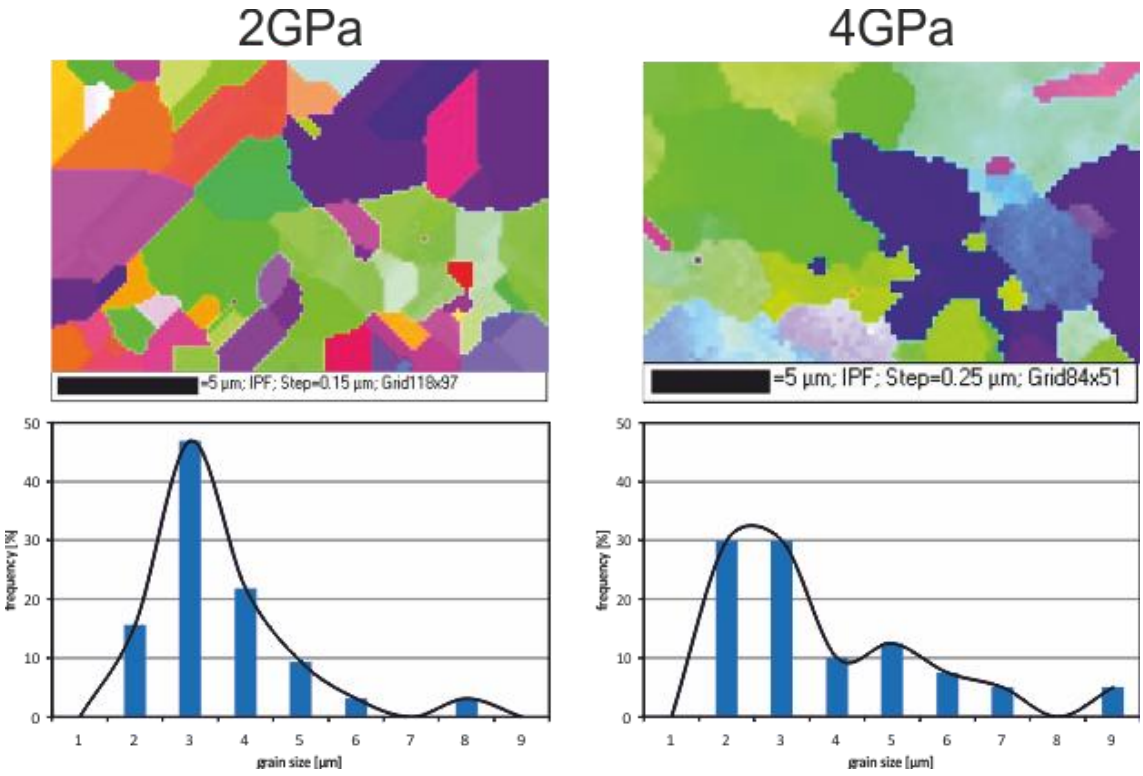

Fig. 4-33. EBSD images and statistics of grain size distribution for the polycrystalline Mg deformed at 2 and 4 GPa (left- and right-hand side, respectively).

Transmission electron microscopy (TEM) imaging was done on the sample cross sections as shown in Fig. 4-34. This specially selected cross section provided the most representative information about the microstructure in the middle of the HPT sample thickness.

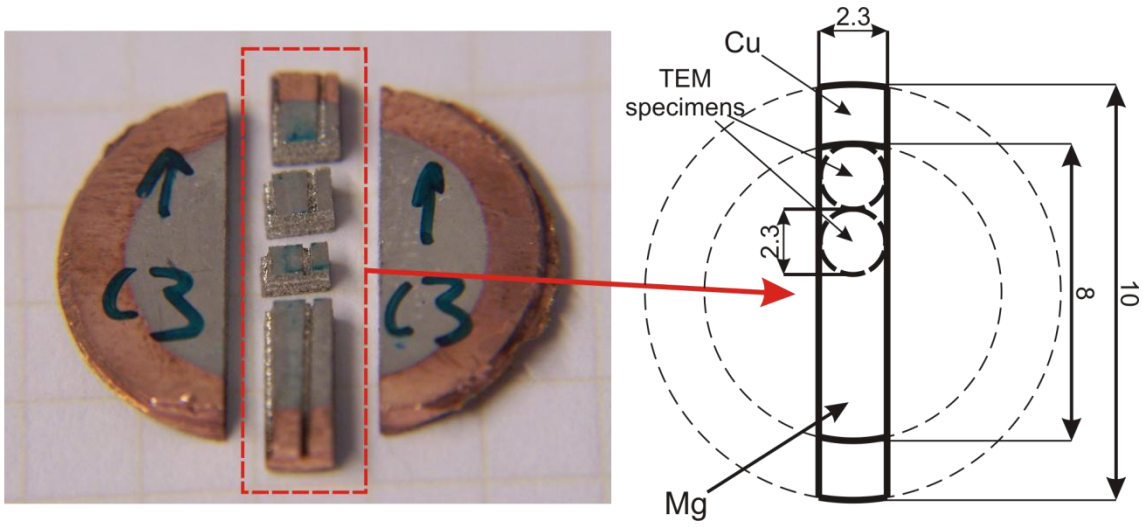

Fig. 4-34. Sample preparation for TEM investigation. TEM specimens are cut off from HPT sample, as shown on the right hand.

Also the TEM investigation were performed on two series of the samples, where the first one was described as Recrystallized (denoted as 'RX'), and the second one was Frozen ones ('F'), respectively (see section 3.1.2.1).

Recrystallized (RX) material

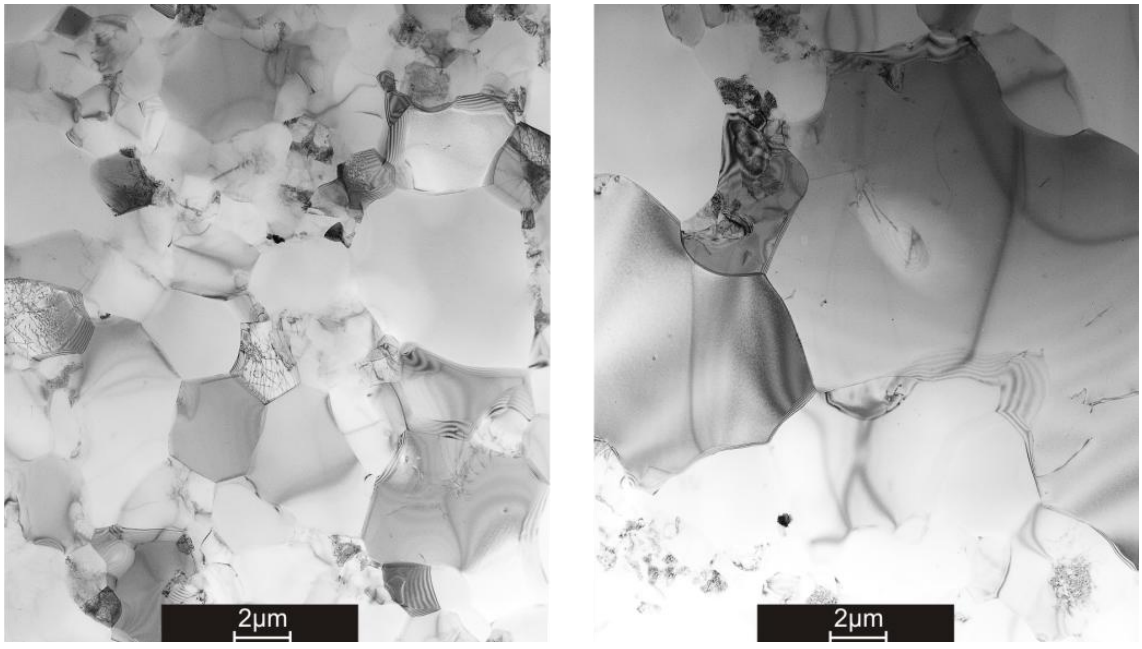

Fig. 4-35. TEM images of recrystallized (RX) HPT sample deformed at 2 GPa up to 1 full rotation (shear strain of about γ≈40).

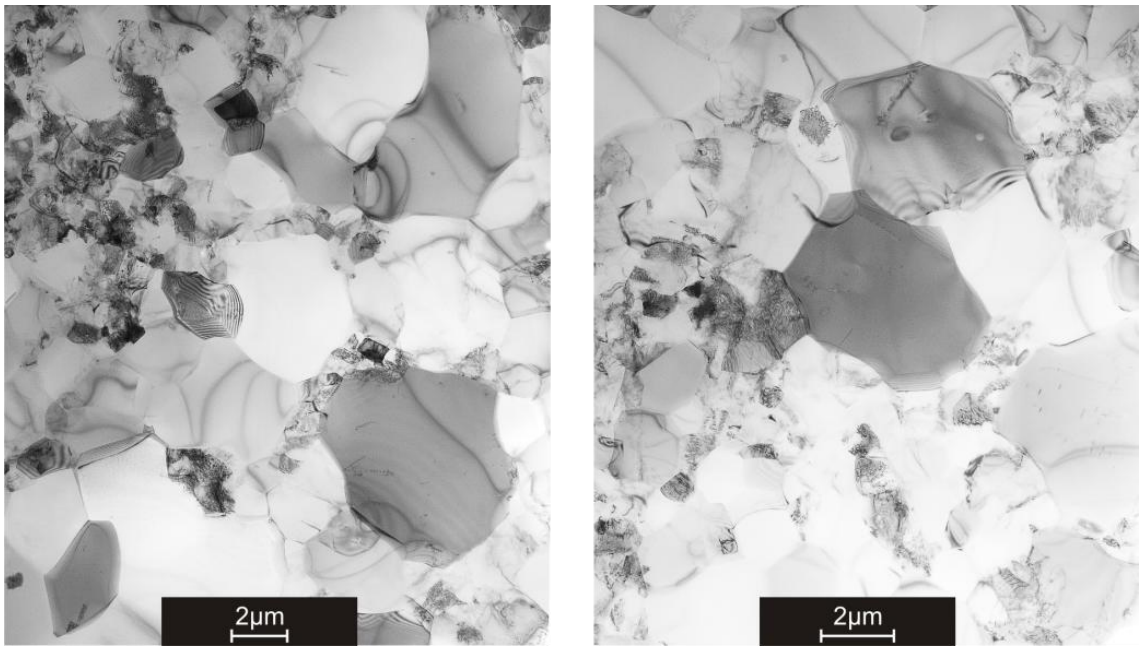

Fig. 4-36. TEM images of recrystallized (RX) HPT sample deformed at 2 GPa up to 2 full rotations (shear strain of about γ≈85).

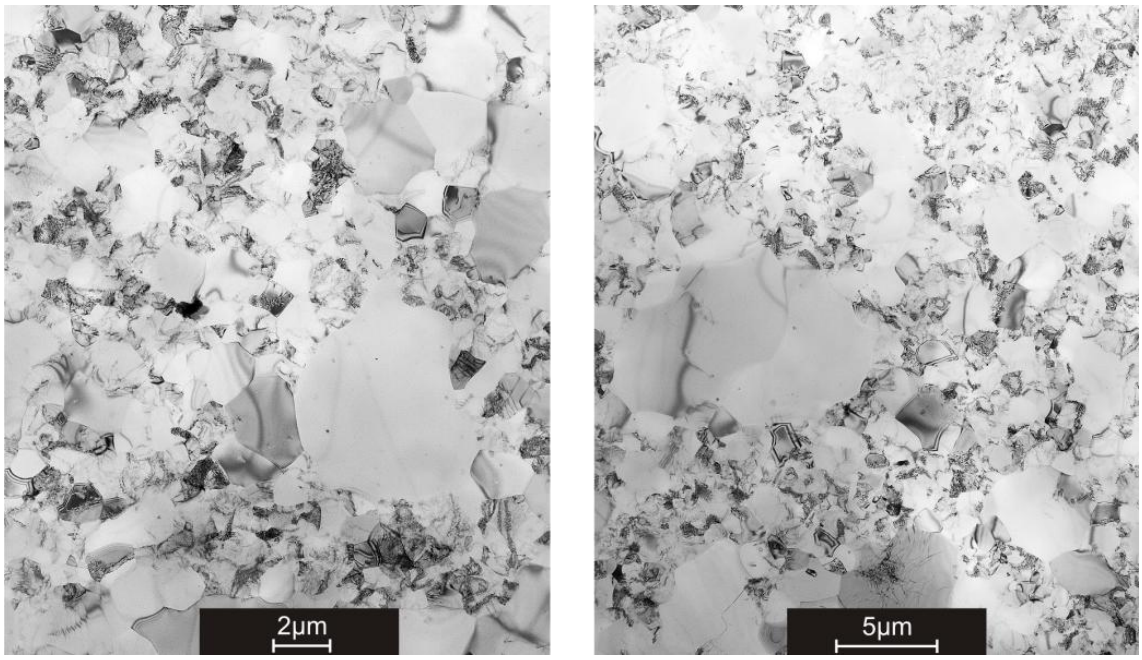

Fig. 4-37. TEM images of recrystallized (RX) HPT sample deformed at 2 GPa up to 4 full rotations (shear strain of about γ≈162).

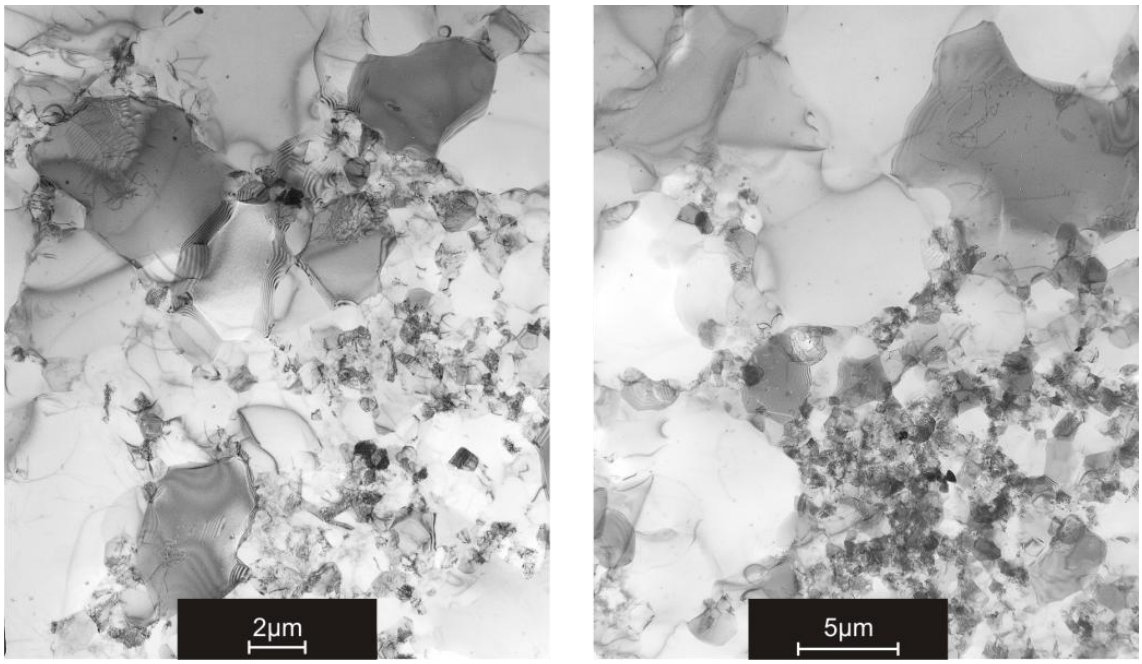

Fig. 4-38. TEM images of recrystallized (RX) HPT sample deformed at 4 GPa up to 4 full rotations (shear strain of about γ≈160).

"Frozen" (F) material

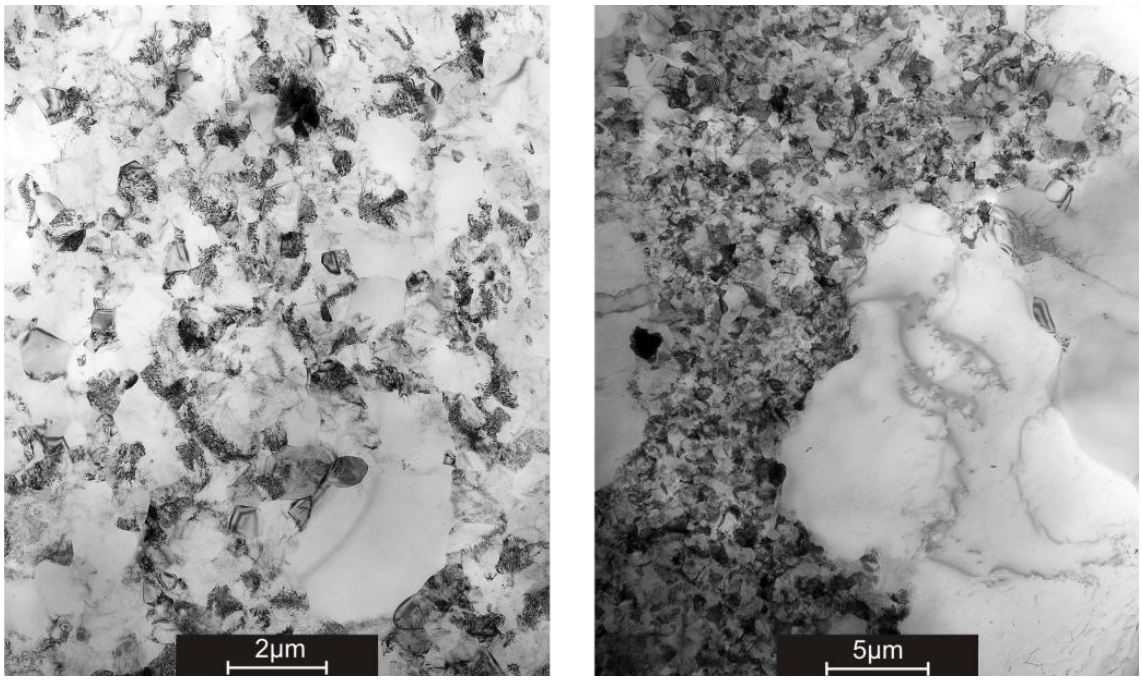

Fig. 4-39. TEM images of frozen (F) HPT sample deformed at 2 GPa up to 2 full rotations (shear strain of about γ≈85).

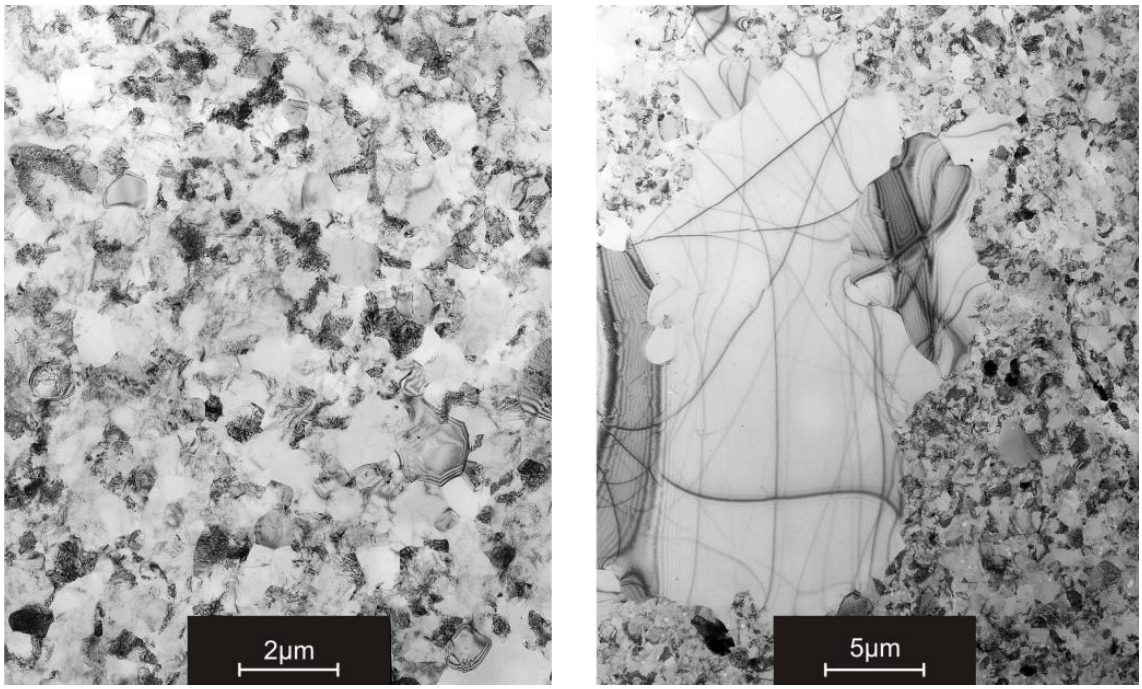

Fig. 4-40. TEM images of frozen (F) HPT sample deformed at 2 GPa up to 4 full rotations (shear strain of about γ≈162).

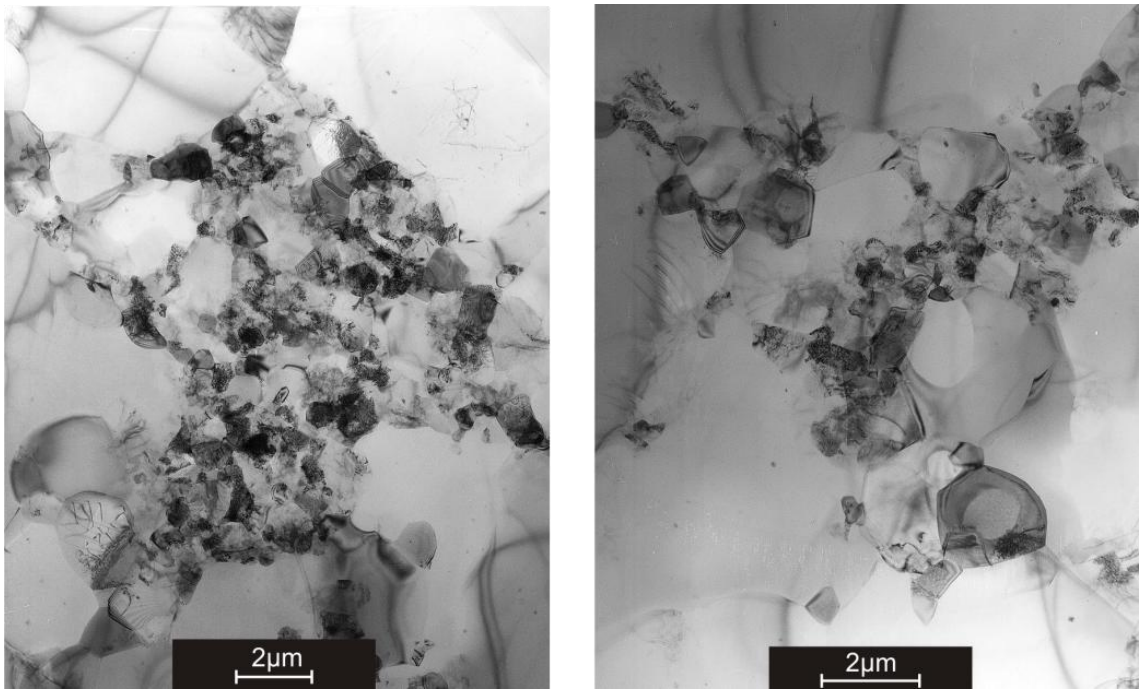

Fig. 4-41. TEM images of frozen (F) HPT sample deformed at 4 GPa up to 2 full rotations (shear strain of about γ≈85).

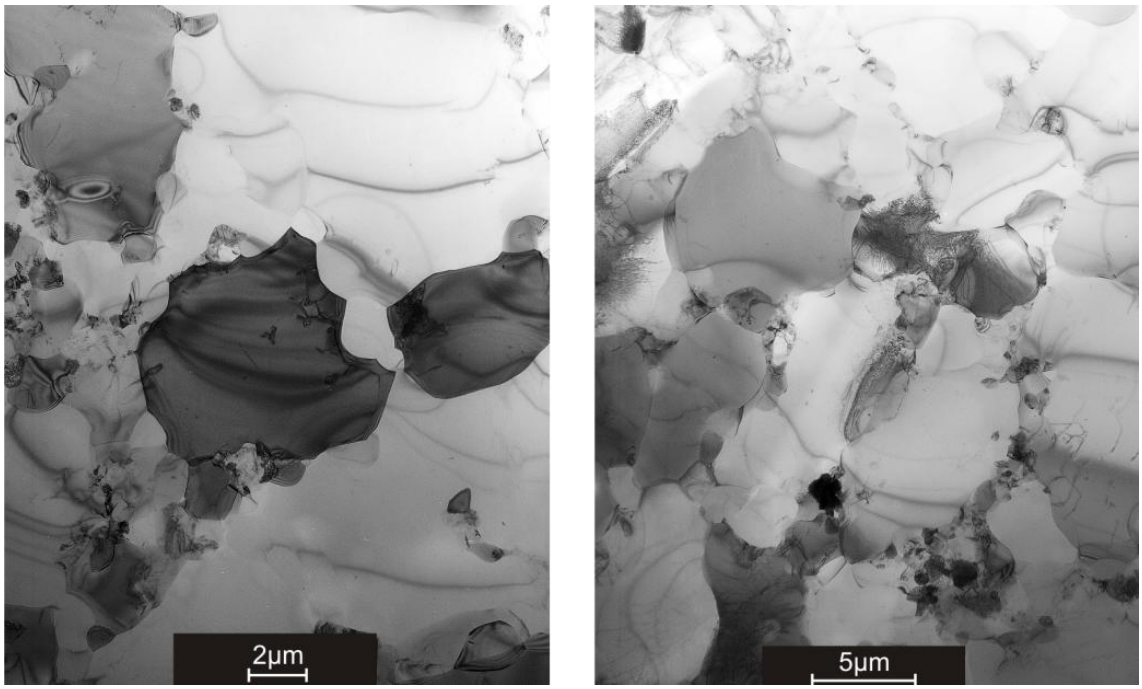

Fig. 4-42. TEM images of frozen (F) HPT sample deformed at 4 GPa up to 4 full rotations (shear strain of about γ≈160).

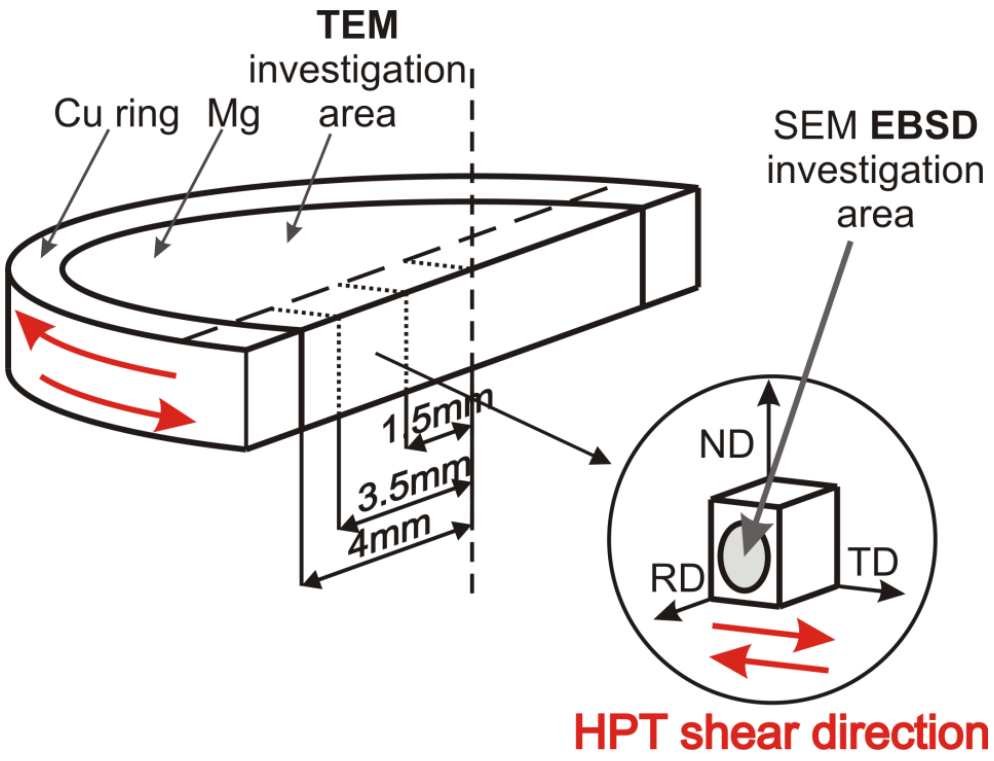

Fig. 4-43. Conventional and radial cross sections for electron microscopy investigations (TEM and SEM EBSD, respectively).

Last not least, Scanning Electron Microscopy (SEM) comprising Electron Back-Scattering Diffraction (EBSD) imaging was used as supplementary research for the TEM microstructure investigations. However, due to the sample preparation procedure, and the intention to correlate the electron microscopy (EM), with results of texture investigation, the sample section was the same as for the texture measurements, as shown in Fig. 4-43.

5 Discussion and conclusions

5.1 Mg single crystals

The single crystalline samples of pure Mg of four selected initial orientations were deformed by High-Pressure Torsion (HPT) at the same amount of hydrostatic pressure of 1.5GPa up to 1 full rotation, which corresponds to the maximum shear strain value of $\gamma \approx 30$ (for an outer perimeter of the sample). All the samples had a diameter of 6mm and the initial thickness of 0.9mm. A careful study of crystallographic texture on the sample surface normal to the torsion axis in the areas along the sample radius (refer to Fig. 4-7) allowed the author to collect the data suitable for determination of texture evolution of the given crystallographic orientation during the HPT deformation process.

Orientation 'I' $[10\bar{1}1]$

From the early beginning of the deformation process the basal component emerges – which can be explained by the compression occurring to the sample at the beginning of HPT deformation (see Fig. 5-3). Then, with increasing torsional strain, the texture slowly changes, revealing a coexistence of the initial $[10\bar{1}1]$ with $[11\bar{2}2]$-fiber components (which has emerged as a result of shear deformation) at first. At the shear strain range from *γ≈3* to about *γ≈6* the enhancement of the initial component can be observed. As the shear strain continues to increase, at the values higher than *γ≈6*, a global decrease of texture intensities can be noticed, which seems to be in good agreement with the global normalized texture sharpness index (J_n) (see section 3.3) characteristics as a function of the shear strain (see Fig. 5-1).

Orientation 'II' $[11\bar{2}2]$

The $[11\bar{2}2]$ orientation seems to be the most stable among the selected ones. From the in-situ HPT deformation curves (see Fig. 4-2) one can see that this orientation can be characterized by its very large material resistance to the shear deformation under the hydrostatic pressure as shown in Fig. 4-2. The reason for this behavior can be explained if one traces its texture evolution. A dominating component (the one which reveals largest volume fraction) is the $[10\bar{1}1]$ one (see Fig. 4-12), which reaches up to 50%, and it is followed directly – with all changes – by the initial $[11\bar{2}2]$ component with volume fractions reaching only about one half of them. The $[10\bar{1}1]$ component is

affected by the escalation of the recrystallization component from an early stage of deformation in a form of a low-intensity spread component near [0001]. This component emerges as a result of static recrystallization, as it is proved for the polycrystalline material (see section 5.2, Fig. 4-17, Fig. 4-18, Fig. 4-19). Initial orientation seems to be affected by the shear deformation fibers $\{10\bar{1}1\}$ and $\{11\bar{2}2\}$, causing its reinforcement arising from active slip systems for this orientation. The component $[11\bar{2}2]$, reaches its maximum at shear strain values *γ≈2* reaching the highest ODF_{max} values among all the selected single crystals initial orientations (highest value achieved by the texture index J_{nmax} = *0.97)*, see Fig. 5-1. In shear strain range of 2 to 5 the dominating component decreases, see Fig. 4-12. When shear strain exceeds the value of 6 a global weakening of texture intensity occurs and spread of the component around the basal position emerges, as a result of recrystallization (Fig. 5-3). Again, it is important to note is the fact that this orientation is the most stable during the deformation, as the initial components are enhanced by the shear deformation and the texture reaches the highest intensities from the point of view of both volume fractions (Vf) and normalized texture Index (J_n) values, and revealing the highest deformation nominal shear stresses (see in-situ HPT curves, Fig. 4-2).

Orientation 'III' $[11\bar{2}0]$ (Prismatic)

The next single crystal orientation to be considered is the one with prismatic planes $(11\bar{2}0)$ oriented in parallel to the sample surface (and at the same time being in parallel to the HPT shear direction). Analyzing the volume fractions and normalized texture index for this orientation some general conclusions can be derived from Fig. 4-14 and Fig. 5-3. Already from the early stage of the deformation one can denote a drastic reconstruction of the existing texture. Shortly after HPT deformation starts, the sample 'loses' its original, prismatic orientation, in favor for the basal orientation. This can be explained by huge effect of the initial compression to the initial prismatic orientation. Due to intense shear deformation of about *γ≈2* even the basal components starts to lose its intensity and $[10\bar{1}1]$ component is arising (see Fig. 4-14 and Fig. 4-13). This component can be believed a consequence of shear deformation, whereas the basal component seems to gain on recrystallization. In the strain range (up to about shear strain of *γ≈10*) one can recognize a slow but monotonic decrease of all components (due to the ongoing shear deformation) except the shear component $[10\bar{1}1]$ this can be confirmed with a global normalized texture index, which reaches its

maximum at $\gamma \approx 10$, with high value of $J_n \approx 0.93$ (high texture sharpness). As it can be expected, the following stage with shear strain of $\gamma > 10$ is characterized by dissipating of deformation component and broad basal (recrystallization) components taking the stage. The prismatic orientation reaches relatively high values of the ODF maximal values, again as a result of the initially strongly evolved basal component.

Orientation 'IV' $[0001]$ (Basal)

Since the basal system is the most easily activated one in Mg hexagonal lattice, it is essential to investigate how a basal-oriented sample will behave in the shear-dominating HPT deformation experiment. At an early stage of deformation, where one can still recognize the influence of the initial compression (see Fig. 4-16), the spread of basal component as well as of deformation component (Fig. 4-15) can be noticed. This configuration remains unstable with increasing shear strain. At shear strain of $\gamma \approx 16$ the recrystallization and deformation components are completely dominating the texture with some coexistence of $[10\bar{1}1]$ component. According to the expectations, when shear strain continues to increase, overall loss of component's intensity can be observed along with the spread of basal (recrystallization) component gaining larger fractions. This setup can be observed since shear strain exceeds the value of $\gamma \approx 15$ (see Fig. 4-16, Fig. 5-3). Because of a relative easiness of deformation in this orientation, one can trace the texture evolution up to the high values, however, as expected, further tendencies are only a prolongation of those observed in shear strain range up to around $\gamma \approx 15$ (see Fig. 5-3, lowest row).

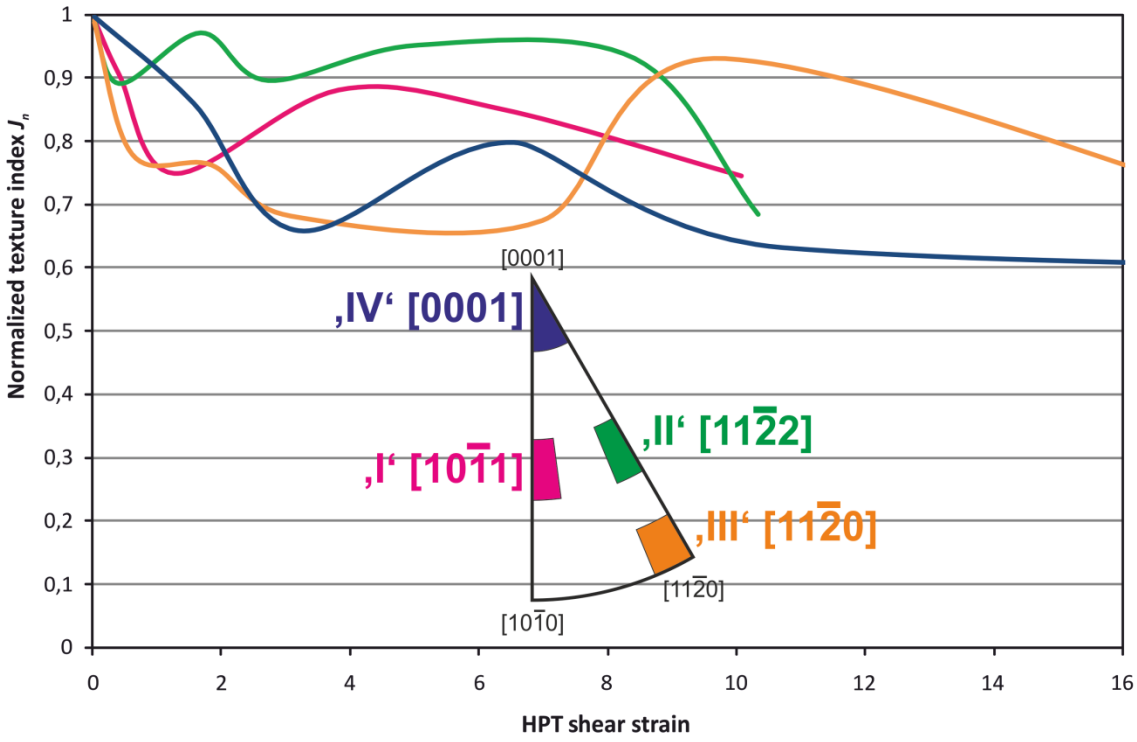

Fig. 5-1. Normalized texture index (J_n) for each of selected single crystal initial orientation as a function of HPT shear strain. Initial orientations according to key map given on the graph.

Fig. 5-1 presents the normalized texture index (J_n) (according to Equ. 3-2) of all orientation of single crystals. The normalized texture index (J_n) provides important information concerning the global texture 'sharpness' for each of the initial orientations in the function of HPT shear strain. Analyzing the texture index changes as a function of HPT shear strain (Fig. 5-1) it can be concluded that its behavior strongly depends on the initial orientation. Each one seems to have its own way of development, but eventually they tend to approach one point with only moderate texture. The pyramidal orientations $[10\bar{1}1]$ and $[11\bar{2}2]$ (denoted as 'I' and 'II') seem to maintain a sharp texture, especially orientation 'II' seems to be the most stable one during HPT deformation. On the contrary, the prismatic $[11\bar{2}0]$ and basal $[0001]$ orientations ('III' and 'IV') shows marked tendency to rebuild the texture. Especially the prismatic orientation tends to a quick and marked texture reconstruction. Both of them show local minima in the normalized texture index – as a function of shear strain which are achieved when orientations 'I' and 'II' are strong. Later, the final 'texture broadening' can be observed (see Fig. 5-1). The normalized texture index evolution (Fig. 5-1) together with a detailed texture development study (Fig. 5-3) seems to be in a good agreement with in-situ HPT deformation

characteristics (presented in Fig. 4-2). Orientation 'II' tends to be the most stable, revealing at the same time the highest nominal shear stress during HPT deformation. Another pyramidal orientation, denoted as 'I', reveals a moderate shear stress level, whereas its texture index shows similar characteristics to orientation 'II'. The a basal orientation ('IV') reveals the lowest shear stress level showing at the same time the biggest loss of texture sharpness along with the HPT deformation. The strong texture rebuild of the prismatic orientation ('III') results with shear stress on the similar level to the basal one ('IV'). As a general conclusion it can be stated that single crystal orientations close to the HPT shear components (both pyramidal ones: 'I' and 'II') tend to reach the high shear stresses (due to the induced activation of the secondary slip systems) while the orientations with easy basal slip system oriented along the HPT shear direction ('IV') or in parallel the HPT compression axis (which induces immediate texture rebuild) – as for orientation 'III' – can be characterized by low shear stress level. The difference in HPT nominal shear stresses can amount to 100%, see Fig. 4-2. The orientation migration of the investigated Mg single crystal orientation can be summarized in terms of the schemata presented in Fig. 5-4.

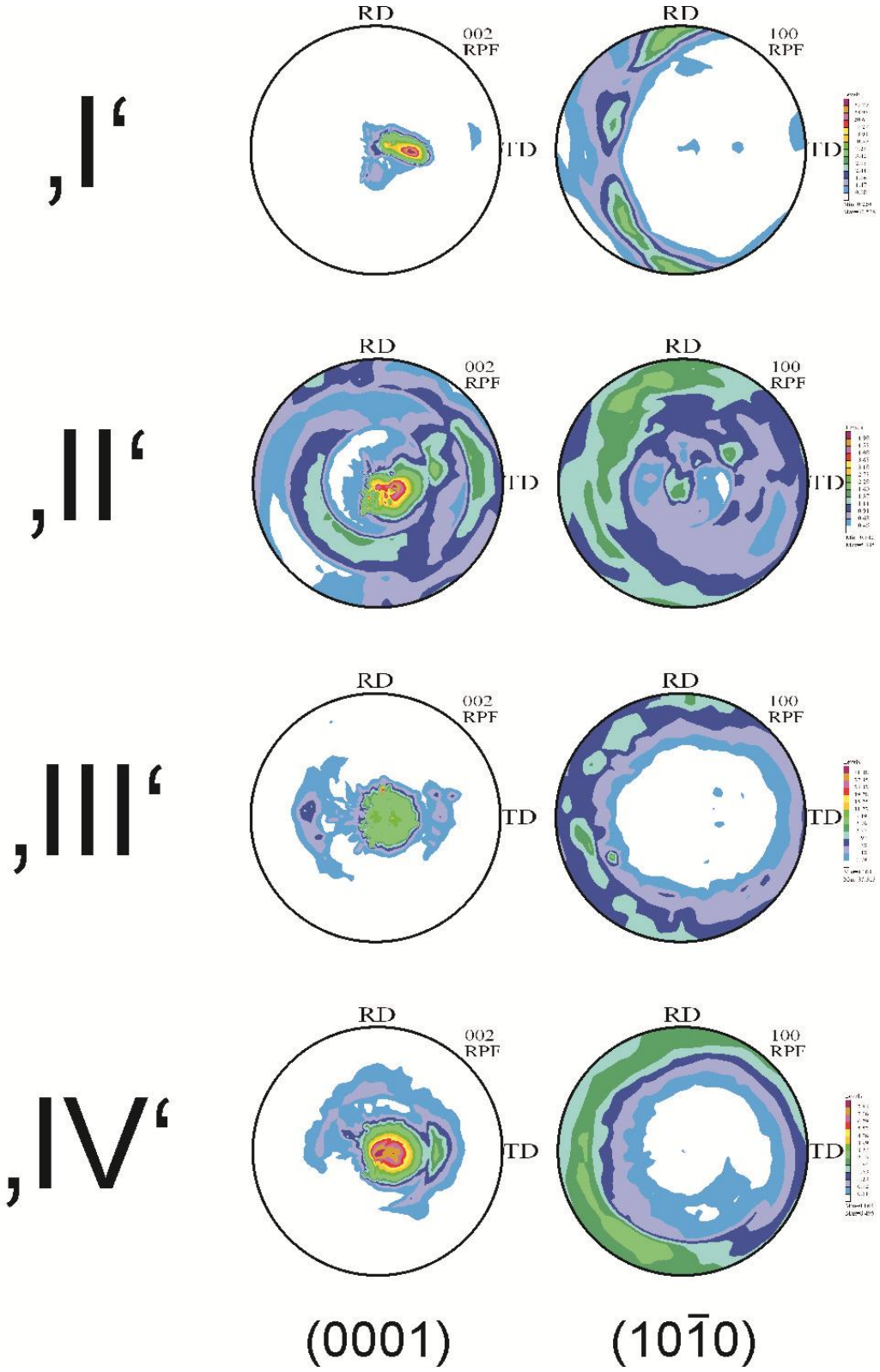

Fig. 5-2. The four investigated initial Mg single crystal orientations after HPT deformation as seen on Complete Pole Figures (CPF) of $\{0001\}$ and $\{10\bar{1}0\}$ reflections, respectively.

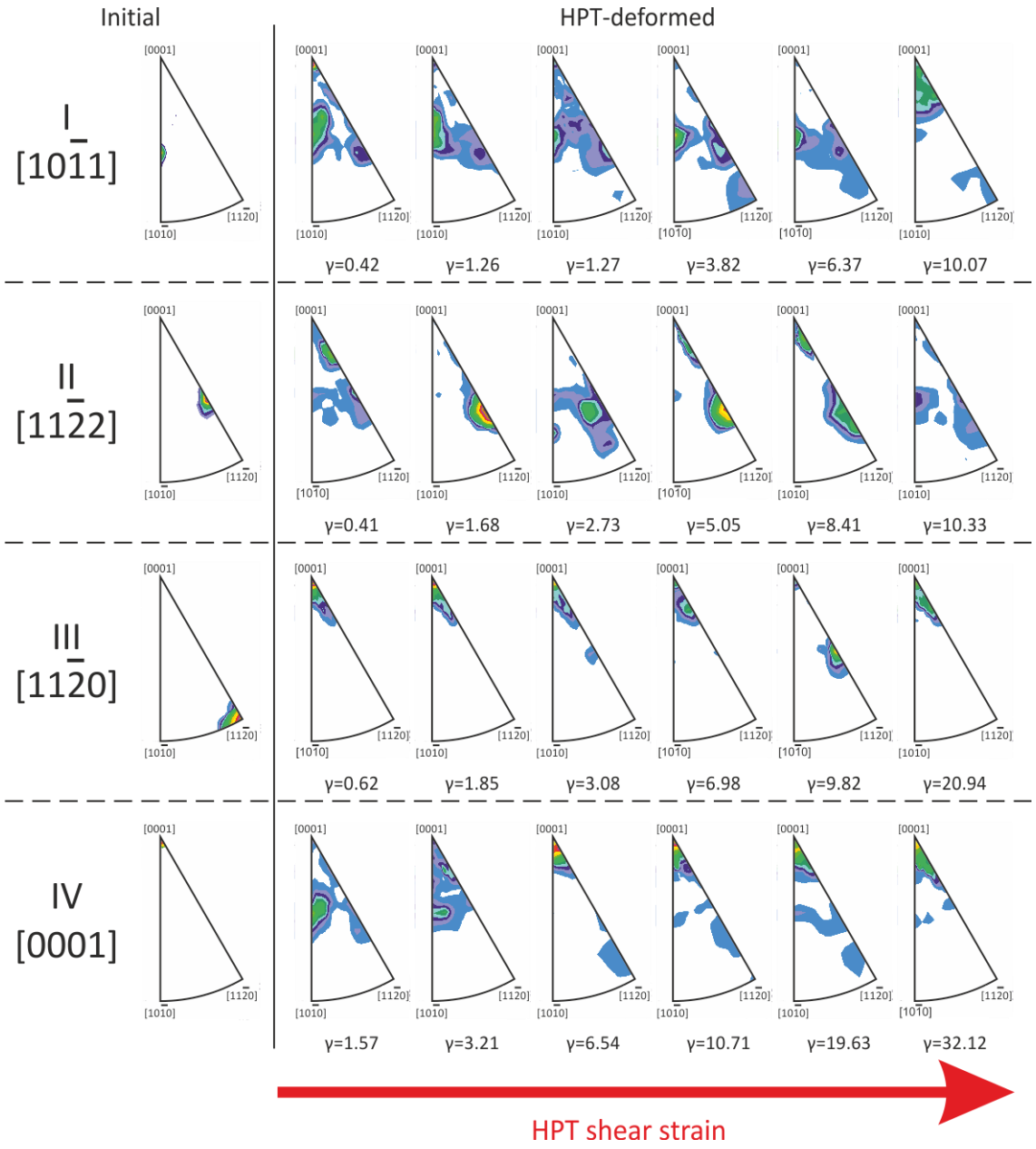

Fig. 5-3. The texture evolution in Mg Single Crystals subjected to HPT deformation as seen on Inverted Pole Figures (INV) of Normal Direction [0001]. Shear strain as given on the graph.

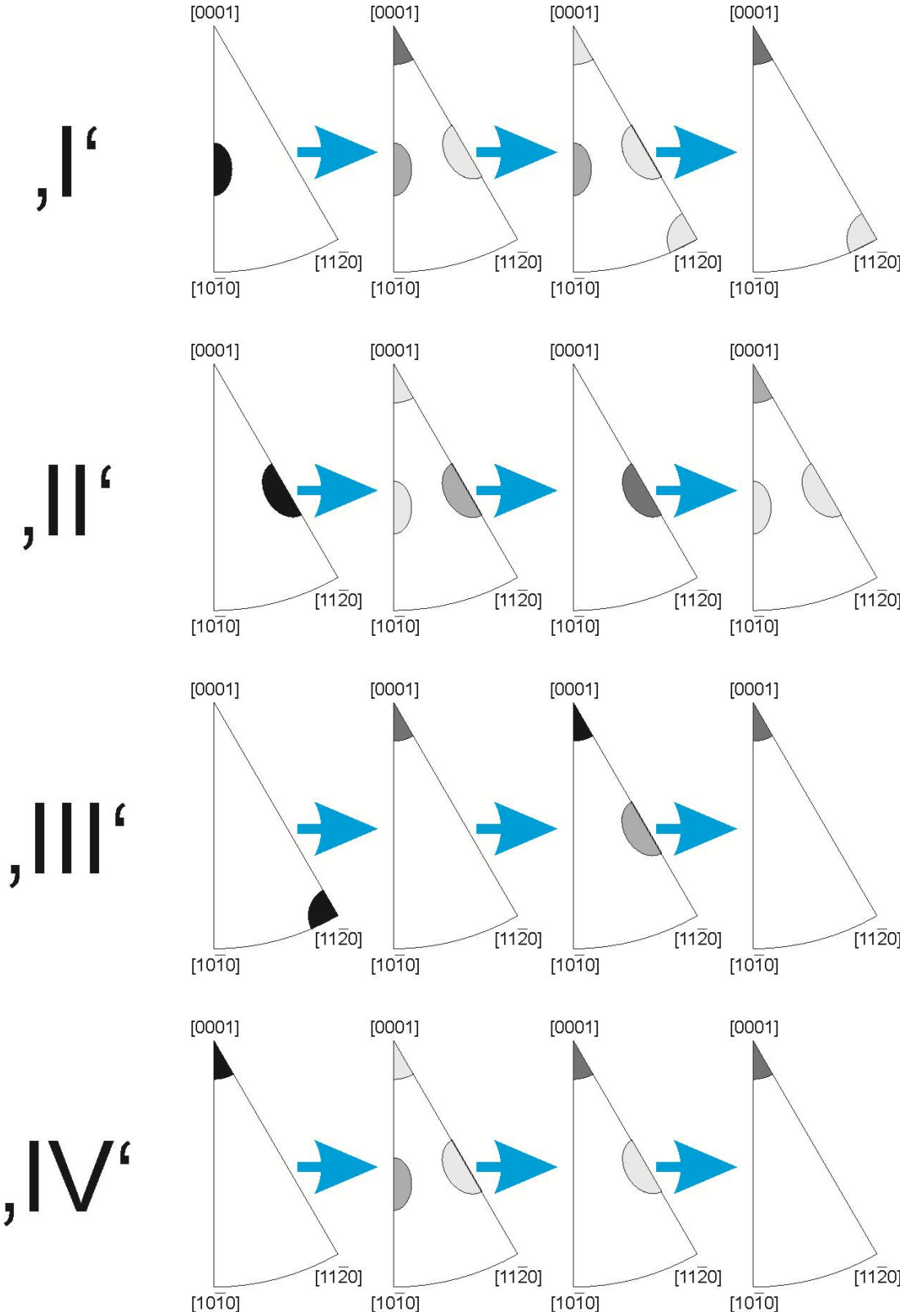

Fig. 5-4. Summary of texture evolution of Mg single crystals during HPT deformation. Grey areas represent intensities of components, the darker the more intense.

5.2 Mg polycrystals

The investigated single crystal orientations, after HPT deformation, are very similar to the textures observed for the polycrystalline material, in the range of shear strain of γ= 10 to 20 (compare Fig. 5-2 for single crystals and Fig. 4-17, Fig. 4-18 and Fig. 4-19 for polycrystalline material). A direct comparison is possible, while these results are shown in the form of RPFs (see section 3.3), measured with the same experimental setup (measurement on normal sample surface, see Fig. 4-7 and Fig. 3-3 a). This similarity comes from the fact that the HPT deformation produces a specific texture in magnesium – both in single and polycrystalline one – although a particular initial single crystalline orientation has a different path of texture evolution, with, however, the same type of final texture after some certain shear strain. Furthermore, it is in good agreement with the Mg polycrystalline samples deformed in HPT results.

As described in section 4.2.2, the crystallographic textures were investigated systematically on the plane normal to the radial direction (see Fig. 3-9 b) on the samples in distances of 1.5 and 3.5 mm from the sample centre (and a rotation axis, at the same time), thus receiving textures of different shear strains from the same sample. From the ECAP deformation [74, 75] and free end torsion of Mg [76, 77] it is known that the shear deformation of Mg can be represented by the so-called 'B-fiber' or 'ideal shear orientation' (Fig. 5-5 b). The initial texture of the above considered HPT-deformed Mg has a strong extrusion character, which means that basal planes have been arranged along the ND direction, and prismatic ones in parallel to TD direction, resulting in a horizontal axis in the corresponding pole figure (Fig. 5-5 a). During HPT processing one expects the horizontal extrusion component to be rotated by 90° in order to approach the shear direction being parallel to the TD direction and finally matching the typical shear component called 'B fiber' or 'ideal shear orientation', see Fig. 5-5a [74-77].

However, the texture of HPT deformed Mg, does not reach the final position of the B-fiber, by stopping the rotation, and leaving a 'deviation angle α' off this ideal shear position (as shown in Fig. 5-5 c and d), see also [78]. The angle α increases with the strain and hydrostatic pressure applied with the HPT processing. Former suggestions by Beausir [75] and Skrotzki [54] and the presented, author's results which include TEM investigations (see section 4.5) led to the conclusion that the limitation of rotation arises from the onset of recrystallization mechanisms [79]. These – at least to some part – tend to re-establish the initial texture as it existed before the HPT processing. However, it is not clear yet whether this recrystallization occurs *during* HPT processing (as a *dynamic* one) or –

driven by the release of enormous hydrostatic pressures at 4 GPa – *after* the HPT processing (as a *static* recrystallization).

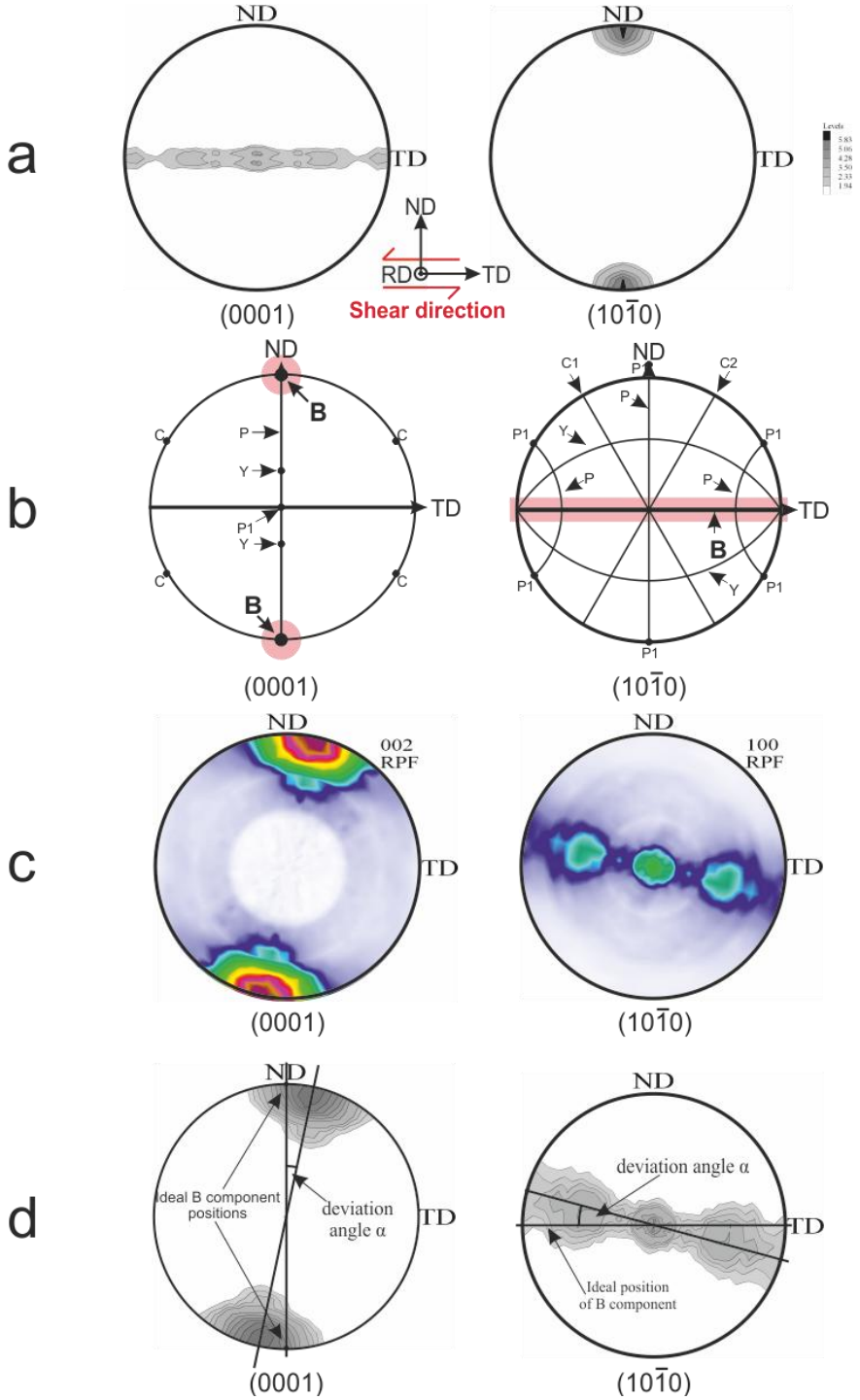

Fig. 5-5. Texture analysis of polycrystalline Mg after HPT deformation: (a) initial texture of fine-grained (Hot-extruded) Mg, (b) expected main shear deformation components positions, (c) experimental texture and (d) α angle representing deviation of experimental textures to ideal position of shear fiber B as seen on (0001) (left) and $(10\bar{1}0)$ (right) Pole Figures.

In this situation, the idea was to produce another set of HPT samples which were to be immediately cooled at 77 K after HPT processing, in order to avoid strong static recovery processes affecting the texture and other properties. In order to distinguish these samples from the previous ones, these samples with mainly dynamic recovery component have been called the 'Frozen' (F) ones, whereas those with a marked additional component of static recovery the 'Recrystallized' (RX) ones. In the 'F' material, where static recrystallization has much less affected the structure, the shear deformation components are stronger. This difference can be seen in the textures achieved with both values of hydrostatic pressures applied, i.e. 2 as well as 4 GPa.

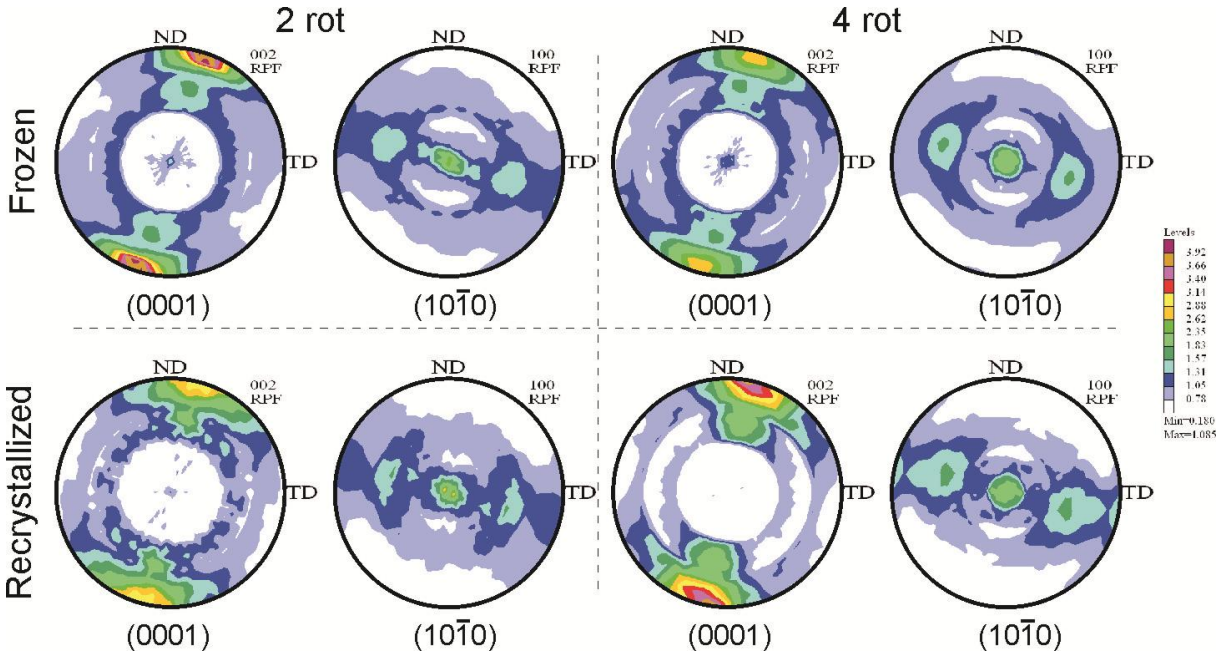

Fig. 5-6. Basal and prismatic pole figures (measured as shown in Fig. 3-9) with 'Frozen' (upper) and 'Recrystallized' (lower) samples deformed under a pressure of 2 GPa, with 2 (left) and 4 (right) rotations, corresponding to shear strains $\gamma = 55$ and $\gamma = 110$, respectively.

The effect of the two different material treatments (F and RX) is best seen on the extend of deviation angle α. Fig. 5-8 gives a survey of how the deviation angle α depends on the pressure and on the type of materials used. The increase of α with increasing pressure applied can be interpreted with a higher contribution of recrystallization process induced through the release of pressure [78]. So one would expect a *lowering* of *deviation* angle α for textures of samples F, as a consequence of suppression of recrystallization by freezing the samples. However, the experiments on F samples show the opposite (Fig. 5-7): frozen samples F exhibit an *increase* of α, and it can be concluded that

dynamic recrystallization (DRX) acting *during* (or immediately after) HPT must play a role here. In fact, it seems that it is the dynamic part of recrystallization which hinders the shear components to form, while the static part of recrystallization (SRX) appears to change the texture in favor of the shear components.

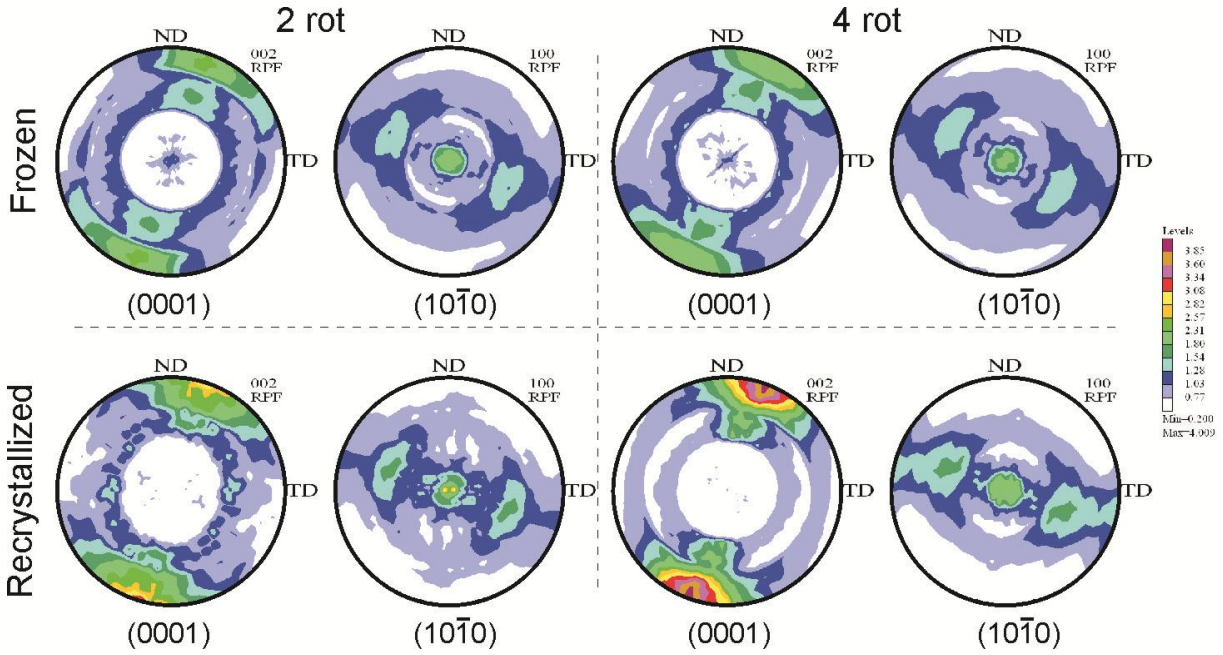

Fig. 5-7. Basal and prismatic pole figures (measured as shown in Fig. 3-9) with 'Frozen' (upper) and 'Recrystallized' (lower) samples deformed under a pressure of 4 GPa, with 2 (left) and 4 (right) rotations, corresponding to shear strains $\gamma = 55$ and $\gamma = 110$, respectively.

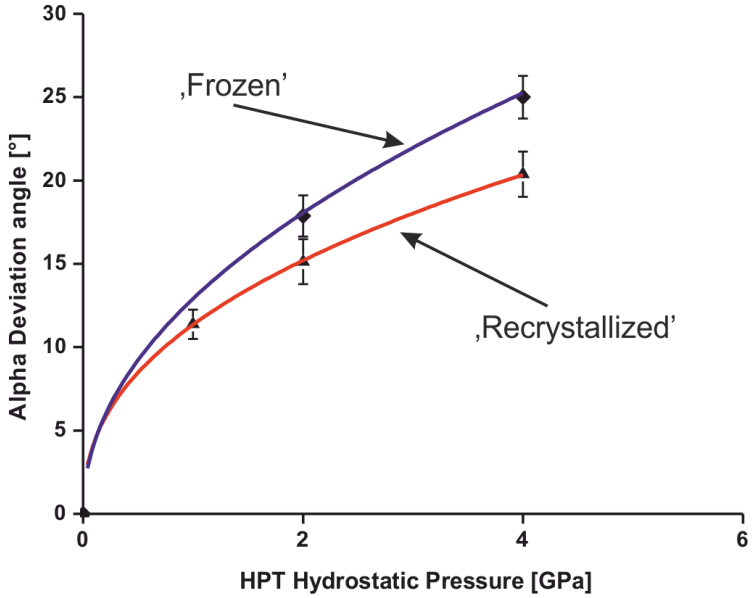

Fig. 5-8. Deviation angle α of B-component (see [76] and Fig. 5-5 b for notation) in HPT-deformed Mg and its dependence on the applied HPT hydrostatic pressure and material state.

The determination of the exact deviation angle together with the exact component for each of the investigated HPT-samples setup (see Tab. 5-1) allowed 'tracing' the dominating, main texture component and providing the exact volume fraction data of this particular component independently of applied pressure or post-processing material treatment. It is essential to correlate the volume fraction as a function of shear strain with global texture sharpness (by means of normalized texture index J_n) – see Fig. 5-9 and Fig. 5-10.

Sample		Averaged deviation angle α [°]	Representative component
'Recrystallized'	1GPa	11.38	(0 1 0)[8 0 1]
	2GPa	15.13	(0 1 0)[6 0 1]
	4GPa	20.38	(0 1 0)[13 0 3]
'Frozen'	2GPa	17.88	(0 1 0)[5 0 1]
	4GPa	25	(0 1 0)[7 0 2]

Tab. 5-1. Averaged deviation angles α and position of corresponding components for RX and F material deformed at different HPT hydrostatic pressures.

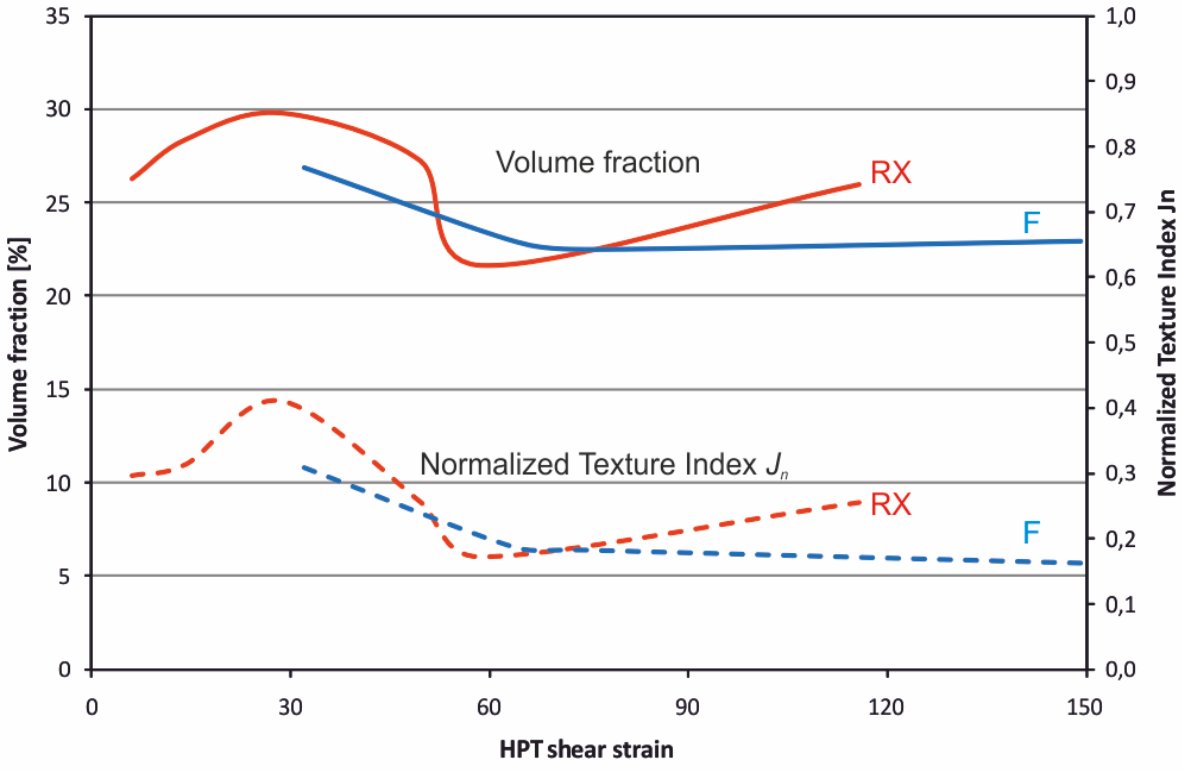

Fig. 5-9. Volume fraction of the dominating component and global normalized texture index J_n as a function of HPT shear strain, for 'Recrystallized' (RX) and 'Frozen' (F) sampled deformed at the HPT hydrostatic pressure. of 2 GPa

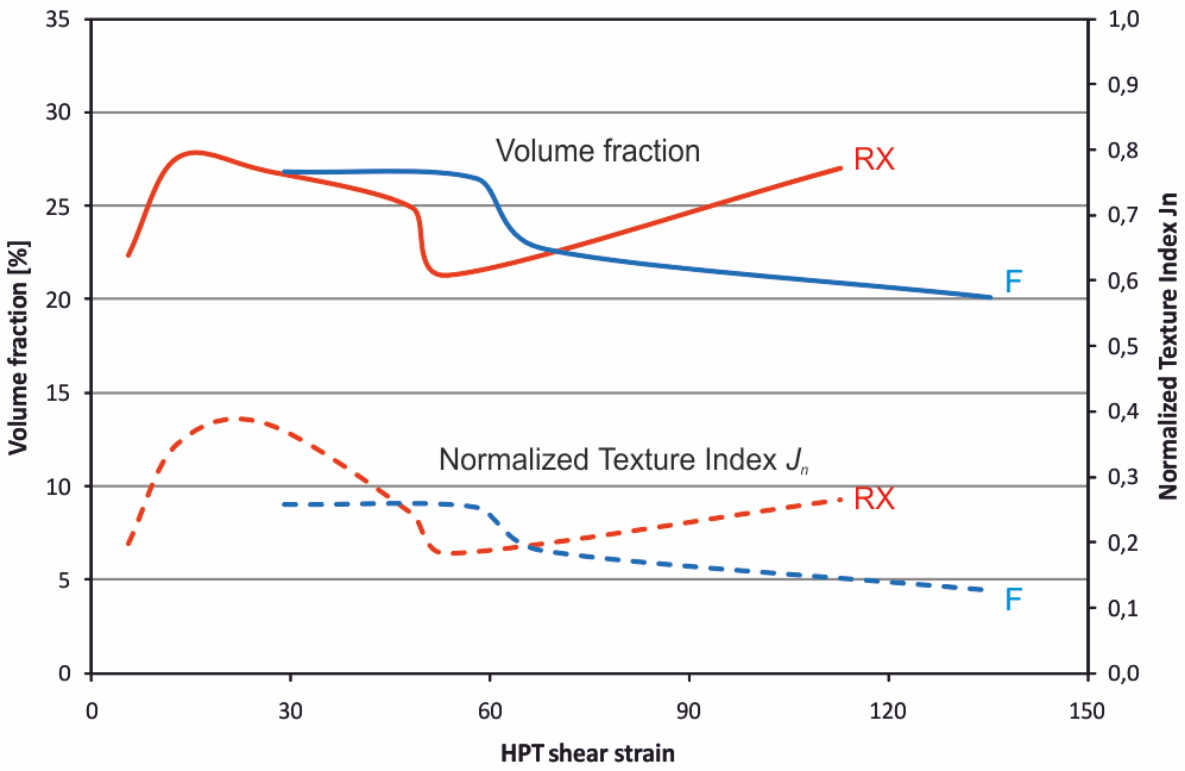

Fig. 5-10. Volume fraction of the dominating component and global normalized texture index J_n as a function of HPT shear strain, for 'Recrystallized' (RX) and 'Frozen' (F) sampled deformed at the HPT hydrostatic pressure of 4 GPa.

As it can be derived from the graphs presented above, the dominating component (which seems to be at a slightly different position at different pressures, etc) rules the overall, global texture 'sharpness'. Note that in comparison to the single crystals results (Fig. 5-1) the texture is markedly 'softer' and broader. When comparing the results from the 'Recrystallized' and 'Frozen' material, deformed at the same hydrostatic pressure, one immediately recognizes that static recovery (SRX, present in RX samples) causes the volume fraction of dominating component to increase at high strains. The same applies to the global texture sharpness. For 'Frozen' material, which has not been affected by SRX, the texture weakens markedly with increasing strain for both 2 and 4 GPa. This difference in texture sharpness between RX and F material, however occur by a certain critical strain (see Fig. 5-9 and Fig. 5-10). This can be observed at HPT shear strains of $\gamma \approx 60$, for both investigated HPT pressures, but it seems to occur earlier in the case of 4 GPa. This may be the result of much stronger 'unloading effect' with higher hydrostatic pressure used for deformation [80]. Nevertheless, the dominating components' analysis showed clearly that the

recovery/recrystallization effects have an outstanding effect on the formation of texture, in such a way that DRX and SRX seem to act in contrary directions.

Besides all of these arguments, again emphasized, it should be that the term 'dynamic recrystallization - DRX' used here includes both the true dynamic recrystallization occurring during HPT as well as the recrystallization which occurs during pressure release. Under 'static recrystallization – SRX' all the processes which operate *after* pressure release of HPT processing are understood

.

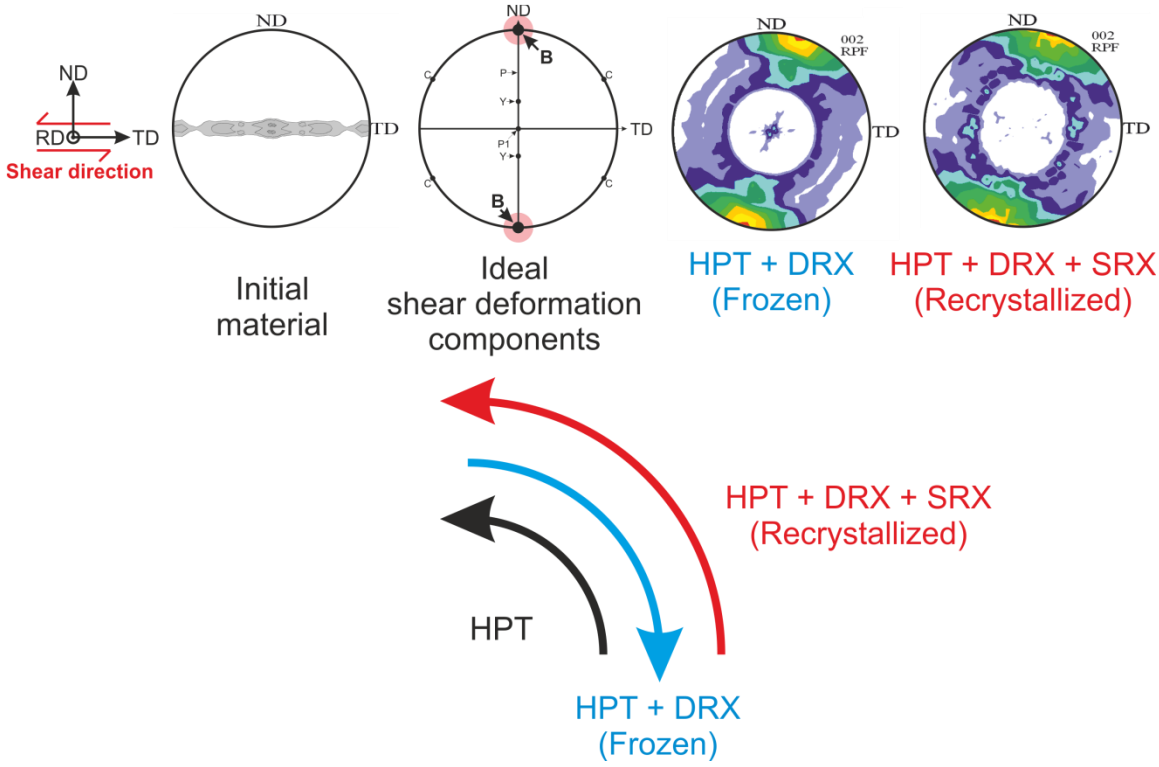

Fig. 5-11. Texture evolution during HPT deformation of polycrystalline Mg. Reference system with shear direction is given on the left hand of upper row.

Tension tests were performed with Mg samples which were HPT deformed at 2 and 4 GPa with 2 rotations ($\gamma = 55$) for both RX and F type, and, for comparison, also with the 'initial' extruded material (Fig. 5-12). It can be seen that HPT deformation achieves an increase of maximum strength from approximately 80 MPa up to 140 – 200 MPa, which corresponds to an increase of more than 100%. More important in connection with the texture investigations is the fact that the ultimate strength of Recrystallized 'RX' –type HPT Mg samples is clearly *higher* than that of Frozen 'F' type samples. However, at the same time, the ductility of RX samples is markedly *smaller* than that of F

samples. All these effects are surprising since one would expect lower strength and higher ductility of samples which have experienced a higher extent of recrystallization, i.e. dynamic *plus* static recrystallization as in the case of RX samples. The situation is somewhat analogous to that of the texture findings where the RX samples showed unexpected behavior concerning *advanced* reaching of the ideal shear texture. Also the influence of the hydrostatic pressure shows the same unexpected tendency as it has been seen from the texture investigations: the higher is the hydrostatic pressure applied, the higher is the deviation from the shear texture, the higher is the ultimate strength and the lower is the resulting ductility. From these all findings one can draw the conclusion that it is the texture variation which strongly affect the mechanical properties rather than grain size.

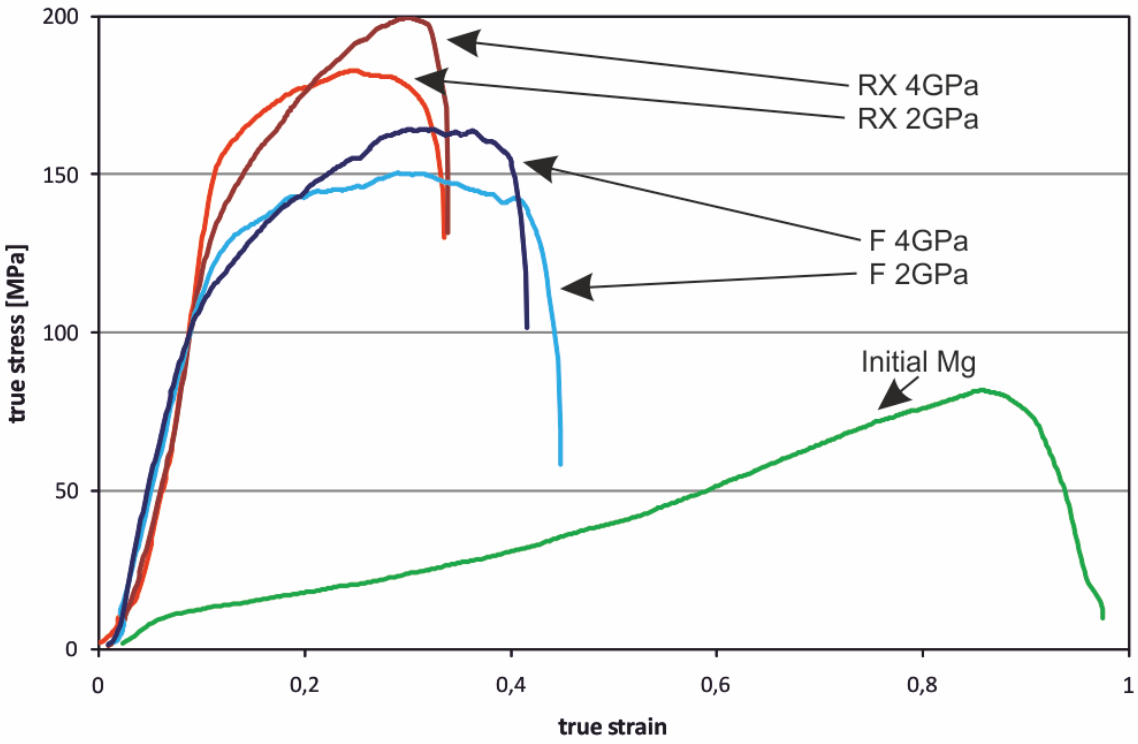

Fig. 5-12. Tension stress characteristics of HPT deformed pure Mg at 2 and 4 GPa comparing 'Frozen' (F) and 'Recrystallized' (RX) samples, as well as pure Mg before HPT treatment. 2 und 4 rotations correspond to shear strains $\gamma = 55$ and $\gamma = 110$, respectively.

In order to have a reliable proof of this interpretation, careful microstructural observations by TEM investigations were initiated, and for optimum comparison, microstructures with the same shear strain $\gamma = 110$ were analyzed. The investigations exhibit the presence of two phases, i.e. as-deformed material with small grains (with an average size of few hundreds of nanometers), and

recrystallized material with grains of micrometer size. The volume fractions of these phases turned out to be independent of the strain applied; however, with increasing pressure, the volume fraction of recrystallized material is markedly increased. Most important is the observation (Fig. 5-13) that the F material exhibits a larger fraction of small grains than the RX material, irrespective of the pressure applied. Moreover, the grain size in both phases is clearly smaller in the F material than in the RX material. All these observations clearly prove that texture of the microstructure which arises from the dynamic part of recrystallization acts in the way usually expected from any structural relaxation process. This part seems to be mainly responsible for the deviation from expected shear texture, for the relatively low stress and, for the enhanced ductility.

TEM findings are in good agreement with SEM EBSD data analysis. As shown in Fig. 4-33, the material deformed at lower hydrostatic pressure (2 GPa) exhibits the smaller, deformation-induced grains, with an average size of 2-3 μm. On the contrary, material deformed at 4 GPa, which experienced more dynamic recovery/recrystallization, show larger, recrystallized grains, with an average size of 5-6 μm, as observed in Fig. 4-33.

The microstructures which experienced additional static recrystallization processes reveal a texture closer to the position of shear texture components, exhibit a higher strength and a lower ductility than the dynamically recrystallized structures. It can be concluded that the textures and mechanical properties observed in HPT Mg (and presumably in other hcp materials) behave much differently to that observed in HPT Cu (as a representative of fcc materials) [65, 81], not at least due to the stronger impact of textures to mechanical properties in the case of Mg (and presumably other hcp materials).

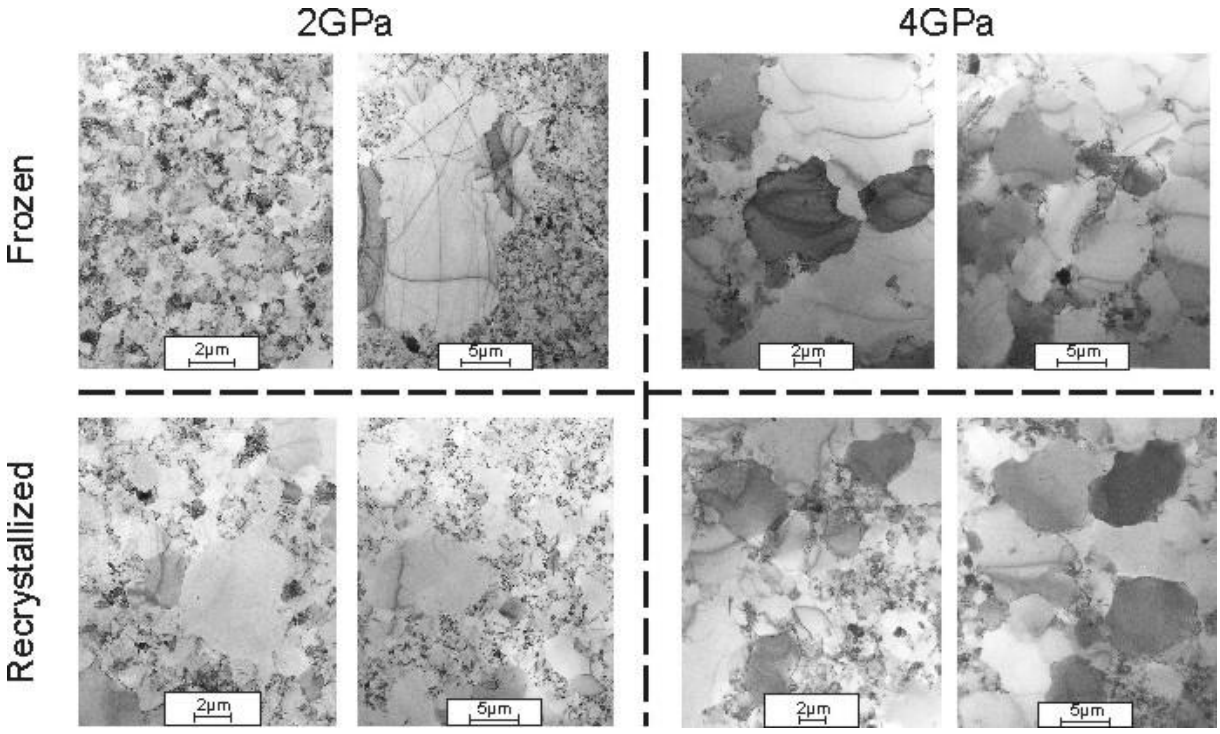

Fig. 5-13. A survey of TEM observations of polycrystalline Mg deformed by HPT at 'Frozen' and 'Recrystallized' samples deformed at 2 and 4 GPa (left- and right-hand, respectively). All samples have been deformed up to approximately the same shear strain of γ = 110.

6 Summary

Samples of single- and polycrystalline magnesium of 99.85 wt. % purity were subjected to deformation by High-Pressure Torsion. In the case of polycrystalline material, a variety of hydrostatic pressures, HPT strains and of material post-processing treatments also was applied. Using an advanced crystallographic texture analysis and correlating its results with selected mechanical properties (such as microhardness and tension tests) in combination with detailed studies of the microstructures (by both TEM and SEM, including EBSD techniques), general conclusions have been stated.

Considering HPT-deformation of selected orientations of single crystals it can be concluded that the orientation strongly affects the deformation process, mainly by differences in activated slip systems. It seems that the High-Pressure Torsion enables activation of non-preferred deformation systems, such as prismatic slip and twinning when the preferred orientations are close to the shear plane. After reaching of certain strain between about γ = 10 to 20, all initial orientations tend to show a global decrease of texture intensity together with enhancement of broad basal component. This feature is similar to the deformation textures in the polycrystalline materials. The latter can be understood as an agglomerate of textures of deformed single crystallites, which tend to reach one specific final texture, regardless of initial orientation and regardless of initial grain sizes. These findings allow a general conclusion that in HPT deformation the initial material state does not affect the final texture nor the microstructure related to it, i.e. that there is no evidence for any texture heritage.

The studies of particular initial orientations of ***single crystals*** allow drawing the following conclusions:

- the pyramidal orientation $[\mathbf{10\bar{1}1}]$ ('I') reveals the activity of two secondary slip systems (of pyramidal type $\langle a+c \rangle$ on planes $\{11\bar{2}2\}$ and $\{11\bar{2}3\}$). In addition, this orientation, due to activation of the secondary deformation modes indicated, seems to be a moderately 'hard' one in comparison to the other initial orientations investigated;
- the other pyramidal orientation $[\mathbf{11\bar{2}2}]$ ('II') enables easy activation of secondary slip system, i.e. pyramidal slip $\langle a+c \rangle$ on planes $\{11\bar{2}2\}$ and $\{11\bar{2}3\}$, being at the same time the

'hardest' orientation with respect of HPT deformation, reaching the highest recorded shear stress values of all single crystal HPT deformations considered. Moreover, this orientation is the most stable one, showing the lowest re-building of texture during HPT deformation among all initial orientations investigated;

- the prismatic orientation $[\mathbf{11\bar{2}0}]$ ('III') reveals operation of the basal system in the beginning, and later the activation of a secondary system, which can be correlated with the strong hardening of the in-situ HPT deformation characteristics at $\gamma = 9.8$. This orientation is characterized by a drastic, immediate change of orientation in the very first HPT deformation stage, from the prismatic orientation to a mainly basal one;
- the basal orientation $[\mathbf{0001}]$ ('IV') seems to be the 'softest' one with respect to HPT deformation, as it is indicated by the in-situ deformation characteristics. Easy activation of basal slip is enabled at the lowest shear stress level until secondary slip systems get active, which is common for all the investigated orientations;
- regardless of the initial orientation, the main part of the HPT deformation is carried by secondary (pyramidal $\langle a + c \rangle$ type) and tensile twinning deformation modes, and after a certain strain level all investigated orientations seem to reach a broadened, basal orientation (already after structure fragmentation is well developed), being typical also of the polycrystalline deformed material.

As it can be derived from the above mentioned findings and from the presented experimental data, a close correlation between the evolved textures in single- and ***polycrystalline material*** can be observed. The higher is the shear strain induced, the more the textures coincide. The main reason of this is the fact that already from the early stages of the HPT deformation, the single crystal samples are subjected to the *sam*e structural fragmentation processes than the polycrystalline ones, making the deformation processes (together with the texture evolution) increasingly similar to those of the polycrystalline material. The approach to the same final texture seems to be entirely independent of the original, initial orientation of the single or polycrystalline sample subjected to the HPT deformation, although the paths to that final texture are different especially in case of the single crystalline samples. That is why the critical shear strain being necessary to reach the final, constant texture depends on the initial orientation. However, coincidence always occurs in a range of shear strains of γ ≈ 10.

The crystallographic textures observed correlate with mechanical properties. The investigations of microstructure provided sufficient data to understand the texture evolution of magnesium during High-Pressure Torsion deformation. It is essential to say at this moment that HPT deformation causes the evolution of a specific, sharp texture being a variant of ideal shear texture expected for Mg. In fact, the HPT texture corresponds to pure shear texture twisted by a certain angle. This angle tends to increase with the applied hydrostatic pressure up to approximately 20°. This 'pressure effect' on the developed texture can be explained by the pressure dependent occurrence recovery/recrystallization processes during and after the HPT deformation. A more detailed analysis of these processes in terms of dynamic (DRX, during HPT) and static (SRX, after HPT) recovery/recrystallization was possible by performing additional experiments suppressing the recovery/recrystallization. It has been shown that the texture evolution in pure Mg subjected to HPT deformation tends to achieve the ideal shear components positions as a result of shear deformation, whereas the dynamic part of recrystallization suppresses this texture development, at the same time being responsible for the deviation of texture from ideal position. When such a deformed material is affected by static recrystallization, however, the main shear texture components are pushed towards their ideal positions. The specific effects of the DRX and SRX have been confirmed by the microstructural investigations, done by EM. These microstructural investigations did not show any evidence of twinning as it has been already indicated by the texture investigations, and thus cannot account for the deviations of dominating texture components from ideal shear position.

To sum up, the investigations of current PhD thesis showed that neither the initial texture nor the initial grain size affects the final HPT texture and microstructure. This observation is also true for the single crystalline material, which tends to reach the same texture as the polycrystalline one. What has a marked effect on the microstructure and mechanical properties of HPT-deformed material are the applied HPT hydrostatic pressure and the post-processing treatment, i.e. the specific influences of the static and/or dynamic recovery/recrystallization. It has been shown that polycrystalline Mg gains ductility with dynamic recrystallization but looses ductility, while static recrystallization enhances the material strength although decreases the ductility at the same time.

7 Appendix

7.1 Hexagonal lattice conventions applied

As the hexagonal close packed (hcp) lattice can be presented in (at least) few conventions (Bunge, Matties [66, 82]), see differences in Fig. 7-1. Keeping the same reference system is a requirement that must be kept in order to process investigation data correctly. Both conventions (Bunge and Matties) can be defined in LaboTex software.

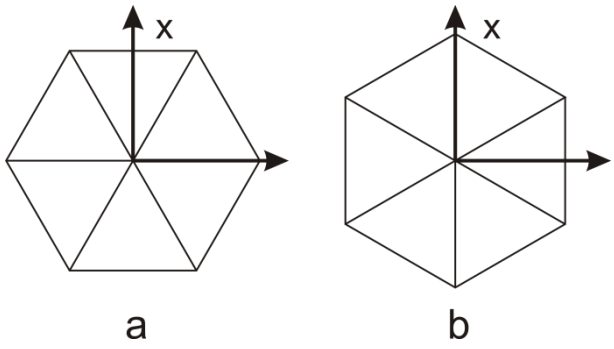

Fig. 7-1. Bunge (a) and Matties (b) conventions of hexagonal lattice notification. Matties convention is used in presented dissertation.

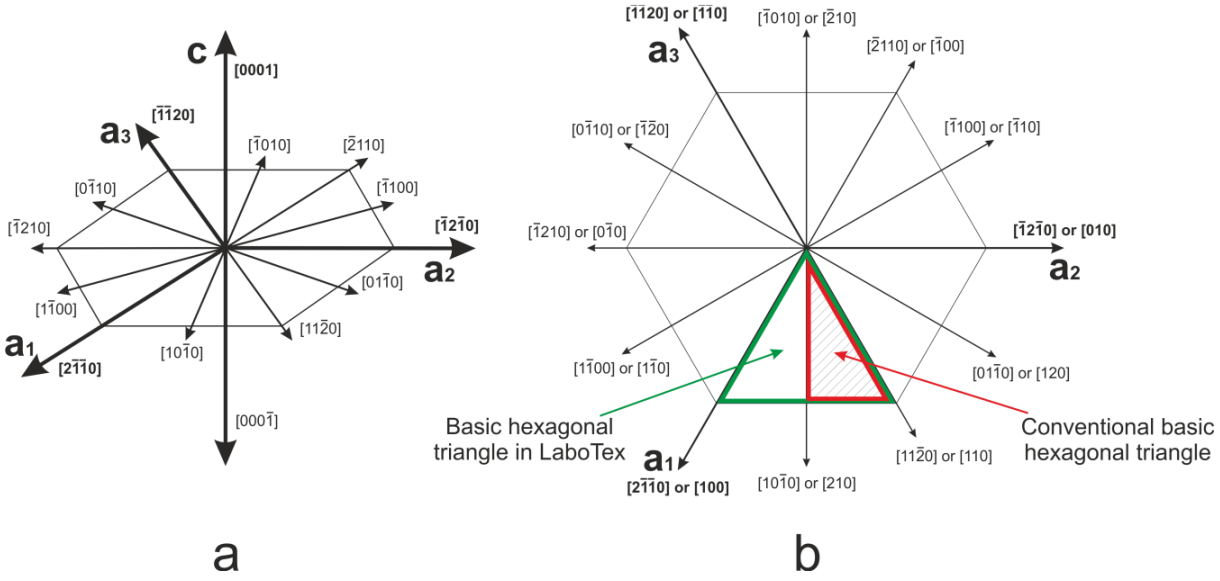

Fig. 7-2. Hexagonal convention used in the presented dissertation (a) and relationship between the basic triangles used in LaboTex software (b).

It is essential to present the data keeping the same reference system. As shown in Fig. 7-2, conventional basic triangle for hexagonal lattice is one half of the basic triangle presented by the LaboTex software, thus all the presented Inverted Pole Figures (INV) of the single crystals investigations are normalized in such a way so they represent the conventional hcp basic triangle (limited by the $[0001]$, $[10\bar{1}0]$ and $[11\bar{2}0]$ axes).

For an additional compatibility of the presented results (which are presented by the software used for data processing) one should be in perfect agreement with converting 3-digit onto 4-digit (used for hexagonal notation) Miller-Bravis indices. Below conversion the principles are gathered and presented.

For the conversion from **regular to hexagonal** lattice (where <uvw> represents regular and <UVTW> hexagonal lattice):

Directions:

$$U = (2u - v)/3$$

$$V = (2v - u)/3$$

$$T = -(u + v)/3$$

$$W = w$$

an example:

$$\langle 100 \rangle \Leftrightarrow \langle 2\bar{1}\bar{1}0 \rangle$$

$$\langle 210 \rangle \Leftrightarrow \langle 10\bar{1}0 \rangle$$

Planes:

$$U = u$$

$$V = v$$

$$T = -(u + v)$$

$$W = w$$

an example:

$$\{002\} \Leftrightarrow \{0002\}$$

$$\{100\} \Leftrightarrow \{10\bar{1}0\}$$

$$\{101\} \Leftrightarrow \{10\bar{1}1\}$$

$$\{102\} \Leftrightarrow \{10\bar{1}2\}$$

For the conversion from **hexagonal** to **regular** lattice (where <UVTW> represents hexagonal and <uvw> regular lattice):

Directions:

$$u = U - T$$

$$v = V - T$$

$$w = W$$

an example:

$$\langle 2\bar{1}\bar{1}0\rangle \Leftrightarrow \langle 100\rangle$$

Planes:

$$u = U$$

$$v = V$$

$$w = W$$

an example:

$$\{2\bar{1}\bar{1}0\} \Leftrightarrow \{2\bar{1}0\}$$

7.2 '4-point Test'

While for the polycrystalline samples the HPT deformation is assumed to be homogenous for the same radius regardless of the radius direction chosen [41, 42, 83], the question about representativeness of the results measured along one arbitrarily selected radius only in the case of the single crystalline samples gains on importance. Although there are assumptions built on the geometry of HPT deformation together with slip planes alignment during the deformation process which indicate that the measurement taken along one selected radius will be representative for the entire sample (with the same radius value, due to strain gradient along sample's radius) [84], an experimental check seemed to be necessary in order to correct the data collection and interpretation.

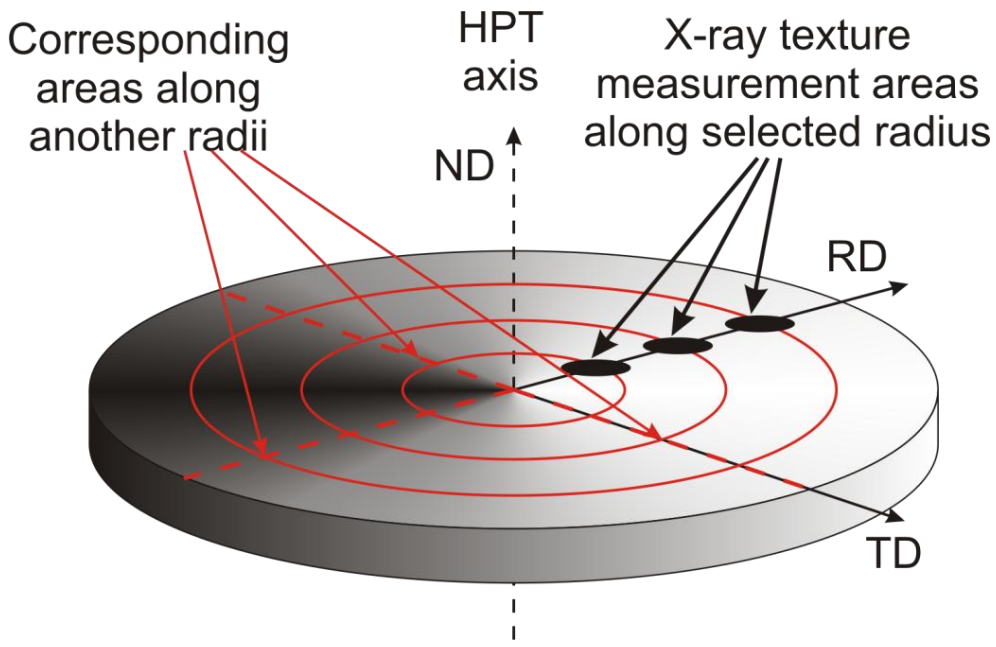

Fig. 7-3. The experimental setup for '4-point Test' texture measurements on a HPT-deformed sample.

Such an idea can be explained in a clear way, more clear with Fig. 7-3, where one can distinguish measured areas along one arbitrarily selected radius and corresponding areas along other non-investigated radii. In order to verify the assumptions of measurements results being

independent on selected radius the texture investigations were carried out for two initial single crystal orientations: the prismatic one $[11\bar{2}0]$ ('III') deformed up to 1.5 rot at 1.5GPa and a basal one $[0001]$ ('IV') one deformed up to 0.5 rot at the same HPT hydrostatic pressure of 1.5GPa. Then for both of the samples all four radii were selected and areas in the same radius distance of 2mm, ensuring good deformation-developed textures, were measured (exactly as shown in Fig. 7-4).

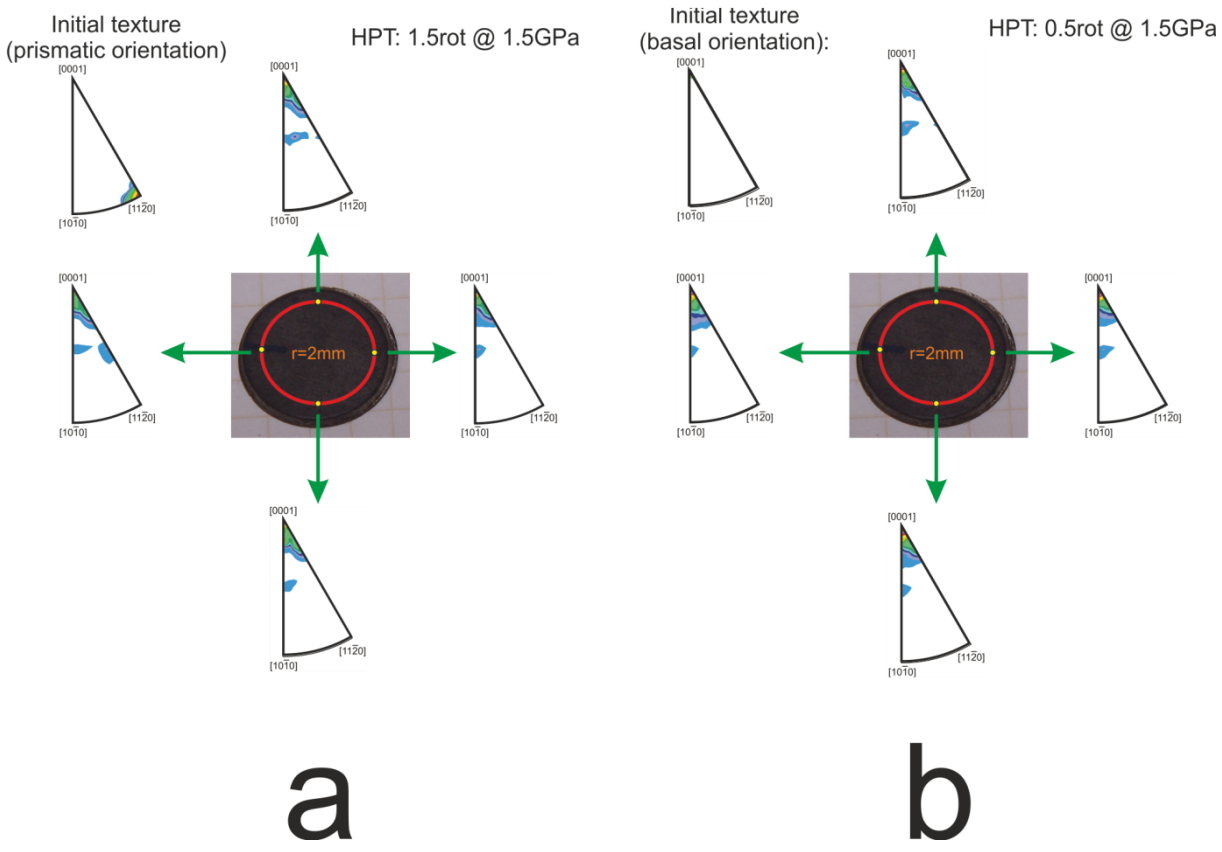

Fig. 7-4. Results of '4-point Test' investigation for (a) prismatic and (b) basal initial single crystal orientations deformed in HPT.

The results are presented in a form of the Inverted Pole Figures (IPF) for the two investigated initial orientation, in Fig. 7-4. The performed experiment proved the correction of the texture analysis of HPT deformed single crystals, by showing that the HPT-evolved texture does not depend on the selected sample radius in Mg single crystal material. Therefore the above presented and analyzed results are considered to be representative for entire single crystalline sample volume, as long as the radius is equal.

7.3 Related papers published

Obtained experimental results, together with detailed discussions were consequently published during this PhD program. A complete list of relevant papers is presented below:

- Bonarski BJ, Mikułowski B, Schafler E, Holzleithner C, Zehetbauer MJ. Crystallographic textures of single and polycrystalline pure Mg and Cu subjected to HPT deformation. Arch. Metall. Mater. 2008;53:117.
- Bonarski B, Schafler E, Mingler B, Skrotzki W, Mikulowski B, Zehetbauer M. Texture evolution of Mg during high-pressure torsion. Journal of Materials Science 2008;43:7513.
- Bonarski BJ, Schafler E, Mikułowski B, Zehetbauer MJ. Texture evolution of magnesium single crystals deformed by high-pressure torsion. Mater. Sci. Forum 2008;584-586:263.
- Bonarski BJ, Enikeev NA, Schafler E, Mikulowski B, Valiev RZ, Zehetbauer MJ. High Pressure Torsion of Cu and Mg - Evolution of Texture and correlation to mechanical properties. 2009;in preparation.
- Bonarski BJ, Schafler E, Mikulowski B, Zehetbauer MJ. Effects of Recrystallization on Texture, Microstructure and Mechanical Properties in HPT-deformed Pure Mg. J. Phys. Conf. Series 2009;in press.

7.4 List of figures

7.5 Curriculum Vitae

I was born on December, 31 in 1981 in Cracow, Poland. I graduated from the secondary school in Cracow in June, 2000 and continued my education at the AGH – University of Science and Technology in Cracow (Poland) at the Faculty of Non-Ferrous Metals. After graduating from AGH University with a Master of Science academic degree I have started the PhD studies at the same University at the Department on Metallic Materials and Nanoengineering. For that purpose I have attended research scholarships founded by Ernst Mach and CEEPUS at the Research Group of Physics of Nanostructured Materials at the Faculty of Physics at the University of Vienna, in 2006 and 2007. In 2007 I have been accepted as a PhD student at the University of Vienna and then continued PhD studies within a bilateral cooperation between AGH (Cracow, Poland) and UW (Vienna, Austria). The doctoral dissertation under the title of: 'Evolution of Crystallographic Texture and Mechanical Properties of Single- and Polycrystalline Mg Subjected to High-Pressure Torsion (HPT) Deformation' has been finished in 2010. Married in September, 2008, I currently live in Cracow, Poland.

Name: **Bartłomiej Jan Bonarski MSc.**

Birthplace: Cracow, Poland, 30th December, 1981

Place of residence: Ul. Doktora Piltza 33/59

PL–30392 Cracow, Poland

Phone: +48 (0) 601 45 55 05

bartek.bonarski@gmail.com

Family status: married, no children

Primary work address: **Department of Metallic Materials and Nanoengineering**

Faculty of Non-Ferrous Metals

AGH – University of Science and Technology in Cracow

Al. Mickiewicza 30/A-2/HA 206

PL-30059 Cracow, Poland

Phone: +48 12 617 26 97

email: bbartek@agh.edu.pl

Secondary work address: Research Group of Physics of Nanostructured Materials

Faculty of Physics

University of Vienna

Boltzmanngasse 5 EG Zi. 32

A-1090 Vienna, Austria

Phone: +43 1 4277 51446

email: bartlomiej.bonarski@univie.ac.at

Education:

2007 – 2010 **- Ph.D. Studies** at the **University of Vienna (Austria)** at the Faculty of Physics, Research Group of Physics of Nanostructured Materials

2005 – 2010 **- Ph.D. Studies** at the **AGH – University of Science and Technology in Cracow (Poland)** at the Faculty of Non-Ferrous Metals, Department of Structure and Mechanics of Solids

2000 – 2005 **- Master Study** at the **AGH – University of Science and Technology in Cracow (Poland)** at the Faculty of Non-Ferrous Metals in field of Materials Science and Engineering, majoring in Metallic Materials Engineering. On July, the 12th 2005 granted degree of Master of Science (MSc.)

Honors and awards:

2006 **-** Diploma thesis under the title of "Developing of anisotropy of structure in titanium proceed by ECAP method" awarded on the 7th Edition of an AGH University's contest "Diamonds of AGH" for the best Diploma Thesis of the AGH University of Science and Technology in Cracow (Poland),

2005 **-** 2nd place on the 42nd Students' Society Session on the Faculty of Non-Ferrous Metals at the AGH – University of Science and Technology in Cracow (Poland) with presented talk under the title: "Odkształcanie tytanu metodą ECAP" *("Plastic deformation of titanium in the ECAP method")*

Conference contributions:

Oral presentations:

- "Tekstura Krystalograficzna Tytanu po Procesie ECAP", **B.J Bonarski***, VIII Seminarium Studentów i Młodych Inżynierów*, Apr. 8, 2005, Gdańsk, Poland;

- „Odkształcanie Tytanu Metodą ECAP", **B.J. Bonarski**, *XLII Sesja Kół Naukowych Pionu Hutniczego AGH,* May 5, 2005, Cracow, Poland;

- "Texture Investigation of HPT-deformed pure Mg", **B.J. Bonarski**; *Workshop*, Feb. 21, 2008, Erich Schmid Institute of Materials Science, Austrian Academy of Science – Leoben, Austria;

- "Texture Evolution of Magnesium Single Crystals Deformed by High-Pressure Torsion", **B.J. Bonarski,** E. Schafler, B. Mikułowski, M.J. Zehetbauer; *The 4th International Conference on Nanomaterials by Severe Plastic Deformation (NanoSPD-4),* Aug. 21, 2008, Goslar, Germany;

- "Correlations Between Texture and Mechanical Properties of UFG Cu and Mg Processed by High-Pressure Torsion", **B.J. Bonarski**, E. Schafler, N. Enikeev, B. Mikułowski, R.Valiev, M.J. Zehetbauer; *The 138th Annual Meeting and Exhibition of The Minerals, Metals and Materials Society (TMS2009)*, Feb. 16, 2009, San Francisco, CA, USA;

- "Effects of Recrystallization on Texture, Microstructure and Mechanical Properties in HPT-Deformed Mg", **B.J. Bonarski**, E. Schafler, M. Perek, M. Szczerba, B. Mikułowski, M.J. Zehetbauer; *15th International Conference on the Strength of Materials (ICSMA-15)*, Aug. 18, 2009, Dresden, Germany;

- "Evolution of Texture and Mechanical Properties of Single- and Polycrystalline pure Mg subjected to High-Pressure Torsion (HPT) Deformation"; **B.J. Bonarski**; Final IC Workshop, University of Vienna, Nov. 20, 2009, Strobl, Austria;

Poster presentations:

- "Crystallographic Textures of Single- and Polycrystalline Pure Mg and Mg-Al-Zn Alloys Subjected to HPT Deformation", **B.J. Bonarski**, B. Mikułowski, E. Schafler, Ch. Holzleithner, M.J. Zehetbauer; *2nd Symposium On Texture And Microstructure Analysis (SOTAMA2007),* Sept. 26, 2007, Cracow, Poland;

- "On the Texture Analysis of High-Pressure Torsion Deformed Mg and Cu", **B.J. Bonarski**, E. Schafler, B. Mikułowski, W. Skrotzki, M.J. Zehetbauer; *The 137th Annual Meeting and Exhibition of The Minerals, Metals and Materials Society (TMS2008)*, Mar. 10, 2008, New Orleans, LA, USA;

- "Evolution of texture and its influence on mechanical properties in Mg and Cu deformed by High-Pressure Torsion (HPT)", B.J. Bonarski, N. Enikeev, E. Schafler, B. Mikułowski, M.J. Zehetbauer; 31. Joint French-German Meeting "Textures", SF2M-DGM, Mar. 19, 2010, Dresden, Germany;

Selected publications:

- **B.J. Bonarski***; Tekstura krystalograficzna tytanu po procesie ECAP;* Proceedings of VIII Seminarium Studentów i Młodych Inżynierów, Gdańsk, Poland, April, 7-8 2005 (2005);
- **B.J. Bonarski**, B. Mikułowski; ***Anizotropia struktury i własności tytanu po procesie ECAP***; Proceedings of the conference Tytan i Jego Stopy, Serock, Poland, 2005 (2005);
- **B.J Bonarski**; ***Odkształcanie tytanu metodą ECAP***; Zeszyty Studenckiego Towarzystwa Naukowego, Nr 7, pp. 67-73, Wydawnictwo Studenckiego Towarzystwa Naukowego, Kraków, Poland (2005);
- **B.J. Bonarski**, E. Schafler, Ch. Holzleithner, B. Mikułowski, M.J. Zehetbauer; ***Crystallographic textures of single and polycrystalline pure Mg and Cu subjected to HPT deformation****;* Arch. Metall. Mater. 53, pp. 117-123 (2008),
- **B.J. Bonarski,** E. Schafler, B. Mingler, W. Skrotzki, B. Mikułowski, M.J. Zehetbauer; ***Texture Evolution of Mg During High-Pressure Torsion,*** J. of Mater. Sci., pp. 1-6 (2008)
- **B.J. Bonarski,** E. Schafler, B. Mikułowski, M.J. Zehetbauer; ***Texture Evolution of Magnesium Single Crystals Deformed By High-Pressure Torsion***; Mat. Sci. Forum 584-586, pp. 263-268 (2008);
- **B.J. Bonarski**, E. Schafler, B. Mikułowski, M.J. Zehetbauer; ***Effects on Recrystallization on Texture, Microstructure and Mechanical Properties in HPT-deformed pure Mg****;* Journal of Physics: Conference Series (JPSC), in press (2010);
- **B.J. Bonarski**, N. Enikeev, E. Schafler, B. Mikułowski, R. Valiev, M.J. Zehetbauer; ***High Pressure-Torsion of Cu and Mg – Evolution of Texture and Correlation to Mechanical Properties****; in preparation;*
- E.D. Tabachnikova, A.V. Podolskiy, **B.J. Bonarski**, C. Mangler, A.N. Velikodny, M.A. Tikhonovsky, V.Z. Bengus, M.J. Zehetbauer**;** ***Mechanical Properties and Microstructure Evolution of Ultrafine grained Zirconium at Low Temperatures****;* Rev.Adv.Mater.Sci, in press (2010);
- B. Mikułowski, G. Boczkal, **B.J. Bonarski**, M.J. Zehetbauer, W. Skrotzki, I. Alexandrov, E. Schafler, C.-G. Oertel, W. Wołczyński; ***Modelling of structure and properties of certain hexagonal metals***; in preparation;
- L. Zhang, A. Grytsiv, **B.J. Bonarski**, M. Kerber, D. Setman, E. Schafler, P. Rogl, E. Bauer, G. Hilscher, M.J. Zehetbauer; ***Impact of high pressure torsion on the microstructure and physical properties of Pr0.67Fe3CoSb12, Pr0.71Fe3.5Ni0.5Sb12 and Ba0.06Co4Sb12***; Journal of Alloys and Compounds 2010;494:78.

Language skills:

- English: fluency in speaking and writing,
- German: intermediate skills in speaking and writing,
- Russian: intermediate skills in speaking and writing,
- Polish: native.

Personal Interests:

Photography, Computers and Networking, Motorcycles, Sports (Martial Arts, Basketball).

8 Acknowledgements

During the time of this PhD project realization, the author has co worked with a number of eminent scientists, without whose help of, this project would have not achieved the desired quality. The author gratefully thanks to acknowledge the cooperation with:

Prof. Werner Skrotzki (TU Dresden, Germany) – for the fruitful discussions and help with the hcp texture understanding,

Dr. Erhard Schafler (UW, Vienna, Austria) – for many excellent expert X-ray hints, equipment operating course and for friendship and warm atmosphere at and outside of the Lab,

Dr. Arkadiusz Wieczorek (UW, Vienna, Austria) – for his friendship and help with the tension tests experiments,

Dr Grzegorz Boczkal (AGH, Cracow, Poland) – for the help with the first steps on the PhD project and advices in the single crystal growth art,

Dr. Nariman Enikeev (USATU, Ufa, Russia) – for the professional help with common publications and fruitful cooperation,

Dr. Bernhard Mingler (UW, Vienna, Austria) – for great help with the TEM investigation of Mg,

Dr Paweł Pałka (AGH, Cracow, Poland) – for great help with the microhardness testing,

Dr Małgorzata Perek (AGH, Cracow, Poland) – for great help with the SEM EBSD investigation of Mg,

Dr. Aleksey Podolskiy (NASU, Kharkov, Ukraine) – for many brilliant comments on the Mg texture,

Dr. Martin Hafok (ESI, Leoben, Austria) – for the support at the HPT experiments,

Dr. Stephan Scheriau (ESI, Leoben, Austria) – for the support at the HPT experiments,

Dr. Daria Setman (UW, Vienna, Austria) – for great help with the DSC experiments and professional and cheerful support at and outside the Lab

Mag. Michael Kerber (UW, Vienna, Austria) – for a lot of advice at excellent scientific quality, support at the X-ray experiments, fruitful conversations, hours of common work, friendship and almost every day help at and outside the Lab,

Mgr Inż. Anna Kula (AGH, Cracow, Poland) – for the great support at the AGH during my absence and many valuable conversations on the common PhD route,

Mgr Inż. Bartosz Sułkowski (AGH, Cracow, Poland) – for the support and mastering the Mg single crystals growth furnace,

Mag. Florian Spieckermann (UW, Vienna, Austria) – for the interesting conversations and brilliant comments at the scientific area and not only,

Christian Holzleithner (UW, Vienna, Austria) – for his great work with HPT in-situ curves analysis and inventing the Cu-ring for the Mg samples.

This dissertation has been completed with the financial support of the CEEPUS and Ernst Mach Scholarships financed by the Austrian government.

The author is grateful for the financial support by the Focus Project "Bulk Nanostructured Materials" of the University of Vienna, by the PhD Program "I022-N Experimental Materials Science – Nanostructured Materials" of the University of Vienna and by the Austrian Science Fund, Project NFN-S10403.

The author kindly acknowledges the financial support by the Polish Ministry of Science and Higher Education within the frame of the "Supervisor's grant" no. N N507 402435.

9 References

1. Beck, A., *Magnesium und seine Legierungen*. Klassiker der Technik. 1939, Berlin: Springer.
2. Kainer, K.U., *Magnesium Alloys and Technology*. 2003: Wiley-VCH, Germany. 285.
3. Berner, R. and H. Kronmüller, *Plastische Verformung von Einkristallen*, in *Moderne Probleme der Metallphysik*, A. Seeger, Editor. 1965, Springer-Verlag: Berlin. p. 35-125.
4. Kainer, K.U., *Magnesium Alloys and Their Applications*. Proceedings of the 7th International Conference on Magnesium Alloys and Their Applications. 2000: Wiley-VCH Weinheim, Germany.
5. Avedesian, M.M., *Magnesium and Magnesium Alloys*. 2 ed. ASM - Speciality Handbook, ed. M.M. Avedesian and H. Baker. 1999, Materials Park, OH, USA: ASM International.
6. Roberts, C.S., *Magnesium and Its Alloys*. Wiley Series on The Science and Technology of Materials, ed. J.H. Hollomon. 1960, New York: Wiley.
7. Winter, M. *http://www.webelements.com/*. 1993; Available from: http://www.webelements.com/.
8. Bakarian, P.W. and C.H. Mathewson, *Slip and twinning in magnesium single crystals at elevated temperatures.* Trans. AIME, 1943. **152**.
9. Burke, E.C. and W.R.J. Hibbard, *Plastic Deformation of Magnesium Single Crystals.* J. Met., 1952: p. 295-303.
10. Dragomir, I.C. and T. Ungár, *Contrast factors of dislocations in the hexagonal crystal system.* Journal of Applied Crystallography, 2002. **35**(5): p. 556-564.
11. Honeycombe, R.W.K., The Plastic Deformation of Metals, 1984.
12. Klimanek, P. and R. Kuzel Jr, *X-ray diffraction line broadening due to dislocations in non-cubic materials. 1. General considerations and the case of elastic isotropy applied to hexagonal crystals.* J. Appl. Cryst., 1988. **21**: p. 59-66.
13. Tonda, H. and S. Ando, *Effect of temperature and shear direction on yield stress by {11-22}<-1-123> slip in HCP metals.* Metall. Mater. Trans. A, 2002. **33**(13): p. 831-836.
14. Busk, R.S., *Magnesium and Its Alloys*, in *Handbook of Materials Selection*, K. Myer, Editor. 2007. p. 259-265.
15. Obara, T., H. Yoshinga, and S. Morozumie, *{11-22}<-1-123> Slip system in Magnesium.* Acta Metall., 1973. **21**: p. 845-853.
16. Akhtar, A. and E. Teghtsoonian, *Solid Solution Strenghtening of Magnesium Single Crystals - I. Alloying Behaviour in Basal Slip.* Acta Metall., 1969. **17**: p. 1339-1349.
17. Akhtar, A. and E. Teghtsoonian, *Solid solution strengthening of magnesium single crystals - II. The effect of solute on the ease of prismatic slip.* Acta Metallurgica, 1969. **17**(11): p. 1351-1356.
18. Ando, S., et al., *The {11-22}<-1-123> slip in magnesium single crystal.* Journal of Japan Institute of Light Metals, 1992. **42**: p. 765-771.
19. Stohr, J.F. and J.P. Poirier, *Etude en microscopie electronique du glissement pyramidal {11-23}<11-23> dans le magnesium.* Philosophical Magazine, 1972. **25**(6): p. 1313 - 1329.
20. Asada, H. and H. Yoshinaga, *Nonbasal Slips and Twins of Magnesium Coarse Grains.* The Journal of the Japan Institute of Metals, 1959. **23**(1): p. 67-71.
21. Aldinger, F., *Flow and Fracture of Single Crystals*, in *Beryllium Science and Technology*, D. Webster and G.J. London, Editors. 1979, Plenum Press: New York. p. 7-114.
22. Graff, S., W. Brocks, and D. Steglich, *Yielding of magnesium: From single crystal to polycrystalline aggregates.* Int. J. Plast., 2007. **23**: p. 1957-1978.

23. Ando, S. and H. Tonda, *Non-basal slips in magnesium and magnesium-lithium alloy single crystals.* Materials Science Forum, 2000. **350**: p. 43-48.
24. Groves, G.W. and A. Kelly, *Crystallography and crystal defects*. 1970, Longman Group: London. p. 428.
25. Wonsiewicz, B.C., *Plasticity of Magnesium Crystals*, in *Department of Metallugry*. 1966, Massachusetts Institute of Technology: Massachusetts. p. 66.
26. Barnett, M.R., *Twinning and the ductility of magnesium alloys: Part I: "Tension" twins.* Mater. Sci. Eng. A, 2007. **464**(1-2): p. 1-7.
27. Akhtar, A. and E. Teghtsoonian, *Substitional Solution Hardening of Magnesium Single Crystals.* Phil Mag, 1972. **25**(4): p. 897-916.
28. Barnett, M.R., *Twinning and the ductility of magnesium alloys: Part II. "Contraction" twins.* Mater. Sci. Eng. A, 2007. **464**(1-2): p. 8-16.
29. Gehrmann, R., *Magnesium - Einfluss der Textur auf das Umformverhalten*. 2004, Aachen, Germany: Shaker.
30. Valiev, R.Z., R.K. Islamgaliev, and I.V. Alexandrov, *Bulk nanostructured materials from severe plastic deformation.* Progr. Mater. Sci., 2000. **45**(2): p. 103-189.
31. Zehetbauer, M.J. and Y.T. Zhu, *Bulk Nanostructured Materials*, ed. M.J. Zehetbauer and Y.T. Zhu. 2009, Weinheim, Germany: Wiley-VCH.
32. Kilmametov, A.R., I.V. Alexandrov, and A.A. Dubravina, *Texture analysis of nanostructured metals produced by severe plastic deformation.* Mater. Sci. Forum, 2004. **443-444**: p. 243-246.
33. Alexandrov, I.V., et al., *Homogeneity of the crystallographic texture and deformation behavior in Cu and Ti under severe plastic deformation.* Archives of Metallurgy and Materials, 2008. **53**(1): p. 237-241.
34. Valiev, R.Z., *Nanostructuring of metals by severe plastic deformation for advanced properties.* Nature Mater., 2004. **3**(8): p. 511-516.
35. Zehetbauer, M.J., et al., *The Role of Hydrostatic Pressure in Severe Plastic Deformation.* Adv. Eng. Mater., 2003. **5**(5): p. 330-337.
36. Jiang, H., et al., *Microstructural evolution, microhardness and thermal stability of HPT-processed Cu.* Materials Science and Engineering A, 2000. **290**(1-2): p. 128-138.
37. Čižek, J., et al., *Microstructure and thermal stability of ultra fine grained Mg-based alloys prepared by high-pressure torsion.* Mater. Sci. Eng. A, 2007. **462**(1-2): p. 121-126.
38. Bridgman, P.W., *On Torsion Combined with Compression.* J. App. Phys., 1943. **14**(6): p. 273-283.
39. Pippan, R., *High-pressure Torsion - Features and Applications*, in *Bulk Nanostructured Materials*, M.J. Zehetbauer and Y.T. Zhu, Editors. 2009, Wiley-VCH Weinheim.
40. Vorhauer, A. and R. Pippan, *On the homogeneity of deformation by high pressure torsion.* Scripta Mater., 2004. **51**(9): p. 921-925.
41. Kim, H.S., *Finite element analysis of high pressure torsion processing.* J. Mater. Proc. Tech., 2001. **113**: p. 617-621.
42. Alexandrov, I.V., et al. *Experimental study and computer modeling of high pressure torsion*. in *TMS Annual Meeting*. 2006.
43. Tóth, L.S., et al., *Texture Development and Length Changes in Copper Bars Subjected to Free End Torsion.* Text. Microstr., 1992. **19**(4): p. 245-262.
44. Tóth, L.S., P. Gilormini, and J.J. Jonas, *Effect of rate sensitivity on the stability of torsion textures.* Acta Metall., 1988. **36**(12): p. 3077-3091.
45. Hafok, M., et al., *HPT-Deformation of Copper and Nickel Single Crystals.* Mater. Sci. Forum, 2006. **503-504**: p. 621-626.

46. Stolyarov, V.V., et al., *Processing nanocrystalline Ti and its nanocomposites from micrometer-sized Ti powder using high pressure torsion.* Materials Science and Engineering A, 2000. **282**(1-2): p. 78-85.
47. Čížek, J., et al., *Defects in ultra-fine grained Mg and Mg-based alloys prepared by high pressure torsion studied by positron annihilation.* Acta Phys. Polonica A, 2005. **107**(5): p. 738 -744.
48. Zehetbauer, M.J. and R.Z. Valiev, *Nanomaterials by Severe Plastic Deformation: Fundamentals-Processing-Applications*. 2004, Weinheim (Germany): VCH-Wiley.
49. Xiang, S., et al., *Microstructure and mechanical properties of PM 2024Al-3Fe-5Ni alloy consolidated by a new process, equal channel angular pressing.* Journal of Materials Science Letters, 1997. **16**(21): p. 1725-1727.
50. Iwahashi, Y., et al., *Principle of equal-channel angular pressing for the processing of ultra-fine grained materials.* Scripta Materialia, 1996. **35**(2): p. 143-146.
51. Iwahashi, Y., et al., *The process of grain refinement in equal-channel angular pressing.* Acta Materialia, 1998. **46**(9): p. 3317-3331.
52. Skrotzki, W., et al., *Microstructure and texture gradient in copper deformed by equal chennel angular pressing.* Acta Mater., 2007. **55**: p. 2013–2024.
53. Schafler, E., et al., *Lattice defect investigation of ECAP-Cu by means of X-ray line profile analysis, calorimetry and electrical resistometry.* Mater. Sci. Eng. A, 2005. **410-411**: p. 169-173
54. Skrotzki, W., et al., *Recrystallization of high-purity aluminium during equal channel angular pressing.* Acta Mater., 2007. **55**: p. 2211–2218.
55. Skrotzki, W., et al., *Influence of dynamic recrystallization on texture formation in ECAP deformed nickel.* Mater. Sci. Forum, 2007. **558-559**: p. 575-580.
56. Agnew, S.R., et al., *Crystallographic texture evolution of three wrought magnesium alloys during equal channel angular extrusion.* Mat. Sci. Eng. A, 2005. **408**(1-2): p. 72-78.
57. Agnew, S.R., et al., *Enhanced ductility in strongly textured magnesium produced by equal channel angular processing.* Scripta Mater., 2004. **50**(3): p. 377-381.
58. Saito, Y., et al., *Novel ultra-high straining process for bulk materials--development of the accumulative roll-bonding (ARB) process.* Acta Materialia, 1999. **47**(2): p. 579-583.
59. Lee, S.H., et al., *Role of shear strain in ultragrain refinement by accumulative roll-bonding (ARB) process.* Scripta Materialia, 2002. **46**(4): p. 281-285.
60. Sun, Y., et al., *Solid-state amorphization of Cu + Zr multi-stacks by ARB and HPT techniques.* Journal of Materials Science, 2008. **43**(23): p. 7457-7464.
61. Richert, J. and M. Richert, *A new method for unlimited deformation of metals and alloys.* Aluminium, 1986. **62**(8): p. 604-607.
62. Richert, M. *Features of cyclic extrusion compression method, structure & materials properties*. in *Diff. Def. Data Pt.B: Solid State Phenomena*. 2006. Warsaw.
63. Richert, M., H.J. McQueen, and J. Richert, *Microband formation in cyclic extrusion compression of aluminum.* Canadian Metallurgical Quarterly, 1998. **37**(5): p. 449-457.
64. Korbel, A. and M. Richert, *Formation of shear bands during cyclic deformation of aluminium.* Acta Metallurgica, 1985. **33**(11): p. 1971-1978.
65. Bonarski, B.J., et al., *Crystallographic textures of single and polycrystalline pure Mg and Cu subjected to HPT deformation.* Arch. Metall. Mater., 2008. **53**(1): p. 117-123.
66. Pawlik, K. and J. Pospiech, *Theoretical methods of texture analysis.*, ed. H.J. Bunge. 1986, Clausthal-Zellerfeld, Germany: Proc. Workshop.
67. Pawlik, K. and P. Ozga, *LaboTex: The Texture Analysis Software*, in *Gittinger Arbeiten zur Geologie und Paläontologie*. 1999.

68. Pawlik, K., *Determination of the orientation distribution function from pole figures in arbitrarily defined cells.* Phys. Status Sol. (b), 1986. **134**(2): p. 477-483.
69. Bonarski, J.T., *X-ray texture tomography of near-surface areas.* Progr. Mater. Sci., 2006. **51**(1): p. 61-149.
70. Xu, C. and T.G. Langdon, *Three-dimensional representations of hardness distributions after processing by high-pressure torsion.* Mater. Sci. Eng. A 2009. **503**: p. 71-74.
71. Enikeev, N.A., et al., *Observations of Texture in Large Scale HPT-Processed Cu.* Mater. Sci. Forum, 2008. **584-586**: p. 367-374.
72. Kilmametov, A.R., R.Z. Valiev, and I.V. Alexandrov, *X-ray analysis of high pressure torsion induced nanostructures in Ti and Ni.* Diff. Def. Data Pt.B: Solid State Phenomena, 2006. **114**: p. 329-336.
73. Kelley, E.W., *The Plastic Deformation of Magnesium*, in *Department of Chemical and Metallurgical Engineering*. 1967, University of Michigan: Ann Arbor. p. 102.
74. Suwas, S., G. Gottstein, and R. Kumar, *Evolution of the crystallographic texture during equal channel angular extrusion (ECAE) and its effect on secondary processing of magnesium.* Mater. Sci. Eng. A, 2007. **471**: p. 1-14.
75. Beausir, B., et al., *Analysis of texture evolution in magnesium during equal channel angular extrusion.* Acta Mater., 2008. **56**(2): p. 200-214.
76. Beausir, B., L.S. Toth, and K.W. Neale, *Ideal orientations and persitence characteristics of hexagonal close packed crystals in simple shear.* Acta Mater., 2007. **55**: p. 2695-2705.
77. Beausir, B., et al., *Texture and Mechanical Behavior of Magnesium During Free-End Torsion.* J. Eng. Mater. Tech., 2009. **131**(1): p. 011108-1−15
78. Bonarski, B.J., et al., *Texture evolution of Mg during high-pressure torsion.* J. Mater. Sci., 2008. **43**(23-24): p. 7513–7518.
79. Al-Samman, T., *Magnesium- The Role of Crystallographic Texture, Deformation Conditions and Alloying Elements on Formability*. 2008: TH Aachen.
80. Schafler, E., *Effects of releasing the hydrostatic pressure on the nanostructure after severe plastic deformation of Cu.* Scripta Materialia, 2010. **62**: p. 423-426.
81. Bonarski, B.J., et al., *High Pressure Torsion of Cu and Mg - Evolution of Texture and correlation to mechanical properties.* 2009. **in preparation**.
82. He, B.B., *Two-Dimensional X-ray Diffraction*. 2009, New Jersey: Wiley. 426.
83. Yoon, S.C., Z. Horita, and H.S. Kim, *Finite element analysis of plastic deformation behavior during high-pressure torsion processing.* J. Mater. Proc. Tech., 2008. **201**: p. 32-36.
84. Estrin, Y., et al., *Strain gradient plasticity modelling of high-pressure torsion.* Journal Mech. Phys. Solids, 2008. **56**: p. 1186–1202.